CHALMERS

Modelling of VSC-HVDC for Slow Dynamic Studies

Master's Thesis in Electric Power Engineering

OSCAR LENNERHAG
VIKTOR TRÄFF

Department of Energy and Environment
Division of Electric Power Engineering
Chalmers University of Technology
Gothenburg, Sweden 2013
Master's Thesis 2013

Modelling of VSC-HVDC for Slow Dynamic Studies
OSCAR LENNERHAG
VIKTOR TRÄFF
Department of Energy and Environment
Division of Electric Power Engineering
Chalmers University of Technology

Abstract

With recent advances in technology and the controllability it offers, Voltage Source Converter based HVDC (VSC-HVDC) is expected to be the preferred choice for integration of renewable energy sources and when building large HVDC grids. As it is a relatively new technology when compared to the more mature Classic HVDC, many studies are aimed at operation and stability of VSC-HVDC interconnecting AC grids. When performing simulations on large systems interconnecting AC grids with VSC-HVDC, the computational load will be heavy due to the complexity of the models associated with VSC-HVDC. It is therefore desirable to develop simplified models suitable for studies where the main interest is in slow dynamics, where such complexity might have a negligible impact on the results.

In this thesis the goal was to implement a simplified model of a VSC-HVDC in the software tool PowerFactory to be used in transient stability studies. First, a detailed model was implemented in PSCAD and PowerFactory for EMT simulations. In order to use the model for simplified RMS simulations in PowerFactory, it was found that several adjustments had to be made in order to get a more similar performance to the detailed models, when considering the slow dynamics of the system. After the simplified model had been implemented it was verified by simulating different cases and comparing the results to the detailed models in PowerFactory and PSCAD. In most cases the simplified model was a good representation of the detailed models. The verified model was then included in a larger multimachine system in order to evaluate the impact of VSC-HVDC on AC systems. It was found that the computational time could be reduced drastically using the simplified model, with negligible differences in the results. From these simulations it was concluded that due to the high controllability of VSC-HVDC and the ability to produce or consume reactive power as needed, it could be used to improve the transient stability of the AC system.

Keywords: VSC-HVDC, EMT, RMS, transient stability, slow dynamic studies, electric power system, transmission system, PowerFactory, PSCAD

Acknowledgements

First of all we would like to express our gratitude to our supervisor at Chalmers, Gustavo Pinares, for his never-ending support. He would always find time to discuss new findings with us or give a helping hand when we were stuck.

We would also like to thank our examiner, Lina Bertling Tjernberg, for believing in us and also for giving us good feedback. We also appreciate the possibility to be a part of the HVDC grid research group at Chalmers, as well as being given the opportunity to participate in several conferences and happenings in the industry.

Also, we would like to thank Tuan Le for, among other things, pointing us in the right direction when we were looking for a thesis.

This project has been supported by STRI AB, who have aided us when looking for information as well as providing equipment and working space. We would like thank everyone at STRI but extra thanks go to our supervisor Susanne Ackeby, for giving us good feedback and for always being positive, as well as Emil Hillberg and Jan Djurström for good insights regarding the project.

The Authors, Gothenburg 22/7 - 2013

List of Figures

List of Abbrevations

AC	Alternating Current
AVR	Automatic Voltage Regulator
CSC	Current Source Converter
DC	Direct Current
DSL	Dynamic Simulation Language
EMT	Simulation mode based on detailed electromagnetic transient models
HVDC	High Voltage Direct Current
IGBT	Insulated-Gate Bipolar Transistor
IMC	Internal Model Control
MIMO	Multiple-Input-Multiple-Output
MTDC	Multi-terminal DC
PI	Proportional Integral
PLL	Phase-locked Loop
PSS	Power System Stabilizer
PWM	Pulse Width Modulation
RMS	Simulation mode based on simplified electromechanical transient models
SCR	Short-Circuit Ratio
SLG	Single-Line to Ground
SPWM	Sinusoidal Pulse Width Modulation
STATCOM	Static Synchronous Compensator
VSC	Voltage Source Converter

Contents

1

Introduction

This chapter provide a background to the thesis, the aim of the thesis and an outline describing the content.

1.1 Background

The first commercial installation of VSC-HVDC was operational in 1999, on the island of Gotland in Sweden, whereas the more mature Classic HVDC has been in use since the 1950s [1]. VSC-HVDC is a relatively new technology and it offers several advantages over Classic HVDC, some which make VSC-HVDC especially suitable for e.g. integration of renewable energy sources such as offshore wind farms, and the construction of HVDC grids which can be used to connect several AC grids together [2]. With recent advances in power electronics, VSC-HVDC is becoming a viable option with several projects in the planning stages, some which have already started construction [3]. One such project is the South West Link in Sweden [4].

There has been a considerable amount of research regarding operation of VSC-HVDC, and its interaction with AC grids. One concern is on how the introduction of VSC-HVDC will impact the power system stability of the connected AC systems [5]. The power system stability is usually evaluated through system studies, performed using computer software, which offer detailed models of components such as synchronous machines and transformers. The VSC models will introduce an increased complexity in the simulations due to the nature of the DC dynamics, switching of the converter etc. which are fast compared to machine dynamics [5]. If a transient stability study is to be performed, focusing on the slow dynamics of the system (e.g. machine dynamics), it would be in the range of seconds to several minutes [6]. If the system include detailed models of VSCs the computational time would then increase drastically due to the complexity of the associated models. However, the high level of detail could have a negligible impact on the mechanical variables, such as rotor speed, torque of power output, when investigating the transient stability of a system [7]. Therefore it is desirable to investigate if the

detailed models can be simplified, decreasing the computational time while still maintaining an acceptable accuracy in the results.

This project originated at STRI AB and have been performed in collaboration with the HVDC grid research group at Chalmers, with the intention to investigate the possibility to develop simplified models of VSC-HVDC for transient stability studies. It is based on previous research on VSC-HVDC by Gustavo Pinares, the supervisor of this project and a member of the research group.

1.2 Aim and Scope

The aim of this thesis is to develop a model of VSC-HVDC suitable for slow dynamic studies, with its limitations and benefits properly identified. The model should then be used to study the impact of VSC-HVDC on the operation of AC systems regarding transient stability.

As the focus of the report is on the development of a simplified model of VSC-HVDC, the following considerations have been made:

- Optimal controller performance is not a part of the objectives of this thesis, what is of interest is that the controller behaves similarly in both the RMS and EMT models.
- Differences between the two EMT models are only investigated if they are deemed large enough to impact the results.

1.3 Thesis Outline

The thesis is organized as follows:

Chapter 1 is an introduction to the thesis, presenting its background and aim.

Chapter 2 presents theory on HVDC and slow dynamic studies based on a literature review, covering power system studies for HVDC, HVDC modelling for slow dynamic studies and HVDC grids - including HVDC topologies, control strategies and protection schemes.

Chapter 3 considers VSCs, showing some advantages of VSC-HVDC over Classic HVDC as well as some more in depth theory regarding modelling of e.g. converters, phase reactors. Also, the modelling of a control system to be used with a VSC is described.

Chapter 4 describes the implementation of a simplified model of a VSC-HVDC in PowerFactory. It also contains a verification of the model when compared to more detailed models in both PowerFactory and PSCAD.

Chapter 5 presents results from simulations carried out in a more complex multimachine system.

Chapter 6 gives the conclusions of the study and it also provides a discussion as well as ideas for future work on this subject.

2

HVDC and Slow Dynamic Studies

This chapter present the results of a literature review covering the following subjects: power system studies for HVDC interconnections, HVDC modelling for slow dynamic studies and HVDC grids, including theory regarding topologies, control and protection.

2.1 Power System Studies for HVDC Interconnections

Power system studies are made in several areas and are an important activity for planning and operation of the power system, but also to streamline the existing system. Studies are done to e.g. propose a power system expansion that might be required and to look at the financial aspect following such an expansion. The cost aspect might also be of concern during operation, where reducing losses might be the goal. Another application of power system studies is a post mortem analysis after undesirable events occur in the power system.

Scenarios that might be of interest include [8]:

- Network interconnections between islands and the mainland.
- Interconnections between countries with the ambition to involve more renewable energy sources.
- Interconnections of asynchronous AC grids.

The stability of a power system is one of the most important areas to study. *Power System Stability* can be defined as the capability of a power system to regain an acceptable state of operational equilibrium when subjected to a disturbance. It can be split into three main categories: *Rotor Angle Stability*, *Frequency Stability* and *Voltage Stability* [9].

Rotor Angle Stability
Rotor angle stability refers to the capability of synchronous machines in a power system to

remain in synchronism. The goal is to keep the equilibrium between the electromagnetic torque and the mechanical torque for every machine in the power system. It can be classified into two categories, *Small-Disturbance Angle Stability* and *Transient Stability*. The main focus of this thesis is within the transient stability area.

In a small disturbance angle stability analysis the ability of the power system to remain in synchronism is studied for small disturbances, such as small variations in generation or loads. For this kind of analysis the disturbances are considered small enough for the system equations to be linearized.

A transient stability analysis aims at studying the power system following a severe disturbance. This could be, for example, in case of large changes in power in generation or load, or due to a fault changing the transmission system configuration. For a transient stability study, the time-frame of interest for the simulation is usually between 3 and 5 seconds after a disturbance. This may be extended for larger power systems [6].

The two main methods for transient stability analysis are [9]:

1. Equal Area Criterion
2. Numerical Integration Methods

The first method, equal area criterion, is based on energy conservation and can be used to graphically visualize and predict the stability scenario. However, this method is not applicable for multimachine systems [9]. In this case numerical integration methods can be used instead. These methods solve the differential equations of the power system for a given initial condition. Computer software for power system simulations use numerical integration, and a general procedure of the process is presented in Figure 2.1.

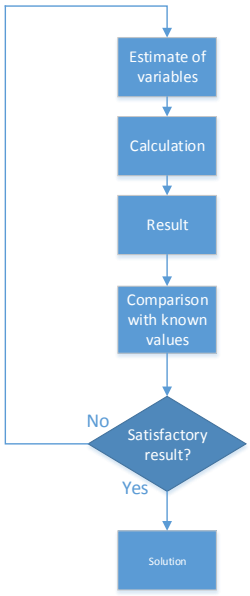

Figure 2.1: A general procedure for numerical integration [10].

Frequency stability

Frequency stability is the ability of a power system to remain at a stable frequency. The goal is to keep the balance between generation and load, and studies which can be of interest may involve coordination of generating units of the power system or response times of certain equipment.

Voltage stability

Voltage stability is the ability of a power system to keep stable voltage levels at all buses in the grid after a disturbance. The goal is to keep equilibrium between demand and supply in the power system. Voltage instability, reaching unacceptable voltages, can occur for several reasons such as equipment reaching operational limits or line/generator outages. Voltage instability can result in an avalanche of events causing voltage collapse where significant parts of the grid will be out of commission. It can be classified into two categories: *Large-Disturbance Voltage Stability* and *Small-Disturbance Voltage Stability*. In large-disturbance voltage stability studies significant events such as fault or loss of generation are present. The time frame can be several minutes to capture characteristics of equipment with slow dynamics. Small-disturbance voltage stability refers to the ability of the system to keep stable voltages when subjected to small disturbances such as a gradual increase in load. Studies of interest include e.g. the performance of the control system.

However, even if it is effective to separate power system stability into different categories during studies, in practice the overall stability of the system should always be considered. Solutions

to problems within one category should not be at the expense of another [9].

In Figure 2.2 the classifications are illustrated.

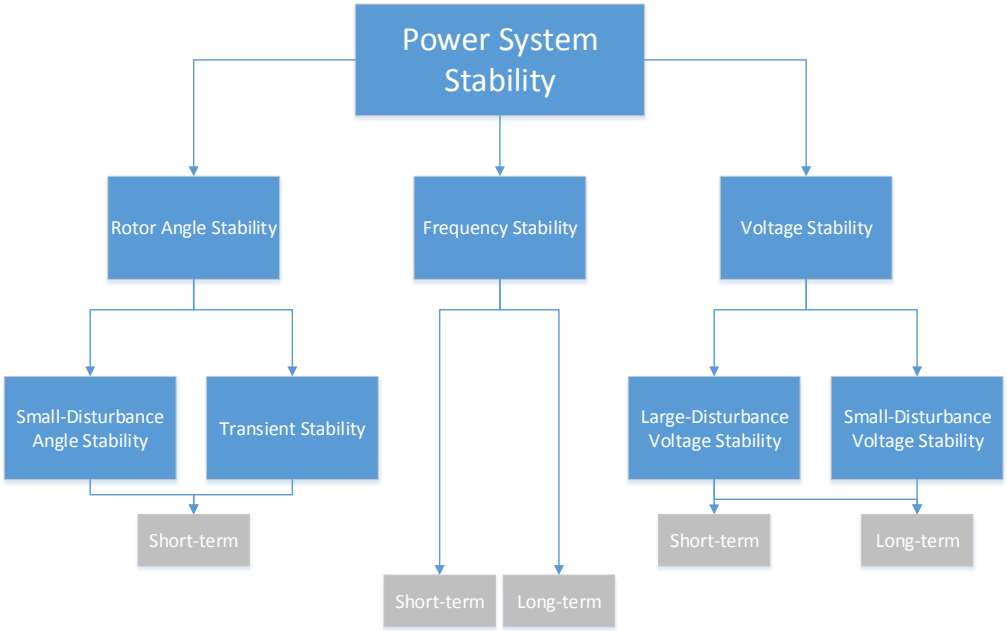

Figure 2.2: Classification of power system stability [6].

There have been previous projects focusing on power system studies regarding introduction of HVDC and VSC-HVDC into AC grids. In [11] several control strategies are presented in order to improve the voltage stability and the transient stability of such a system. Main conclusions are that with a proper strategy for the control, the introduction of VSC-HVDC gives the possibility to increase the transmission capacity as well as increasing both the voltage and the transient stability of the overall system.

Another report, [12], which also study the effect of the integration of a HVDC link into an AC system conclude that a HVDC link will contribute to increasing the stability of the network it is connected to. A model for the DC link was developed using the software SIMPOW and was tested on a simplified model of the Nordic network. The author states that if the link is installed at a proper location, in some cases it can even save the system from a total collapse.

2.2 HVDC Modelling for Slow Dynamic Studies

Several reports have focused on the modelling of VSC-HVDC and Multi-Terminal HVDC (MTDC) for power system stability studies. In [13], a general VSC-MTDC model is derived mathematically. It includes the converter, its controllers, DC circuit equations and AC/DC coupling equations. The authors transform the converter equations into a rotating dq reference frame,

assuming that the angle given by the PLL will align the system voltage with the q axis. The current controller and outer controllers are implemented as standard Proportional Integral (PI) regulators as the development of control systems for VSC-MTDC is not the aim of the study. Then equations are derived for the DC circuit and generalized for any number of converters in an MTDC configuration. For the converter controlling the DC voltage, the DC circuit dynamics are approximated by a time constant, determined by the DC capacitors.

The authors use the principle of active power balance to couple the AC and DC equations, finally arriving at the full model of a VSC-MTDC system with one converter controlling the DC voltage. As the model is aimed at transient stability studies the level of detail in the HVDC system is limited, but it can be used for studying the influence of the VSC-MTDC system on the AC system and also the dynamics of the DC circuit. According to the obtained results from the performed simulations the proposed model seems to be a good representation of an MTDC system for transient stability studies.

In [14], the interaction between an MTDC grid and a multimachine AC system is investigated. The authors aim to create a general model of an asymmetric, bipolar MTDC grid for stability analysis when the system is subjected to e.g. DC-side faults, cable outages or converter outages. The stability analysis is comprised of a modal analysis and transient simulations.

First, the entire system was transformed to the rotating dq reference frame following the IEEE convention, with the converters represented by their averaged models. All converters, except for one, are considered to control active power, with a single converter operating in the DC voltage control mode. A generic π-model was used for the DC cable as a distributed model of the cable has an infinite number of states associated with it and was therefore deemed unsuitable for modal analysis. It was determined that using four cascaded π-sections a close approximation could be obtained compared to the distributed model. Then a mathematical model of the DC network was described, using both algebraic and differential equations. Following this a combined AC-MTDC grid was modelled, with the generators, excitation systems, loads etc. in the multimachine AC system described by their respective algebraic and differential equations.

The authors claim that the model is generic enough to handle any:

- Bipolar MTDC grid configuration.
- Grounding options.
- π-section approximations.
- DC side faults (location and type).
- Cable or converter outages.

Using a detailed model in PSCAD, the model was tested for both small and large disturbances, and the obtained results indicate that the model was a good representation in the case of small disturbances, and a good enough approximation for large disturbances. Following this, a modal analysis was performed and from this the conclusion could be made that instability in some cases could only be associated to the DC side state variables.

The study performed in [15] consider small signal stability of VSC-MTDC. A generic model of VSC-MTDC grids is developed and an analogy between AC and DC parameters is made. In

the converter model a perfect decoupling between the d and q axes is assumed and the energy stored in the AC filter, and its losses, is neglected to simplify the model for dynamic studies. The modelling is simplified further by splitting the DC network into three elementary blocks, one for each converter substation and one for the line. Contrasting to the previous two papers presented in this section the cable is modelled using a T-model rather than a π-model. The state space model was validated using the software EMTP-rv, and even though there was a small static error due to the linearization, the dynamics of the state space model matched the detailed model for small disturbances. Based on these models, a parametric study is performed on the DC voltage droop parameter for a point-to-point link as well as a three terminal MTDC grid to show its influence on the stability of the system.

2.2.1 Model Reduction

A model reduction can be done in order to decrease computational time at the cost of accuracy that may not be needed for the specific study. In case of a long-term stability study for example, transients that disappear quickly might not be of interest. The model reduction should be performed in order to eliminate small time constants related to the system, and this coincide with the assumption that fast dynamics are instant compared to slower.

Possible actions for the DC side could be to eliminate the dynamics of the DC cable and the converter capacitor, making the network purely resistive. This would result in no dynamics in the DC voltage and the current flowing through the lines. For the AC side, e.g. the fast dynamics of the phase reactor could be eliminated.

In [7] it is suggested to keep the DC capacitors and phase reactor as they are the dominant elements in the DC and AC side respectively. Time constants that can be removed are related to the dynamics associated with the DC line, DC current and AC voltage, and their removal will reduce the number of differential equations. Advantages of this include the need for less data and the possibility to use a larger integration step size, increasing the calculation speed.

2.3 HVDC Grids

There are several areas of interest regarding HVDC grids, such as how they should be controlled, how to implement protection schemes and what topology they should be arranged in. This section aims to give a brief overview on these subjects.

2.3.1 HVDC Topologies

HVDC converters can be arranged in several different topologies, the most common being:

Monopolar
The monopolar configuration, as shown in Figure 2.3, uses a single line to connect two converters. A positive or negative DC voltage can be used for the power transmission and the second terminal of each converter is connected to ground. The path of the return current can go through the ground or sea, or a metallic conductor used for the return current between the two earthed terminals [9].

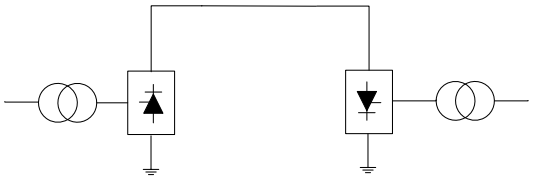

Figure 2.3: Monopolar topology.

Bipolar

The bipolar configuration is the most commonly used topology in HVDC transmission [16]. It uses a pair of conductors at positive and negative potential relative to ground respectively. It is a more expensive topology than monopolar due to the increased transmission line cost but it has several advantages over the monopole configuration. In case of the loss of a line, approximately half the rated power can still be transmitted by using the bipolar configuration, by using the remaining line in monopolar operation [9]. It is shown in Figure 2.4.

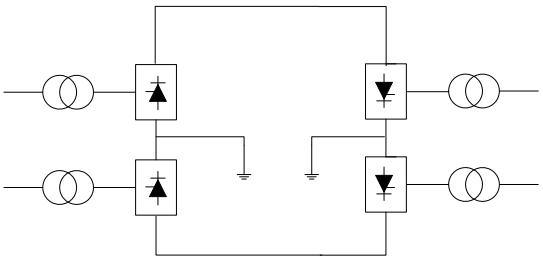

Figure 2.4: Bipolar topology.

Back-to-Back

The back-to-back configuration, as shown in Figure 2.5, has two converter stations located in close proximity; at the same site or in the same building. In this configuration a transmission line is not used. Back-to-back stations are used for connecting AC systems with either the same or different nominal frequencies [9].

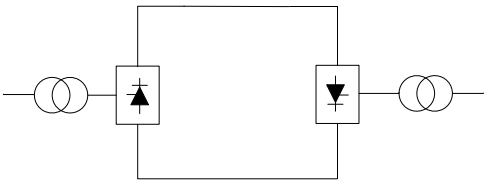

Figure 2.5: Back-to-back topology.

Multi-terminal
An MTDC system connects three or more converter stations together and it provides the possibility to interconnect several AC systems together. It can be arranged in several different ways. If connected in series the current is controlled by one converter and it will be the same for the whole system. The power is then controlled at the other converters by changing the DC voltage. If the system is connected in parallel one converter will control the voltage and the others will control the power by varying the current [9]. A series and parallel configuration can also be used together in a so called hybrid configuration. Figure 2.6 show both configurations.

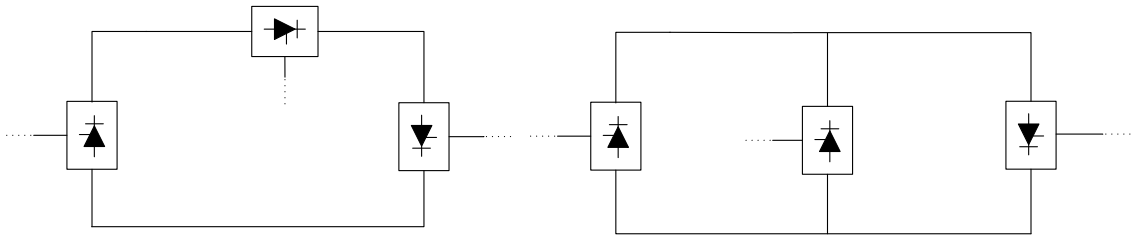

Figure 2.6: Series and parallel topologies of MTDC.

2.3.2 Control Strategies

The subject of control of VSC-HVDC have been considered in several reports, such as [5] and [17], and depending on the characteristic of the AC grid connected to the VSC the control objective will differ.

There are two types of AC grids: active and passive. If the AC grid is said to be passive, the only power source in the grid is the VSC. If it is active, there are more sources than just the VSC. The main concern for the VSC, if connected to a passive AC grid, is keeping the AC line-line voltage constant [17].

In case of an active AC grid, the control objective of the VSC will depend on if the grid is weak or strong. The strength of the AC system is defined by its Short-Circuit Ratio (SCR). It is defined in [9] as:

$$SCR = \frac{\text{Short-circuit MVA of AC system}}{\text{MW rating of DC converter}} \tag{2.1}$$

where the short-circuit MVA of the AC system is defined as

$$\text{Short-circuit MVA} = \frac{V_{AC}^2}{Z_{th}} \tag{2.2}$$

where Z_{th} is the thevenin equivalent impedance of the AC system and V_{AC} is the commutation bus voltage at rated DC power.

The AC system strength is then classified as [9]:

- High, for an SCR higher than 3.
- Low, for an SCR between 2 and 3.
- Very low, for an SCR below 2.

In a strong grid the AC voltage is constant unlike in a weak grid, where the AC voltage should be controlled by reactive power compensation. Furthermore, when connected to an active AC grid one must choose to either control for a constant DC voltage or for a constant power flow [17].

Figure 2.7 shows suitable control-modes of the VSC depending on the classification of the AC grid connected to it.

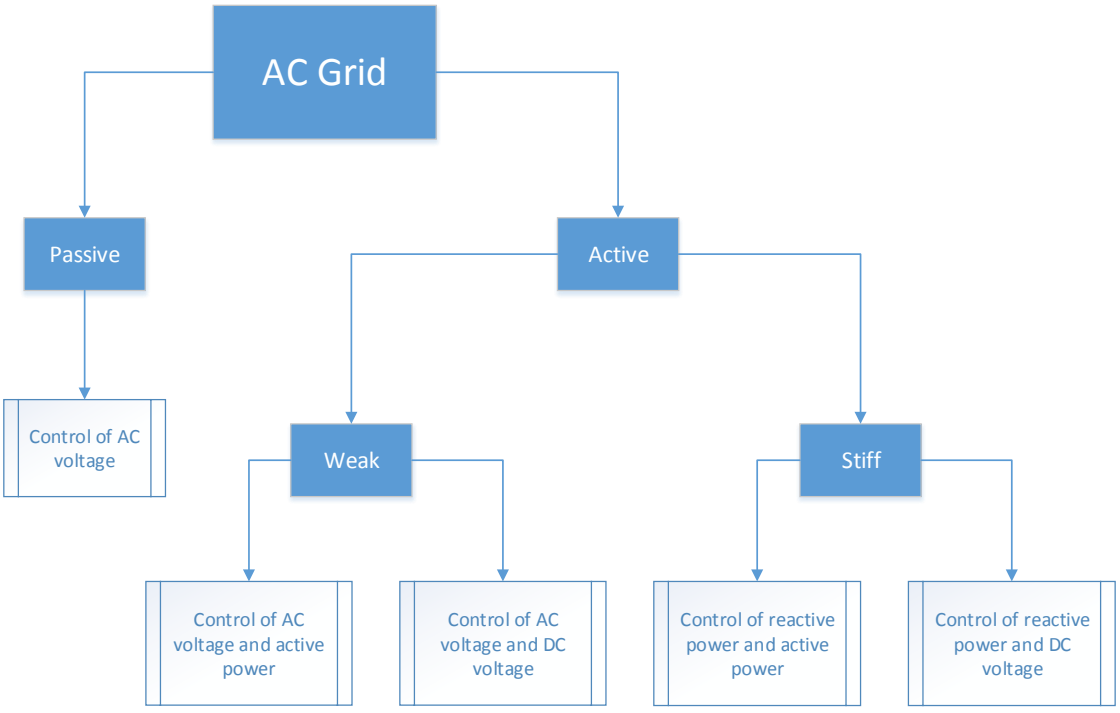

Figure 2.7: Classification of AC grids and control strategies [17].

From this it can be seen that there are five different ways of controlling the VSC depending on the characteristic of the AC grid. This thesis will only consider active AC grids.

To be able to attain a power balance in the DC link at least one converter should always regulate the DC voltage. In a point-to-point configuration it is common that one converter controls the DC voltage with the other controlling the active power injection from the AC grid.

The DC voltage controlled converter will then adjust its active power injection to ensure that there is always a balance in the power flow [5, 17].

The most common control implementation for VSC-HVDC is called *Vector Current Control*, which is discussed in detail in [18–21]. The main advantage of vector current control is the ability to achieve independent control of active and reactive power. Currents and voltages are transformed to a synchronous reference frame, called the dq reference frame, which is synchronized to the AC system. In order to do this, a PLL is used to align the d axis to the voltage of the filter-bus. Then the active and reactive power can be controlled by controlling the d and q components of the current, respectively. Depending on what quantity should be controlled, e.g. DC voltage or reactive power, an outer controller is implemented which outputs the desired current reference to the current controller.

Even though it is the most widely used implementation, vector current control has some limitations, as discussed in [21–23]. It is found that the potential of VSC-HVDC is not fully utilized in the case where it is connected to very weak AC systems. Some of the problems include low-frequency resonance and a negative impact on the performance of the VSC caused by the PLL [22]. In order to overcome these limitations, a different control strategy called *Power Synchronization Control* is suggested. The main feature is that an active power control loop is used to synchronize the VSC with the AC system, similarly to a synchronous machine. Thus, no PLL is required and the VSC can be seen as emulating a synchronous machine and there is no requirement for the short-circuit capacity of the connected AC system [23]. In [22], the control design is verified using PSCAD and it is also compared to vector current control. It was found that by using power synchronization control it was possible to operate the VSC under worse conditions than when using vector current control.

In an MTDC system, the control principles from the point-to-point configuration can be extended with one converter controlling the DC voltage and the others the active power flow. However, in [24] the authors illuminate the problems associated with having only one such DC slack converter. The slack converter must be overdimensioned to be able to manage all transients emerging from connected grids and if there is an outage of this DC slack converter, the whole system will collapse. The authors also indicate that the decision of the geographical placement of a DC slack converter will be problematic for these reasons, especially considering a potential HVDC grid crossing national borders. One way to solve these problems could be by migrating the voltage regulation objective to another converter; this is called voltage margin control. However, while using a backup DC slack converter will help in case of an outage, the need for overdimensioning of that converter will remain. Also, at the point where one converter stops to regulate the voltage and another one starts, there might be some unwanted behaviour of the controllers. To solve this issue, voltage droop control is introduced, where several converters contribute to the objective of regulating the voltage, to lessen the impact of e.g. changes in power. The voltage regulation is done via a droop characteristic at each converter which will determine how much it should participate in regulating the DC voltage.

To avoid problems associated with a single DC voltage controller in an MTDC grid, [17] have proposed a distributed voltage control. The strategy, based on mixture between voltage margin control and voltage droop control, is concluded to be the most reliable and robust way to control an MTDC system with no need of communication between the involved terminals.

2.3.3 Protection Schemes

With large and complex MTDC grids interconnecting several systems, protection must be a priority in order to ensure that the system can survive contingencies following faults. The main challenge when extinguishing faults in DC systems compared to AC systems is the lack of a zero-crossing in the current, making the development of an HVDC circuit breaker a challenge. In the literature several different strategies have been proposed for VSC-HVDC protection, e.g. in [25], [26] and [27]. Also, the new HVDC breaker proposed by ABB in November 2012 is an interesting prospect for the future of HVDC protection [28]. Unlike existing mechanical breakers, it uses power electronics and fast mechanics combined and is fast enough to secure a reliable MTDC operation, with the capability to break up to 9 kA of current. The hybrid DC breaker has been verified for voltages up to 320kV and rated currents of 2 kA in laboratory experiments but it has not yet been tested under continuous operation [29].

In [26] the authors propose the *handshaking method* for locating and isolating DC faults in MTDC systems. It is based on the assumption that DC circuit breakers are expensive, meaning that it would not be economically feasible to use them extensively. A solution where the AC circuit breakers of the converters are used together with cheap DC disconnectors to isolate the fault is suggested. Cost is one of the driving factors, and it is stated that by using the suggested method, significant savings can be achieved. The drawback is that the MTDC system will suffer from a short interruption of service. The main challenge is considered the identification of the faulted line, since it is desired that no communication is used between converters in the system.

The handshaking method can be explained using Figure 2.8 and Figure 2.9, showing a small three-terminal MTDC system.

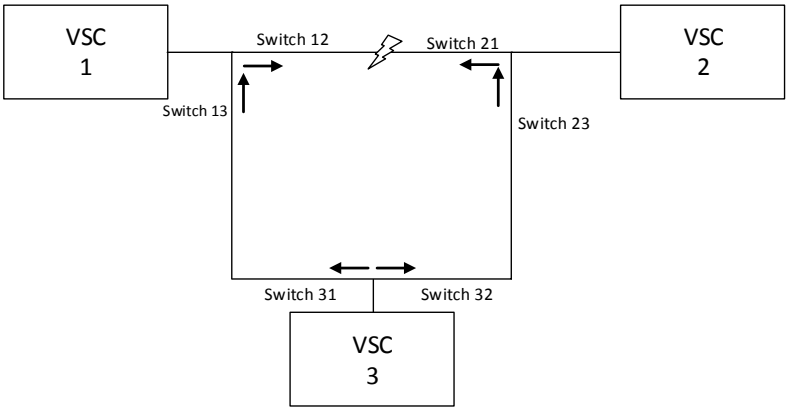

Figure 2.8: Handshaking method, part 1.

The currents at the end of the three lines are monitored at the VSC stations. Considering a positive-line-to-ground fault, the DC fault current is defined as the difference between the pre-fault and post-fault measurements, and its direction is indicated by the arrows in Figure 2.8. After the fault is extinguished using the AC circuit breakers, the protection system then selects one line as the faulted line, opening the fast DC disconnector associated with it. The

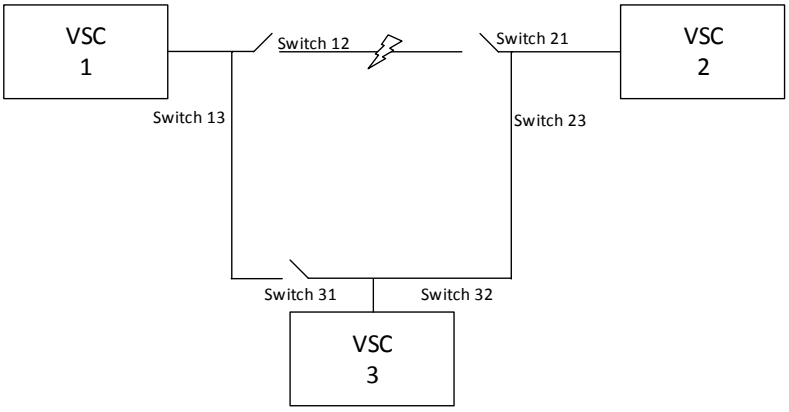

Figure 2.9: Handshaking method, part 2.

rule of selection is the *largest positive DC current*, positive meaning away from the converter. This means that VSC station 1 will identify the line between itself and VSC station 2 as the faulted line, VSC station 2 the same line as VSC station 1 and VSC station 3 either of the two lines connecting it to the other converters, depending on the amplitude of the currents. As can be seen in Figure 2.9, the faulted line is now isolated and each non-faulted line has its switch open at only one end, if at all. Then the AC circuit breakers are closed and the DC capacitors are recharged. Every non-faulted line will then be recharged to high DC voltages, and when the voltage at both sides of the open fast DC switch is the same it is allowed to close again, bringing the system back into operation with the faulted line successfully isolated.

The reviewed literature agrees on that AC side protection is a good, cheap, solution for point-to-point systems but it would cause unnecessary downtime in MTDC systems.

3

Voltage Source Converters

This chapter gives an introduction to VSCs, including advantages over Classic HVDC, modelling of VSC-HVDC and an explanation of how it operates. It also includes an overview of the vector current control method.

3.1 Introduction

The development of HVDC technology came from a desire to increase the efficiency of the transmission in a power system, as the losses of equally rated lines are lower for DC lines compared to AC lines [30]. Today, there exist two types of HVDC systems: Classic HVDC, which is line commutated, and VSC-HVDC, which is self-commutated. Classic HVDC is a Current Source Converter topology (CSC) where the direction of the current in the DC link does not change. For a VSC, the voltage polarity in the DC link stays unchanged [31]. In contrast to Classic HVDC, which was introduced in the 1950s, VSC-HVDC is a relatively new technology and the first commercial system was implemented on Gotland in 1999 [1].

Even if VSC-HVDC is less mature than Classic HVDC, the interest in VSC-HVDC is increasing as it offers several benefits including [2]:

- Flexibility and controllability of the power flow.
- Multiterminal configurations.
- Fast response in case of disturbances.

3.2 VSC vs Classic HVDC

From a power system point of view a VSC can be seen as a voltage source which operates with the same frequency as the AC system to which it is connected, controlling active and reactive power independently of each other [30]. Classical HVDC consumes reactive power and needs

a present AC voltage source for commutations, which is not the case for VSC-HVDC. This makes VSC-HVDC suitable for restoration scenarios and it is claimed to possess a "black start capability" [30]. If a power reversal is desired, the VSC changes the direction of the current, in contrast to Classic HVDC which changes the polarity of the DC voltage [31]. This makes Classic HVDC unsuitable for MTDC configurations as changing the polarity of the voltage at one converter would invert the polarity of all converters connected to the same DC grid, which may not lead to the desired power flow [31]. VSC does not have this problem as the power flow can be reversed at a single VSC without inverting the DC voltage polarity of the whole system. Also, reversal of the power flow for Classic HVDC involves time consuming mechanical maneuvers but with VSC it can be achieved almost instantaneously. Furthermore, Classic HVDC needs to be connected to a strong AC grid as fluctuations in voltage or frequency may result in errors in the commutation which can interrupt the power flow. With VSC, the power flow will only be reduced in case of a voltage drop, depending on how large the reduction of the AC voltage is [31]. The main disadvantage for VSC-HVDC is the switching losses, which are higher compared to Classic HVDC. Since the introduction of VSC in the 1990s the conversion losses have been reduced from around 3% to 1%, for Classic HVDC the conversion losses is around 0.5% [32]. For point to point links, where large amounts of power need to be transferred, Classic HVDC is still preferable. There are projects commissioned with a DC voltage of ±800kV and rated power of 7200 MW [33]. For VSC-HVDC, projects commissioned have voltage ratings up to ±350kV and rated power up to approximately 900 MW [3].

In table 3.1 below a summary is shown.

Table 3.1: Comparison of Classic HVDC and VSC-HVDC

Classic HVDC	**VSC-HVDC**
Line-commutated	Self-commutated
Controls active power only	Control active and reactive power independently
Controls the power direction by the polarity of the voltage	Controls the power direction by the polarity of the current
Limited power reversal capability	Power reversal almost instantaneous
Requires a strong AC grid	Can supply a weak AC grid
Not feasible for MTDC configurations	Feasible for MTDC configurations
Needs reactive power support	Can inject or withdraw reactive power depending on what is needed
Needs a present AC voltage	Black start capability
Conversion losses around 0.5 %	Conversion losses around 1 %

3.3 VSC-HVDC Components

In order to understand the operating principle of VSC-HVDC it is important to understand the components that such a system consist of. Figure 3.1 show a typical VSC-HVDC system with converters, phase reactors, transformers, DC capacitors, AC filters and DC cables. These components will be described in more detail in the subsequent sections.

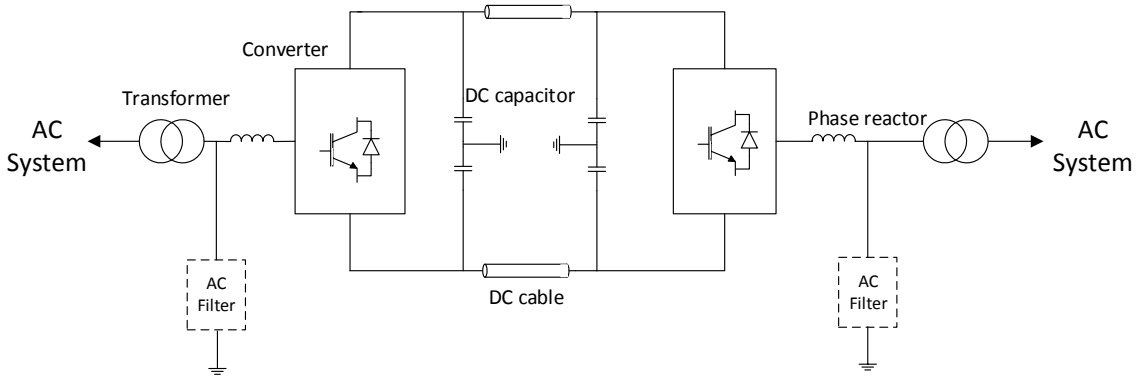

Figure 3.1: A typical VSC-HVDC system and its components.

Converter
The converter is the most important component of the VSC-HVDC system and it is used to transfer power from the AC side to the DC side when operating as a rectifier, or to inject power into the AC side operating as an inverter. It uses Pulse Width Modulation (PWM) to generate the desired voltage waveform. In this thesis, Sinusoidal Pulse Width Modulation (SPWM) is considered where the basic principle is to compare a sinusoidal control voltage to a triangular wave, also called a carrier wave. If the control signal is larger than the carrier wave, it will switch on the corresponding valve in the converter and if the control signal is smaller it will be switched off instead [34]. This is shown in Figure 3.2, which show the control voltage, carrier wave and the actual voltage.

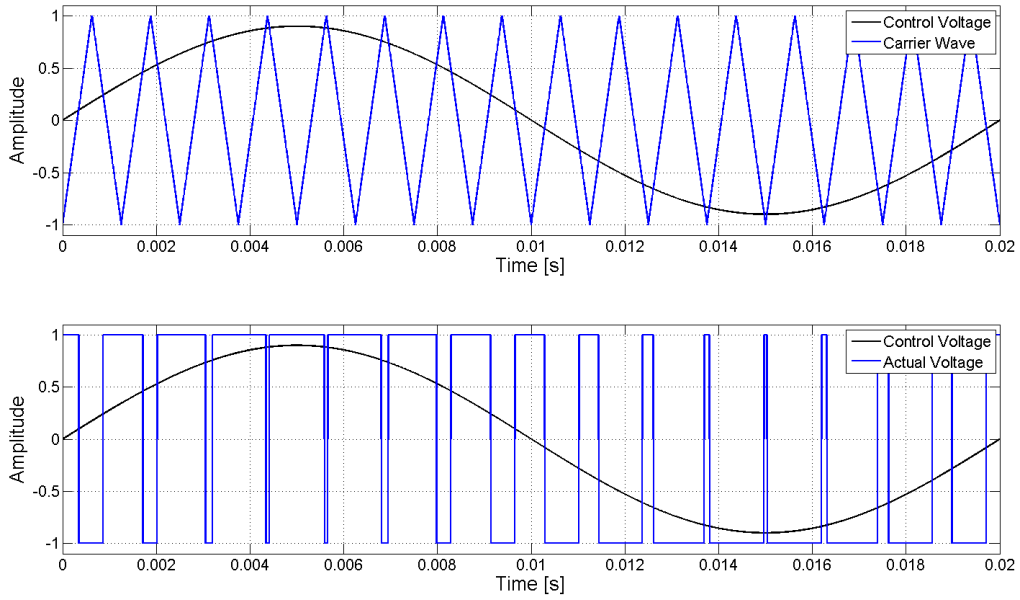

Figure 3.2: Pulse width modulation

The modulation index, M, is defined as:

$$M = \frac{v_{ctrl}}{v_{tri}} \tag{3.1}$$

where v_{ctrl} is the amplitude of the control voltage and v_{tri} the amplitude of the triangle wave.

The converter valves are usually Insulated-Gate Bipolar Transistor (IGBT) semiconductors and can be arranged in several different configurations. The simplest configuration is the two-level configuration, consisting of six valves. It is shown in Figure 3.3.

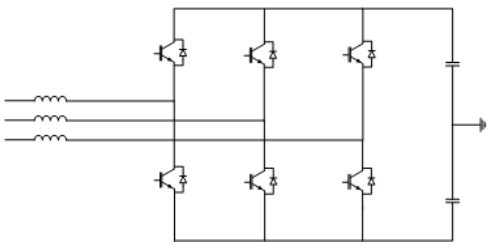

Figure 3.3: Two-level bridge configuration

The two-level configuration can produce two output voltages, $+u_{DC}$ and $-u_{DC}$, at each phase [35]. The main advantages of the two-level configuration are its simplicity and the reduced size of DC capacitors. The main drawback of the two-level converter is that the obtained AC waveform has a high harmonic content. While the switching frequency can be increased to make the

harmonics appear at higher frequencies, to make them easier to filter, this will cause an increase in switching losses [36].

In Figure 3.4, a three-level (12-pulse) bridge is shown.

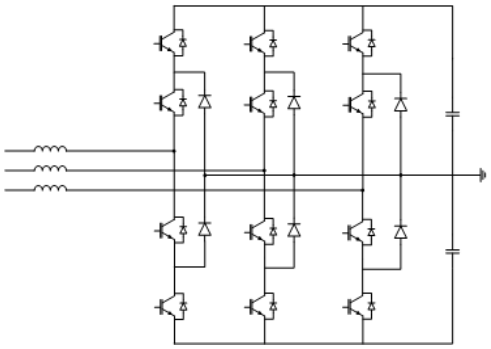

Figure 3.4: Three-level bridge configuration.

In this configuration, the AC voltage waveform is generated by going through multiple intermediate voltage levels. This will result in several advantages over the two-level bridge, including lower losses, higher power density and a waveform with lower harmonic content [36].

Transformer

The transformer connects the AC grid with the converter and the main objective for the transformer is to transform the voltage level to a suitable level for the converter [17]. Besides transforming the voltage to a suitable level, the transformer can help with the regulation of the voltage with its tap-changer.

Phase reactor

The phase reactor has several uses: to regulate the active and reactive power flow and it also functions as an AC filter to reduce high frequency harmonics caused by the switching in the converter [9]. It will also limit the short circuit current in the case of a fault [37].

DC Lines

DC lines used can be either overhead lines or cables. Several factors impact the choice between them, including the environmental impact and reliability of the system. Generally, cables are used to reduce the risk of faults and to mitigate the environmental impact [38].

DC Capacitor

The DC capacitor is necessary to maintain a steady DC voltage during the switching of the valves. In order to control the average DC voltage the capacitor can be charged or discharged by exchanging active power between the AC and DC sides [39]. The choice of the capacitor size is a trade-off between how much ripple is acceptable and the dynamic performance. A large capacitor will smooth out the ripple at the cost of increased response time during changes in voltage. A small capacitor will instead result in greater ripple but with reduced response time [20].

AC Filters
AC filters are used to filter out unwanted harmonics. They form part of the low-pass filter together with the phase reactor. The goal of the AC filters is to make sure that as little harmonics as possible enter the AC system [19].

3.4 VSC-HVDC Modelling and Design

In order to use VSC-HVDC in simulations, equations are needed to represent its behaviour. This section will give a brief overview of how the VSC-HVDC system is designed and modelled for use in simulations.

Converter
When modelling VSC-HVDC, in the AC side the converter can be considered as an equivalent AC voltage source with independent control of amplitude, phase and frequency [20]. The instantaneous phase voltage v_c of the VSC bridge can be described as

$$\hat{v_c} = \frac{1}{2} u_{DC} M sin(\omega_e t + \delta) + \text{harmonics} \tag{3.2}$$

Where M is the modulation index, ω_e the fundamental frequency and δ the phase shift of the voltage.

Transformer
To represent the transformer, a π-equivalent model can be used together with an ideal transformer [7]. In this thesis, however, it is represented only by its leakage reactance to reduce the complexity of the model. The reasoning behind this representation is that even if the tap changers can help in regulating the voltage, they are not expected to operate within the time frame of interest in this thesis [20]. The value of the reactance is usually between 0.1 to 0.2 p.u. and a value of 0.10 p.u. was chosen, in series with a small resistance of 0.01 p.u. representing the losses [40, 41].

Phase Reactor
The phase reactor is represented by an inductance in series with a small resistance. The parameters were chosen according to [42], with a reactance of 0.15 p.u. and a resistance of 0.015 p.u.

DC Lines
DC lines can be modelled using e.g. a π-model or a distributed model. The required detail of the model depend on what type of study is of interest, and the length of the cable that is modelled [9].

DC Capacitor
In steady state, if the converter losses are neglected, the DC side power equals the AC side power. If the power balance is broken the difference is stored in or extracted from the DC

capacitor. This will lead to fluctuations in the DC voltage [20]. The current flow in the DC link is given by

$$i_C = C_{DC}\frac{du_{DC}}{dt} \tag{3.3}$$

As mentioned in Section 3.3, the choice of capacitor size depends on whether the ripple should be small or if the dynamic response should be fast. Even if it is assumed that there will be no harmonics from the PWM, and therefore no ripple, in reality there will be. Therefore it was decided that it should be designed with ripple in mind in order to get as realistic results as possible, rather than overdimensioning it.

The size of the DC capacitor is characterized by the time constant τ_C, defined as the time needed to charge the capacitor to u_{DC} when supplied with a constant power P_N.

$$\tau_C = \frac{0.5C_{DC}u_{DC,N}^2}{P_N} \tag{3.4}$$

In this thesis, a time constant of 5 ms was chosen. It will give a sufficiently small ripple and a small transient on the DC voltage [19].

3.5 Control of VSC-HVDC

In this thesis, the control system for the VSC-HVDC system was implemented based on vector current control since it is the one which is the most well-documented and widely used today [22]. It was also the implementation used in [42], which this project used as a starting point.

3.5.1 Vector Control Method

As stated in Chapter 2, the main benefit of using vector current control for grid-connected VSCs is to control the active and reactive power independently through an inner current control loop. It uses the *dq* synchronous reference frame to represent three-phase quantities as constant vectors in steady state [20], using PI-regulators to remove static errors in voltages and currents.

The vector current control method can be formulated using the single line diagram representation of a VSC connected to a grid shown in Figure 3.5.

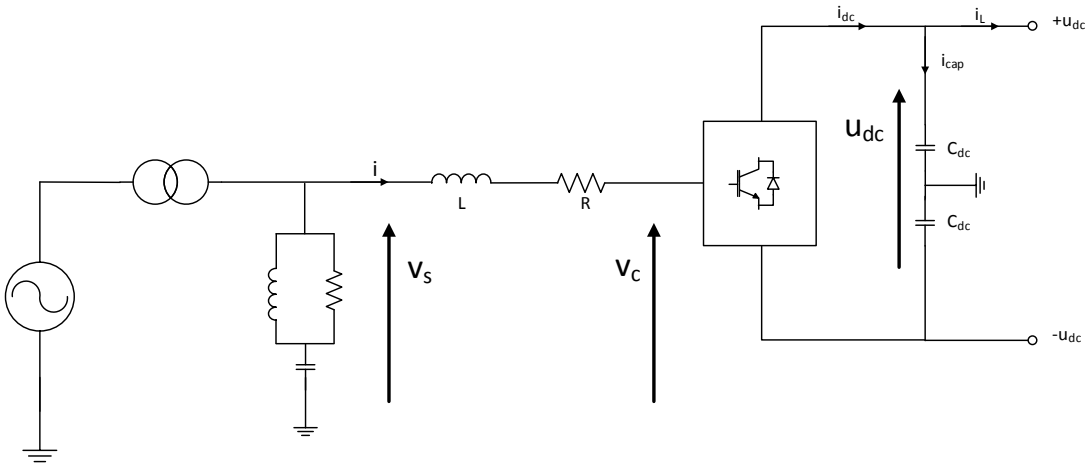

Figure 3.5: Single-line representation of a VSC-HVDC system.

If all voltages and currents on the AC side are in the $\alpha\beta$ stationary coordinate system, the AC dynamics of the system are given by the dynamics of the phase reactor according to:

$$L\frac{d\boldsymbol{i}_{\alpha\beta}}{dt} = \boldsymbol{v}_{s,\alpha\beta} - \boldsymbol{v}_{c,\alpha\beta} - R\boldsymbol{i}_{\alpha\beta}. \tag{3.5}$$

By transforming these into the rotating dq reference frame:

$$L\frac{d\boldsymbol{i}_{dq}}{dt} = \boldsymbol{v}_{s,dq} - \boldsymbol{v}_{c,dq} - (R + j\omega L)\boldsymbol{i}_{dq} \tag{3.6}$$

where the term $j\omega L$ represent the time derivative of the rotating of the reference frame. If Eq. 3.6 is split into its real and imaginary parts:

$$L\frac{di_d}{dt} = v_{s,d} - v_{c,d} - i_d R + i_q \omega L \tag{3.7}$$

$$L\frac{di_q}{dt} = v_{s,q} - v_{c,q} - i_q R - i_d \omega L. \tag{3.8}$$

The dq reference frame can then be aligned so that:

$$v_{s,d} = v \text{ and } v_{s,q} = 0 \tag{3.9}$$

which will give the power from the AC system as:

$$P = v_{s,d} i_d \tag{3.10}$$

$$Q = -v_{s,d} i_q. \tag{3.11}$$

For the DC side, the power is given as::

$$P_{DC} = u_{DC} i_{DC} \tag{3.12}$$

and the DC side dynamics is given by Eq. 3.3, where:

$$i_C = i_{DC} - i_L. \tag{3.13}$$

Figure 3.6 shows a typical control system for a VSC using vector current control, including the PLL, inner current controller and outer controllers. This will be described further in the coming sections.

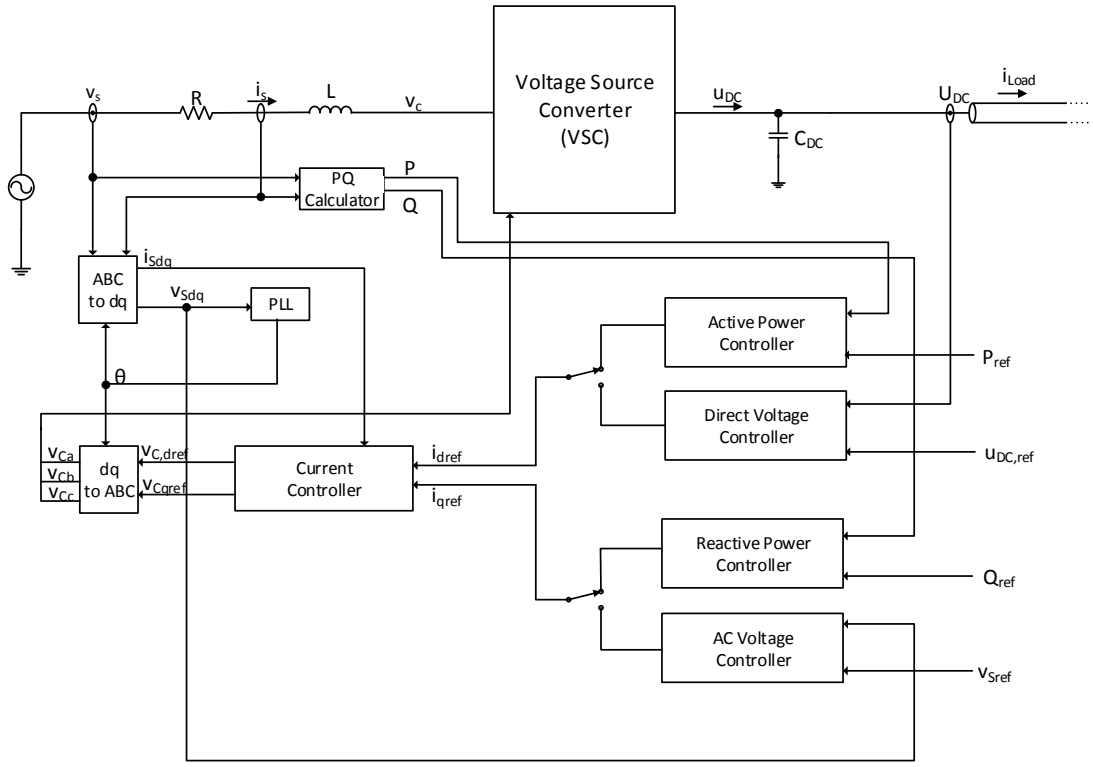

Figure 3.6: VSC-HVDC control system overview with vector current control.

PLL

In order to represent the currents as DC quantities to be controlled by a PI regulator it is necessary to align the *dq* reference frame with the rotating voltage vector. The PLL is used

to determine the phase angle of the voltage and to lock the dq axes to this angle [43]. In this thesis the voltage vector is aligned to the d axis. This means that if the dq axes are aligned correctly, v_q will be zero. Therefore, v_q can be considered an error and used as an input to a PI regulator. Figure 3.7 shows the structure of a PLL including a feed-forward of the nominal frequency which is used to reduce the time it takes for the PLL to lock on to the voltage.

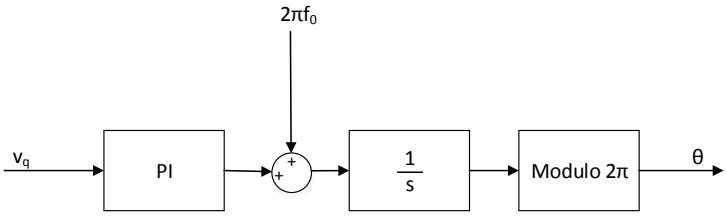

Figure 3.7: Block representation of PLL.

3.5.2 Current Controller

Based on the equations derived in the previous sections the inner current controller can be implemented in the dq-frame. The basic block diagram of the current controller is shown in Figure 3.8.

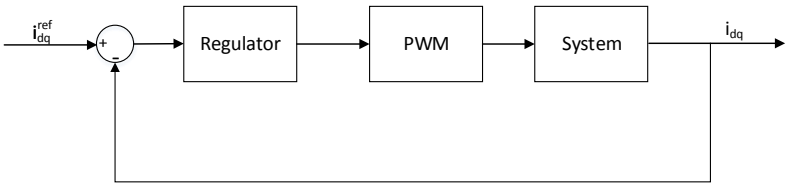

Figure 3.8: Simple block representation of current controller.

A further description of each block follows below.

Regulator
The regulator used is a standard PI regulator:

$$F(s) = K_p + \frac{K_i}{s} = K_p \frac{(1/K_p + sT_i))}{sT_i} \tag{3.14}$$

where K_p, K_i and T_i are the parameters to be determined.

PWM
The input of the PWM converter is the voltage reference generated by the current control loop, transformed from dq to $\alpha\beta$. It can be assumed that the converter voltage will follow the

reference without any delay and that the harmonics caused by the switching will be removed by the phase reactors and AC filters [20]. Thus, the operation of the PWM can be expressed in the dq reference frame as:

$$v_{c,dq} = v_{c,dq}^{ref}. \tag{3.15}$$

System
Eq. 3.7 and 3.8 describe the system behaviour, and can be rewritten as:

$$v_{s,d} - v_{c,d} = L\frac{di_d}{dt} + i_d R - i_q \omega L \tag{3.16}$$

$$v_{s,q} - v_{c,q} = L\frac{di_q}{dt} + i_q R + i_d \omega L. \tag{3.17}$$

From these equations it can be seen that the model of the VSC in the dq reference frame is a nonlinear Multiple-Input Multiple-Output (MIMO) system, and due to the speed/frequency induced term present in each equation there will be a cross-coupling between the two axes [18]. This cross-coupling term can be considered a disturbance from a control point of view. In order to achieve a good performance, a dual-close-loop current controller is required, with cross-coupling and voltage feed-forward compensations [18, 20]. With separate inner loop controllers for i_d and i_q, the output of the current controller will be the voltage references for each axis respectively, $v_{c,d}^{ref}$ and $v_{c,q}^{ref}$. Taking into consideration the cross-coupling compensation and voltage feed-forward the output of the regulator block will be:

$$v_{c,d}^{ref} = -(i_{d,ref} - i_d)F(s) + i_q \omega L + v_s,d \tag{3.18}$$

$$v_{c,q}^{ref} = -(i_{q,ref} - i_q)F(s) - i_d \omega L + v_{s,q}. \tag{3.19}$$

If these are combined with Eq. 3.16 and 3.17 it will result in:

$$(i_{d,ref} - i_d)F(s)G(s) = i_d \tag{3.20}$$

$$(i_{q,ref} - i_q)F(s)G(s) = i_q \tag{3.21}$$

where $G(s)$ is defined as

$$G(s) = \frac{1}{sL + R}. \tag{3.22}$$

Thus the cross-coupling terms are eliminated and independent control of the d and q axes will be achieved. The complete current controller block diagram is shown in Figure 3.9 below.

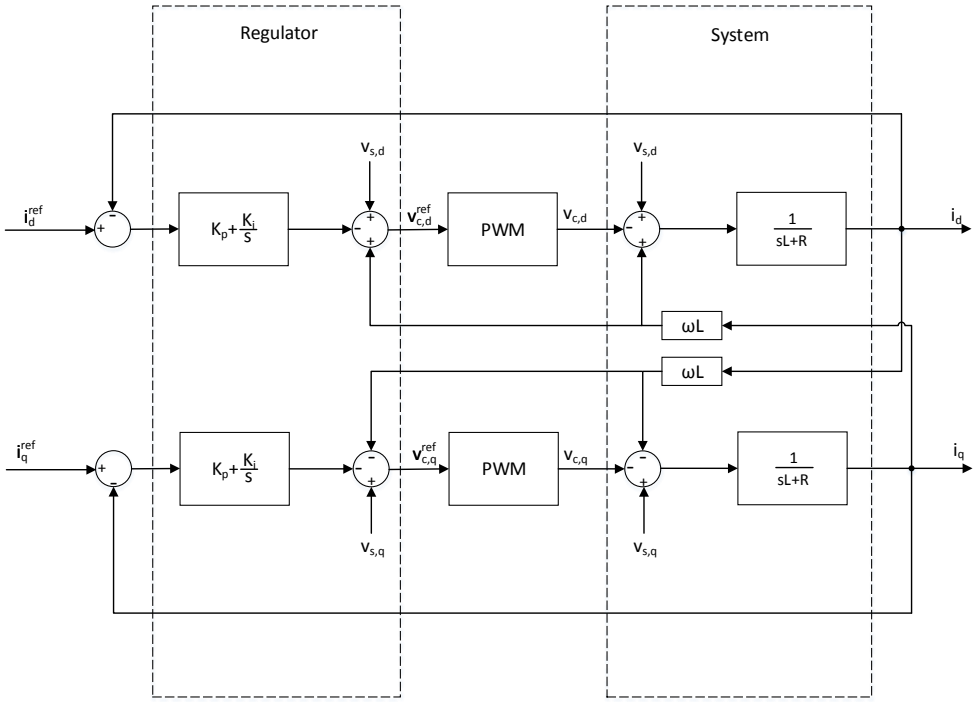

Figure 3.9: Detailed current controller

3.5.3 Outer Controllers

As is shown in Figure 3.6, the outer controllers consist of an active power controller, DC voltage controller, reactive power controller and an AC voltage controller. Figure 3.10 use a DC voltage controller to illustrate the cascaded structure of the control system.

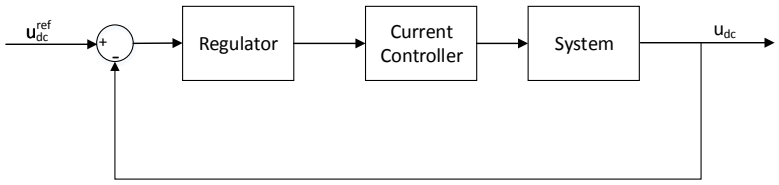

Figure 3.10: Block representation of an outer controller.

A criterion when designing the outer controllers is that the outer control loop must be slower than the inner control loop to ensure stability [44]. The inner current control loop can then be considered instantaneous, so the current controller can be represented simply as:

$$\boldsymbol{i}_{dq} = \boldsymbol{i}_{dq}^{ref}. \tag{3.23}$$

DC Voltage Controller

Control of the DC voltage is important since it ensures power balance between converters. According to [19] the DC voltage can be controlled using a PI regulator. Adding a feed forward of the current, the equation is:

$$(u_{DC}^{ref} - u_{DC})(K_p + \frac{K_i}{s}) + \frac{u_{DC} i_L}{v_{s,d}} = i_d^{ref}. \tag{3.24}$$

In order to relate the d axis current to the DC side current, as the power is assumed to be the same on the DC and AC side of the converter Eq. 3.10 and 3.12 can be equalized, which gives:

$$u_{DC} i_{DC} = v_{s,d} i_d \tag{3.25}$$

which can be rewritten as:

$$i_{DC} = \frac{v_{s,d} i_d}{u_{DC}}. \tag{3.26}$$

Also, taking into account the DC side dynamics, Eq. 3.3 and 3.13 can be combined, which result in:

$$C \frac{du_{DC}}{dt} = i_{DC} - i_L. \tag{3.27}$$

Laplace-transforming this and rewriting it gives:

$$u_{DC} = \frac{i_{DC} - i_L}{sC} \tag{3.28}$$

which together with Eq. 3.24 and 3.26 complete the equations needed to describe the DC voltage controller.

Figure 3.11 shows the block diagram of the DC voltage controller including the feed forward of the current.

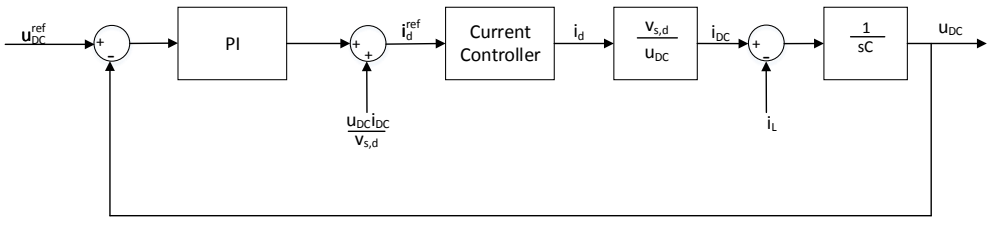

Figure 3.11: Block representation of a DC voltage controller.

Active and Reactive Power Controllers

The active and reactive powers can be controlled in a simple way by the use of an open loop controller, with the current references being generated as:

$$i_d^{ref} = \frac{P^{ref}}{v_{s,d}} \text{ and } i_q^{ref} = -\frac{Q^{ref}}{v_{s,d}}. \tag{3.29}$$

The accuracy can be improved using a feedback loop with PI regulators, as is shown in Figure 3.12.

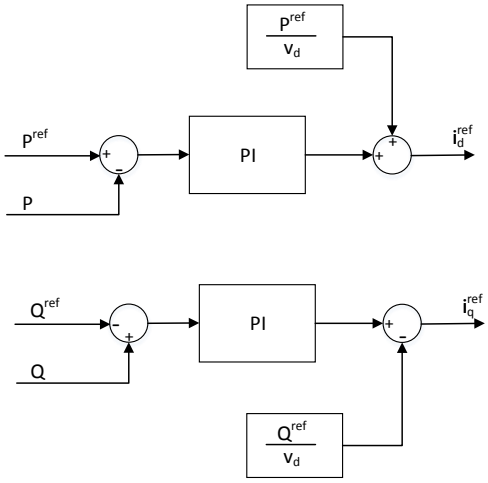

Figure 3.12: Block representation of active and reactive power control.

In this thesis, however, the power controller was implemented as an open loop controller as the accuracy of this particular controller was not considered important.

AC Voltage Controller

The AC voltage controller was implemented as a simple droop controller. The basic principle of a droop control is shown in Figure 3.13.

If the AC voltage magnitude differ from the desired level, reactive power should either be produced or consumed by the converter in order to increase or decrease the voltage, thus improving the voltage profile.

This is implemented according to Figure 3.14, where R_{AC} is the droop gain which represent the slope in Figure 3.13.

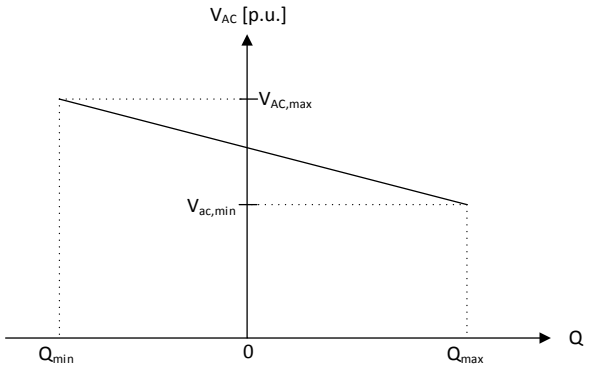

Figure 3.13: AC voltage droop graph.

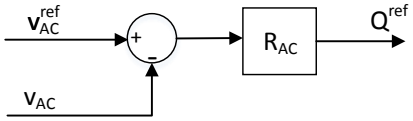

Figure 3.14: Block representation of the AC voltage droop controller.

3.5.4 Tuning

The current controller was tuned using Internal Model Control (IMC) based on the methods used in [18, 20, 40]. This resulted in the following choice of parameters:

$$K_p = \alpha L \ , \ K_i = \alpha R \text{ and } T_i = L/R \tag{3.30}$$

where α is the closed loop bandwidth, which was selected as 10 times slower than the switching frequency of the converter, as suggested in [42].

Tuning of the DC voltage controller is outlined in [5, 21]. In this thesis it was done according to [5] which led to the following parameters:

$$K_{p,DC} = \alpha_{DC} \xi C \text{ and } K_{i,DC} = \frac{\alpha_{DC}^2 C}{2} \tag{3.31}$$

with α_{DC} selected as 10 % of the closed loop bandwidth of the current controller and ξ selected as 3, as suggested in [5].

The tuning of the PLL is based on [45, 46] where it is suggested to select the PLL parameters according to:

$$K_{p,PLL} = 2\alpha_{PLL} \text{ and } K_{i,PLL} = \alpha_{PLL}^2 \tag{3.32}$$

with α_{PLL} being the PLL bandwidth, which is typically in the range of 3-5 Hz [46]. In this thesis it was selected to 5 Hz.

3.5.5 Current Limiter

Compared to electromechanical devices, such as motors and generators, VSC-HVDC do not have any inherent overload capability. In some situations the outer controllers might set the current reference higher than the current capability, which may damage the valves. In order to avoid exceeding the current limitation due to control actions, the control system must have a current limiter implemented [19, 20].

The current limiter is implemented by comparing the current limit, i_{max}, with the current magnitude calculated as $\sqrt{i_d^2 + i_q^2}$. If the limit is exceeded, the reference currents will be limited according to the chosen limiting strategy. Three different limiting strategies are discussed in [41] and [20]. They are visualized in 3.15.

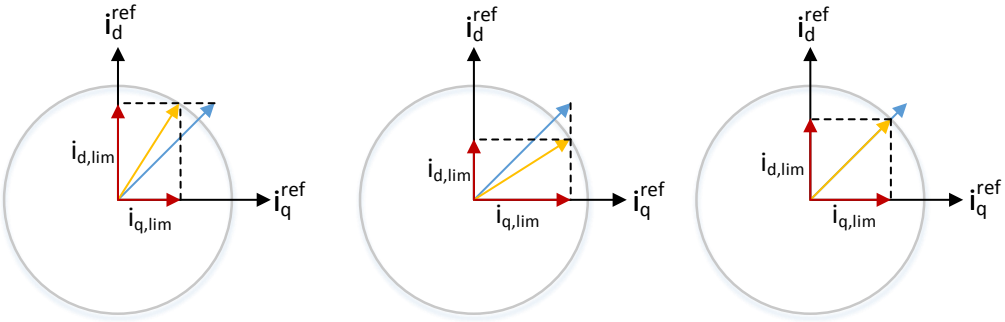

Figure 3.15: Different current limitation strategies.

One strategy is to prioritize the current reference controlling the active power. This strategy is suitable for cases when the converter should transfer as much power as possible, e.g. when connected to a strong grid. In cases when the converter is instead connected to a weak grid it could be a good idea to prioritize the current reference controlling the reactive power. A third strategy suggested is to keep the angle but limit the current magnitude.

The current limitation implemented in this thesis prioritizes the current reference controlling the active power.

4

Modelling and Implementation for Slow Dynamic Simulations

This chapter give an introduction to the computer software used in this thesis, PowerFactory. Then a description of the implementation approach is presented as well as an overview on how the models of VSC-HVDC defined in PowerFactory differ from those defined in Chapter 3. Later sections will explain the implementation of the system in PowerFactory and compare the models to a more detailed model in PSCAD.

4.1 Introduction

In this thesis, the modelling and analysis was carried out in PowerFactory (version 14.0.525.4), which is developed by DIgSILENT GmbH. PowerFactory can be used for steady state studies, such as load flow and short-circuit calculations, as well as dynamic studies, such as transient stability and electromagnetic transient analysis. Models with different levels of detail are provided depending on the purpose of the study. It is also possible to implement user-developed models that can be interfaced with the built-in network models in order to design e.g. control systems.

4.2 Implementation Approach

In order to develop a simplified model it was decided to use the RMS simulation mode in PowerFactory, and to investigate to what extent the built-in models could be used. The developed RMS model was then compared with an EMT model implemented in PSCAD, and another EMT model implemented in PowerFactory. The goal was that the final RMS model should have a response as similar as possible to the EMT models.

When comparing the models, some criteria had to be determined for whether or not results could be deemed acceptable. Considering the focus on transient stability of this thesis, the

following considerations were made:

- Differences between the models in DC side transients might be negligible as they are fast compared to machine dynamics.
- Differences in reactive power during fast transients should have a small impact on machine dynamics.
- Active power in the AC side is considered the most important quantity as that is what will have the most influence on the machine dynamics.

4.3 RMS and EMT Simulations

For dynamic studies, PowerFactory has two simulation options that can be used: RMS, based on simplified electrical transient models, and EMT, based on detailed electromagnetic transient models.

In RMS simulations, electromagnetic dynamics of the electric network is neglected and voltages and currents are defined as phasors, represented by the magnitude and the phase angle of the steady-state sinusoidal waveforms. In this way, currents and voltages in the network are found from algebraic equations rather than differential equations, i.e. in RMS simulations [47]:

$$\underline{u} = j\omega L\underline{i} \text{ and } \underline{i} = j\omega C\underline{u}. \tag{4.1}$$

The only differential equations that are considered are for the dynamic behaviour of controllers and mechanical transients, e.g. the swing equation:

$$\omega J\frac{d\omega}{dt} = P_{mech} - P_{el}. \tag{4.2}$$

In PowerFactory, RMS simulations can be performed in two different ways, using either a symmetrical steady-state network model suitable for balanced network conditions, where the network is simplified to only one phase, or a three-phase model suitable for unbalanced conditions e.g. studies involving asymmetrical faults.

In EMT simulations, voltages and currents are represented by their instantaneous values and the dynamic behaviour of network elements is also accounted for. In contrast to Eq. 4.1 above, the voltage and current in an EMT simulation would be expressed as [47]:

$$u = L\frac{di}{dt} \text{ and } i = C\frac{du}{dt}. \tag{4.3}$$

Models used in EMT simulations are more detailed and are suitable for simulations of fast transients under either balanced or unbalanced conditions. For transient stability studies as well as evaluation of control systems, the RMS simulation modes are preferable as the simplified network models allow for shorter computational times.

4.4 PowerFactory Models

PowerFactory comes with a library of pre-defined components including models for e.g. synchronous machines, cables and converters. There is also the possibility to use custom-made models or macros together with the pre-defined models via the use of so called composite frames. Models written in the Dynamic Simulation Language (DSL), which can be represented either mathematically or graphically, can be connected to the grid elements via input/output relations [48]. The following sections will describe built-in models that were relevant in this thesis.

4.4.1 PWM Converter Model

The PWM converter model in PowerFactory is based on a fundamental frequency approach where at fundamental frequency, the ideal converter can be modelled as a DC voltage controlled AC voltage source [49]. It can be described by the following equations (for values of $|P_m| < 1$, P_m being the modulation index):

$$v_{AC,r} = K_0 P m_r u_{DC} \tag{4.4}$$

$$v_{AC,i} = K_0 P m_i u_{DC} \tag{4.5}$$

and the active power conservation between AC and DC-sides:

$$P_{AC} = Re(\underline{v_{AC}} \underline{i^*_{AC}}) = u_{DC} i_{DC} = P_{DC} \tag{4.6}$$

where K_0 will depend on the modulation mode used for the PWM. In case of SPWM, as is used in this thesis, K_0 will be:

$$K_0 = \frac{\sqrt{3}}{2\sqrt{2}}. \tag{4.7}$$

No-load losses and load losses are included in the model, represented by a resistance between the DC terminals and a series resistance respectively. Also included in the model is a series reactance to simplify the modelling of the converter. The DC link capacitor, however, is not included in the model so it has to be added externally. Figure 4.1 shows the complete model without the DC link capacitor.

Depending on the type of study, the PWM converter model can be controlled as indicated in the following sections.

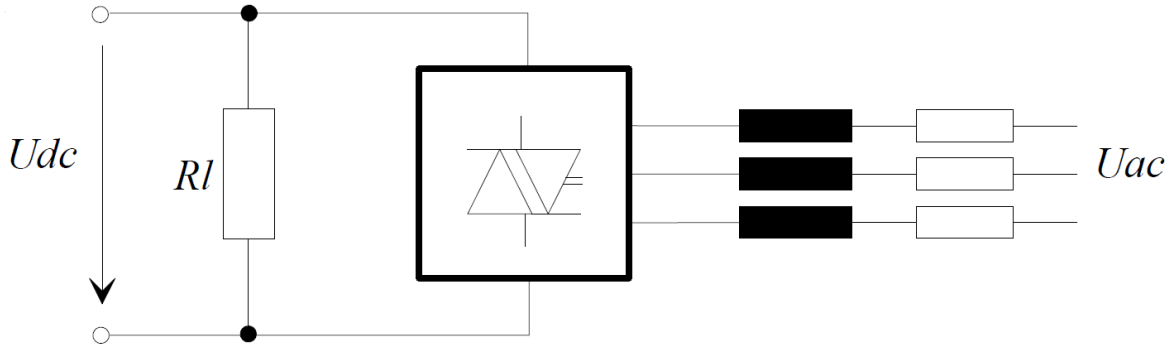

Figure 4.1: PowerFactory PWM converter model [49].

Power-flow
For a power-flow analysis, several control objectives can be specified:

- **Vac-phi** - The magnitude and phase of the AC terminal are specified. This control mode is typically used with motor-side converters in variable speed drive applications.
- **Vdc-phi** - The DC voltage and AC voltage phase are specified. No typical applications.
- **PWM-phi** - Directly sets the PWM factor in magnitude and phase.
- **Vdc-Q** - The DC voltage and reactive power flow are specified. Typical applications include Static Sycnronous Compensators (STATCOM) and VSC-HVDC.
- **Vac-P** - The AC voltage magnitude and active power flow are specified. Typical applications include VSC-HVDC and grid-side converters of converter driven synchronous machines.
- **P-Q** - The active and reactive power flows are specified. Typical applications are the same as for Vac-P.
- **Vdc-Vac** - The DC and AC voltages are specified. Typical applications are similar to those of Vdc-Q.

In cases where the voltage or power flow is specified the controlled cubicle or bus-bar needs to be specified.

Stability model
For stability simulations, the same fundamental frequency model as described above is used and the converter is controlled by the PWM indices. Depending on the application, the PWM indices of the converter can be determined in a number of different ways:

- **Pmr, Pmi** - In this setting, the inputs to the converter are the real and imaginary parts of the PWM index. This set of inputs requires the use of phase measurement devices as they are in the global reference frame.
- **Pmd, Pmq, cosref, sinref** - When using this set of input variables, the PWM index can be specified in a reference frame determined by cosref and sinref. This is convenient when the control system is implemented in the dq frame and is combined with a PLL, as is the case in this thesis.
- $\boldsymbol{id^{ref}}$**,** $\boldsymbol{iq^{ref}}$**, cosref, sinref** - This set of inputs uses the converters built-in current controller, described in more detail below, which is defined in a reference frame determined by cosref and sinref.
- $\boldsymbol{Pm_{in}}$**, dphiu** - This set of input variables is essentially the same as using Pmr and Pmi.
- $\boldsymbol{Pm_{in}}$**, f0** - In this case, the magnitude of the PWM index can be set whereas the frequency f0 allows for the frequency of the output voltage to be varied.

Current Controller

The built-in current controller of the PWM model is shown in Figure 4.2. It uses the i_d and i_q reference currents as inputs to calculate the voltage references. These are then transformed back to the global reference frame inside the converter model.

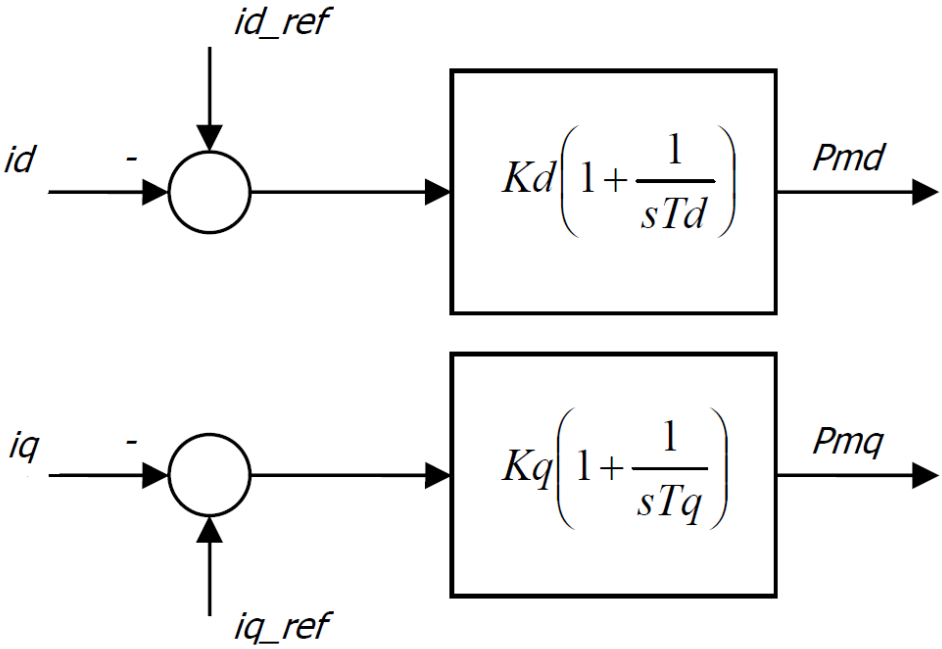

Figure 4.2: PowerFactory built-in current controller [49].

4.4.2 DC Cable

For the modelling of the DC cable it was decided that a π-model would be sufficient as the cable length used was 100 km [9]. There is a built-in cable model in PowerFactory which was used.

The cable parameters are based on the values given in [42] and are shown in Table 4.1. The rating of the cable is 600 MW and $\pm$ 300 kV.

Table 4.1: Cable parameters

Resistance (Ω/km)	**Inductance** (mH/km)	**Capacitance** $(\mu F/km)$
0.0376	0.189	0.207

4.4.3 PLL

The use of PLL models will differ greatly between RMS and EMT simulations. In EMT simulations it will be used to lock on to a rotating quantity. In RMS, however, the voltages will not rotate as they are represented by phasors, so the PLL will be used simply to correct the angle of the steady-state phasor. PowerFactory has a built in PLL model for both RMS and EMT simulations. Figure 4.3 show how it is implemented as described in the PowerFactory technical reference documentation.

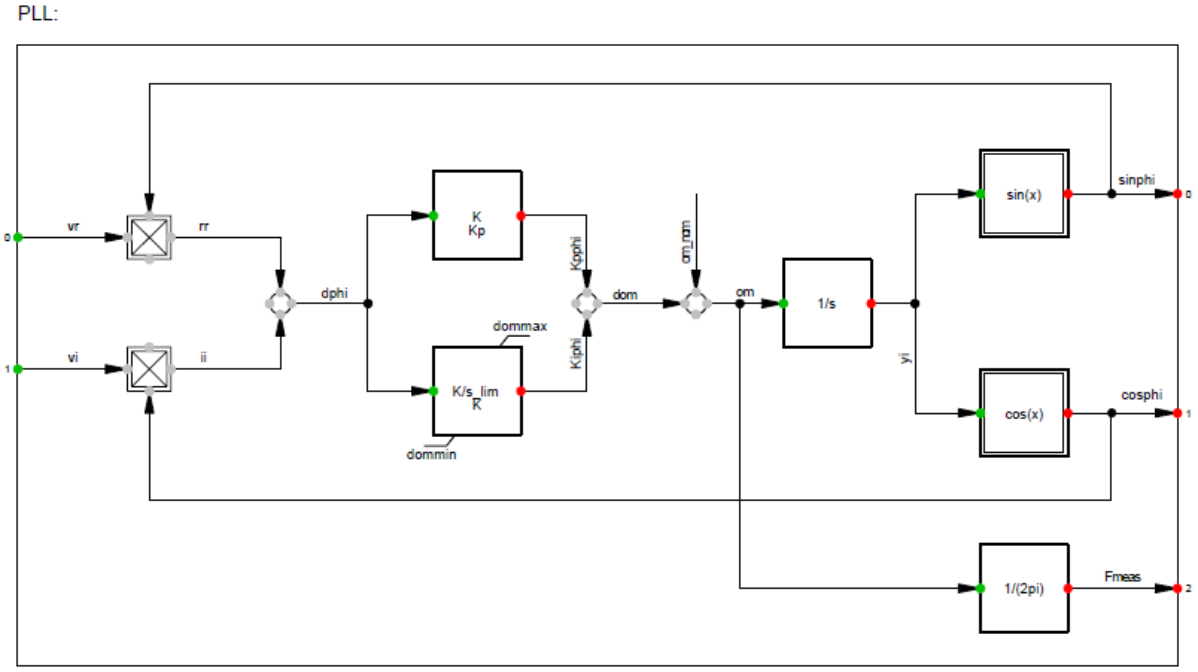

Figure 4.3: PowerFactory built-in PLL [50]

4.5 Implementation

The following sections provide an overview of the system used in the implementation, as well as a description of how each part of the system was implemented.

4.5.1 Point-to-point System Overview

The system was implemented using pre-defined models in PowerFactory to represent DC cables, AC sources, DC link capacitors and the converters. Figure 4.4 shows the system used in this thesis for verification purposes.

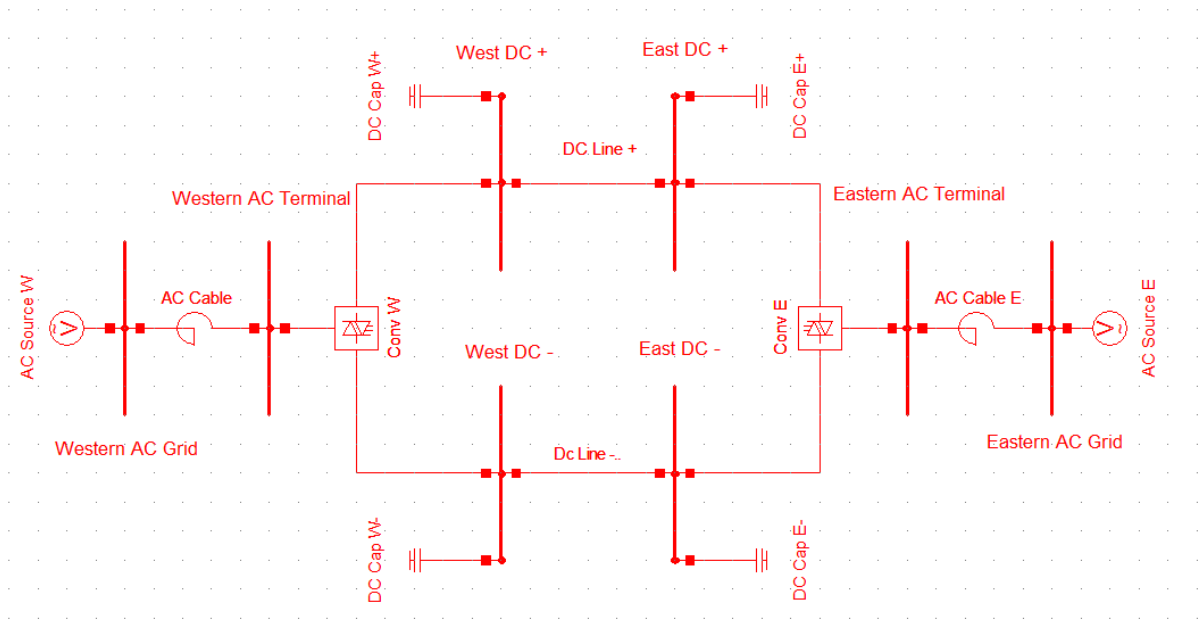

Figure 4.4: Overview of the point-to-point system used in simulations in PowerFactory.

The system consists of two VSC-HVDC systems connected together via DC cable, making up the DC link. From now on they will be referred to as the *western converter* and the *eastern converter*. The converters are then connected to different AC grids on both sides. The western converter was set to control the DC voltage and the eastern converter to control the power. Parameters used for this system can be found in Appendix A. The upcoming sections will describe the model in more detail.

4.5.2 AC Grid

The AC grid that each converter was connected to was modelled by an AC voltage source in series with an inductance. By varying the value of the reactance different SCRs could then be achieved. For the initial calculations both converters were assumed to be connected to strong AC grids, with an SCR of 6.

4.5.3 Current Controller

The current controller was initially implemented based on the derivations presented in Chapter 3. However, it was found that for RMS simulations the controller had to be modified. As explained in Section 4.3, PowerFactory use phasors to represent all voltages and currents in the AC side for RMS simulations and the dynamic behaviour of e.g. inductances is not considered. Therefore Eq. 3.5 has to be rewritten accordingly:

$$v_{s,\alpha\beta} - v_{c,\alpha\beta} = i_{\alpha\beta}R + i_{\alpha\beta}j\omega L. \tag{4.8}$$

Splitting this into the real and imaginary parts will give:

$$v_{s,\alpha} - v_{c,\alpha} = i_{\alpha}R - i_{\beta}\omega L \tag{4.9}$$

$$v_{s,\beta} - v_{c,\beta} = i_{\beta}R + i_{\alpha}\omega L. \tag{4.10}$$

Due to the use of phasors there will be no rotating quantities, so assuming that the PLL adjusts to any difference in angle these equations can easily be transformed into the dq reference frame:

$$v_{s,d} - v_{c,d} = i_{d}R - i_{q}\omega L \tag{4.11}$$

$$v_{s,q} - v_{c,q} = i_{q}R + i_{d}\omega L. \tag{4.12}$$

If the system transfer function in Section 3.5.2 is derived with this taken into account, the system transfer function becomes:

$$G(s) = \frac{1}{R} \tag{4.13}$$

rather than:

$$G(s) = \frac{1}{sL + R}, \tag{4.14}$$

which is the case in EMT simulations. This means that the current controller parameters need to be changed in order for the RMS model to have the same response as the EMT models. From Figure 3.9 it could be seen that:

$$(i_d^{ref} - i_d)(K_p + \frac{K_i}{s}))(\frac{1}{sL + R}) = i_d \tag{4.15}$$

which can be rewritten as:

$$\frac{i_d}{i_d^{ref}} = \frac{K_p + \frac{K_i}{s}}{sL + R + K_p + \frac{K_i}{s}}. \tag{4.16}$$

If $K_p = \alpha L$ and $K_i = \alpha R$:

$$\frac{i_d}{i_d^{ref}} = \frac{\alpha(\frac{sL+R}{s})}{sL + R + \alpha(\frac{sL+R}{s})} \tag{4.17}$$

which becomes:

$$\frac{i_d}{i_d^{ref}} = \frac{\frac{\alpha}{s}}{1 + \frac{\alpha}{s}} \tag{4.18}$$

and finally:

$$\frac{i_d}{i_d^{ref}} = \frac{\alpha}{s + \alpha}. \tag{4.19}$$

Figure 4.5 show the current controller as it is represented in RMS simulations.

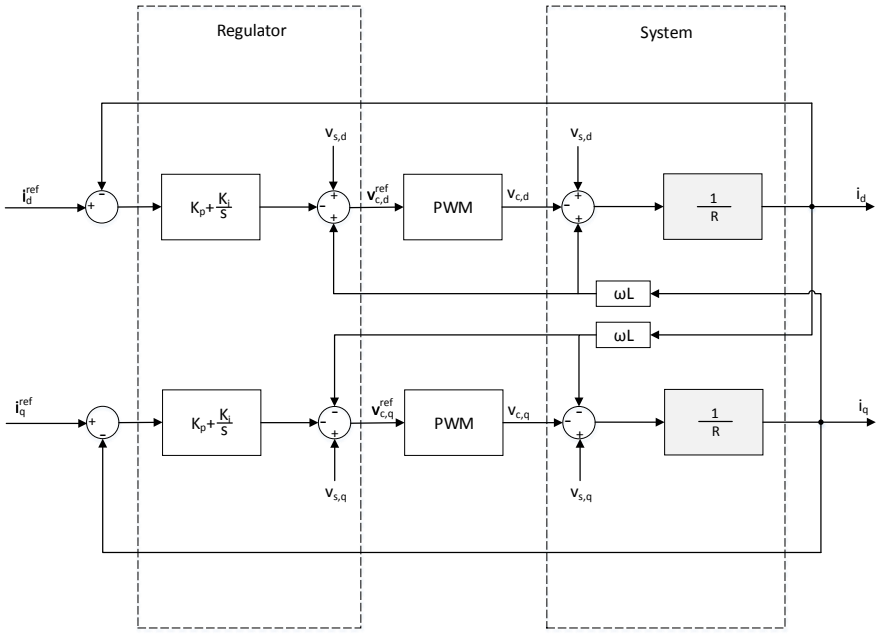

Figure 4.5: Current controller for RMS

In the d axis this can be expressed as:

$$(i_d^{ref} - i_d)(K_p + \frac{K_i}{s})(\frac{1}{R}) = i_d \tag{4.20}$$

which can be rewritten according to:

$$\frac{i_d}{i_d^{ref}} = \frac{K_p + \frac{K_i}{s}}{R + K_p + \frac{K_i}{s}} \tag{4.21}$$

which becomes:

$$\frac{i_d}{i_d^{ref}} = \frac{sK_p + K_i}{s(R + K_p) + K_i}. \tag{4.22}$$

If K_p is changed to:

$$K_p = 0 \tag{4.23}$$

with K_i remaning as before, it will result in:

$$\frac{i_d}{i_d^{ref}} = \frac{\alpha R}{sR + \alpha R} \tag{4.24}$$

which can be rewritten as:

$$\frac{i_d}{i_d^{ref}} = \frac{\alpha}{s + \alpha}. \tag{4.25}$$

As can be seen in Eq. 4.20 to 4.25, selecting the parameters of the current controller adequately for the RMS model results in the same transfer function obtained for the EMT model. It should be noted that the implementation of the current controller is not straight forward in PowerFactory since the voltage references cannot be used directly as inputs to the PWM converter. Instead the PWM indices Pm_d and Pm_q are used as inputs. In order to get the desired voltages from the PWM converter, the PWM indices should then be:

$$Pm_d^{ref} = \frac{v_{c,d}^{ref}}{u_{DC}} \frac{2\sqrt{2}}{\sqrt{3}}. \tag{4.26}$$

$$Pm_q^{ref} = \frac{v_{c,q}^{ref}}{u_{DC}} \frac{2\sqrt{2}}{\sqrt{3}}. \tag{4.27}$$

The controllers in PowerFactory were implemented in per unit, whereas the input to the PWM should be in real values. Considering this, the indices should be (shown for the d axis):

$$Pm_d^{ref} = \frac{v_{c,d,p.u.}^{ref}}{u_{DC,p.u.}} \frac{v_{c,d,base}}{u_{DC,base}} \frac{2\sqrt{2}}{\sqrt{3}} \tag{4.28}$$

which will give that:

$$Pm_d^{ref} = \frac{v_{c,d,p.u.}^{ref}}{u_{DC,p.u.}} \frac{\sqrt{2}}{\sqrt{3}}. \tag{4.29}$$

The current controller was then implemented in PowerFactory for RMS simulations, which is shown in Figure 4.6.

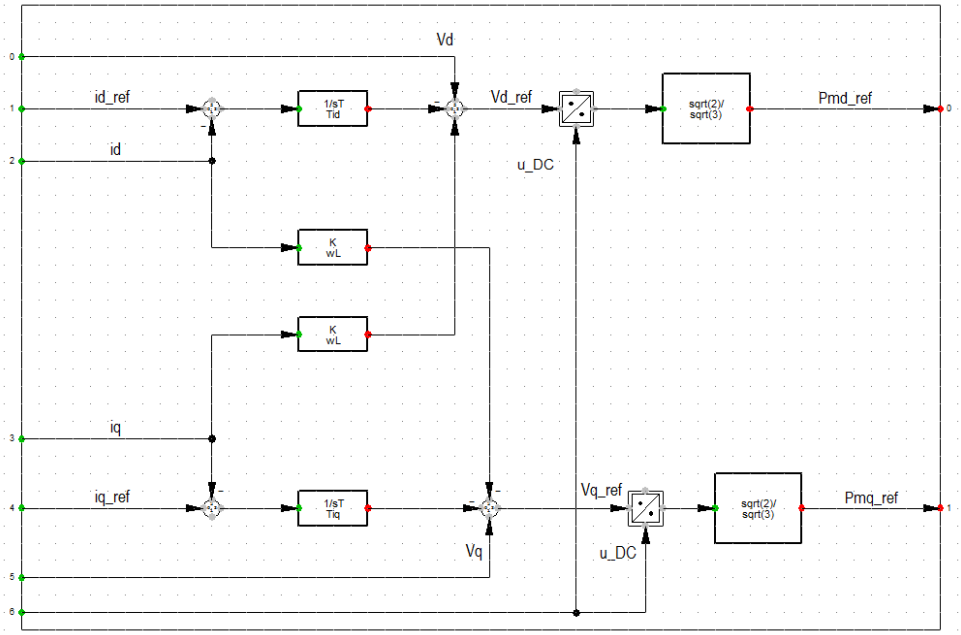

Figure 4.6: Current controller implementation in RMS.

It should be noted that the current controller was implemented using a user-defined model instead of the built-in current controller in the converter model. The main reason was the way in which the PI-regulator was implemented in the built-in model:

$$F(s) = K_p(\frac{1 + T_i s}{T_i s}). \tag{4.30}$$

As stated before, the proportional part of the regulator should be set to zero in order to obtain the same response from the RMS model as the EMT model. However, if the proportional would be set to zero in Eq. 4.30 the output from the regulator would always be zero. Thus it would be difficult to obtain the same performance in the RMS and EMT models using the built-in current controller. Other reasons were the lack of voltage feed forward and cross-coupling compensation.

4.5.4 PLL

When investigating the performance of the built-in PLL models in PowerFactory and PSCAD, the PLL in PowerFactory performed poorly while the PLL in PSCAD performed acceptably, using the same parameters for both. Since no reference for the PLL model in PSCAD was provided, a user-defined model of the PLL was implemented in PSCAD according to [50]. This model was then compared to the built-in PLL model in PSCAD and, using the same parameters, the results in PSCAD were similar if either PLL model was used. Based on this, it was concluded that the PLL was implemented differently in PowerFactory than what was stated in [50]. In order to verify this, the user-defined PLL model was implemented in PowerFactory as well and

the results were then similar to the ones in PSCAD. Thus, the user-defined PLL model was used in this thesis. Similarly to the current controller, the PLL had to be changed for RMS simulations to accommodate the use of phasors. To achieve the same performance as for the EMT models, the feed forward of the nominal frequency is not added in the PLL model for RMS [50]. The resulting models for EMT and RMS simulations are shown in Figures 4.7 and 4.8.

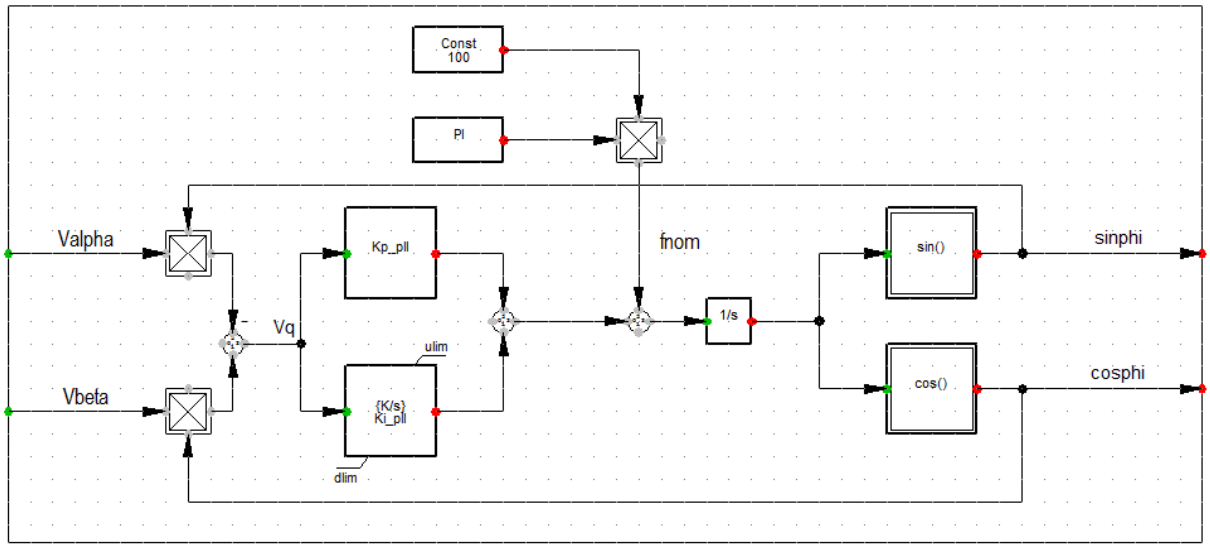

Figure 4.7: Custom PLL implementation, EMT.

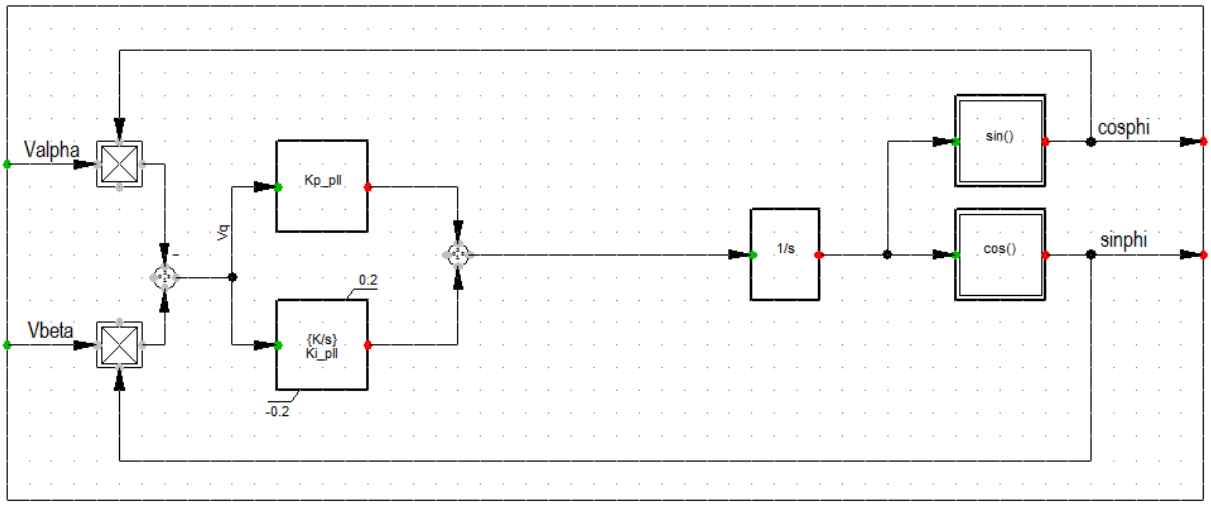

Figure 4.8: Custom PLL implementation, RMS.

4.5.5 Outer Controllers

As there are no built-in models for outer controllers they had to be implemented using user-defined models. Figure 4.9 shows the complete control system for a converter controlling active power, including an active power controller, measurements coming from the grid models, PLL and the current controller described in the previous section.

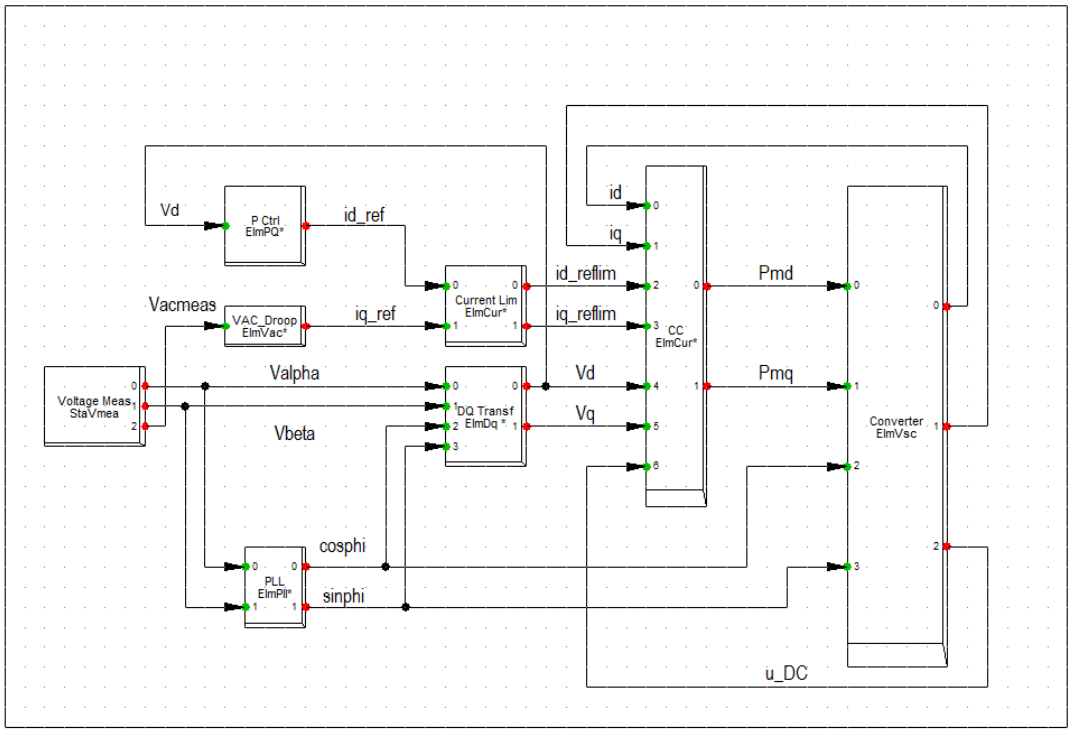

Figure 4.9: Active power control system implementation.

The DC voltage control system was modelled in the same way and it is visualised in Figure 4.10. Figure 4.11 shows the implementation of the DC voltage controller, and Figure 4.12 shows the AC voltage droop controller.

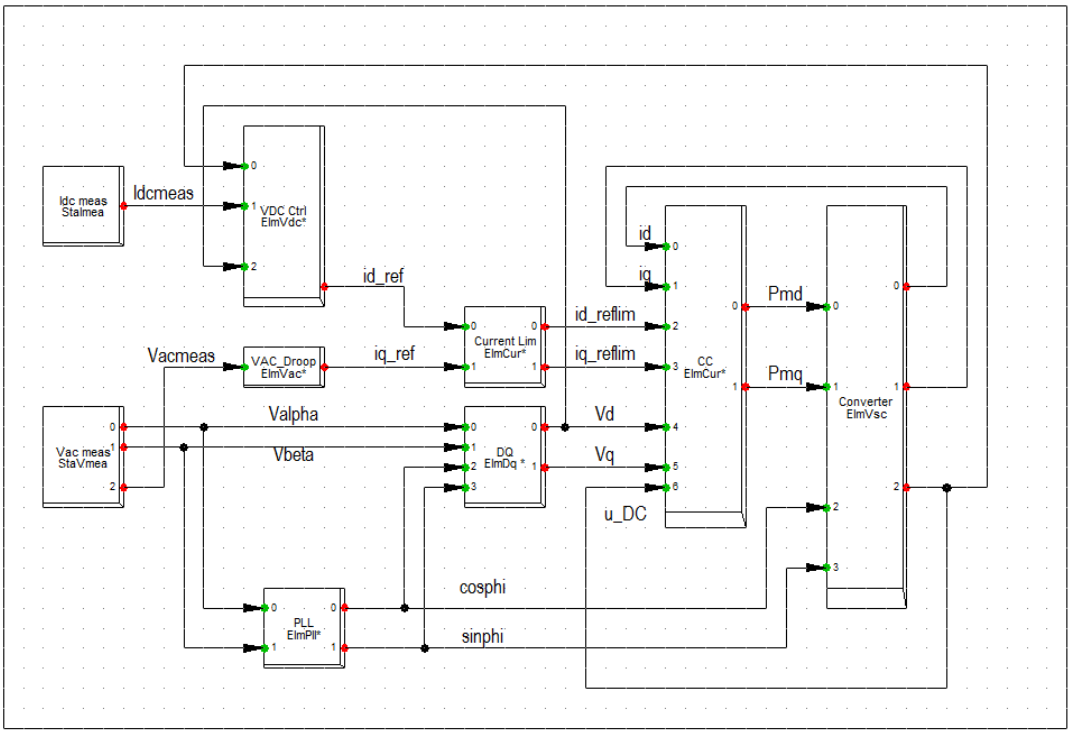

Figure 4.10: DC voltage control system implementation.

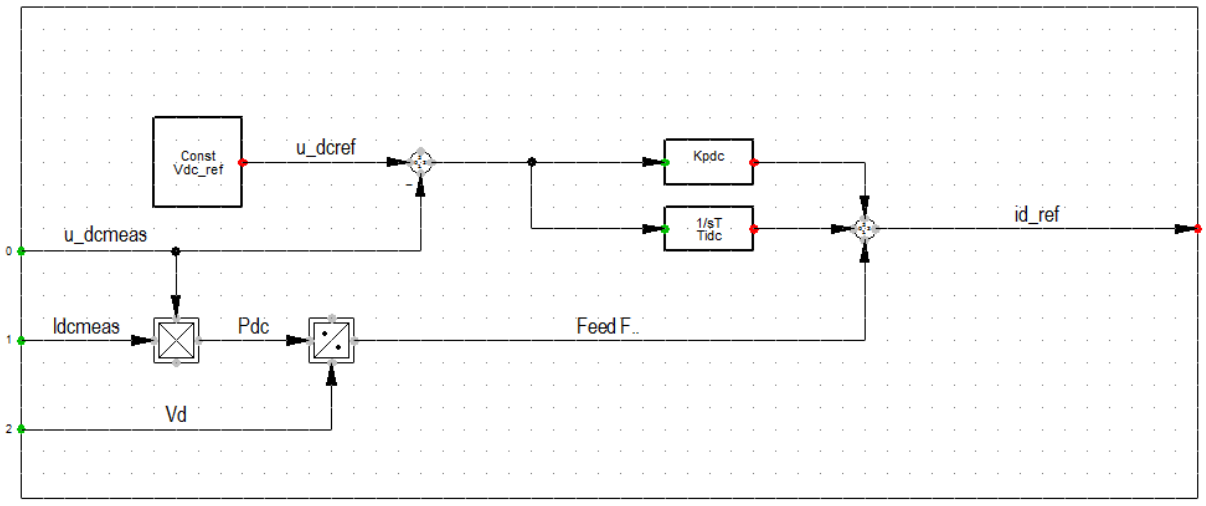

Figure 4.11: DC voltage controller implementation.

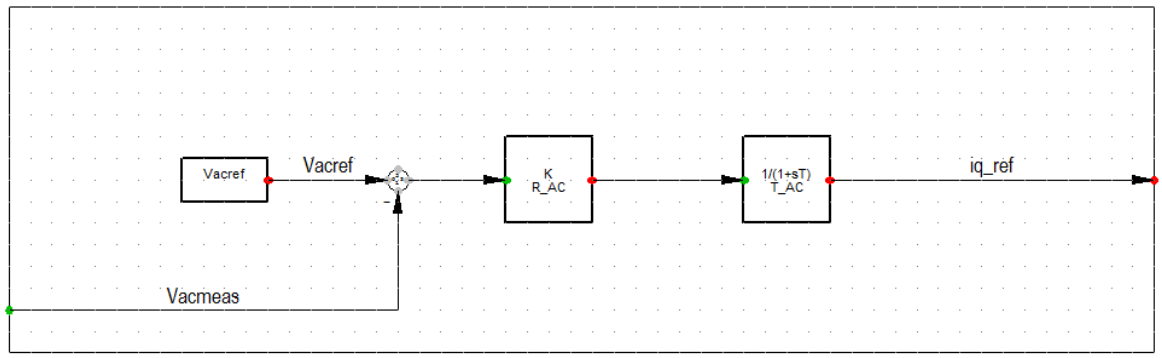

Figure 4.12: AC voltage droop control implementation.

4.6 Model Verification

The model verification was performed by simulating different cases which are detailed below. From now on a power flow from the converter to the AC grid will be referred to as a *positive* power flow and the opposite will be referred to as a *negative* power flow.

4.6.1 Negative Setpoint change

In this simulation the current reference is changed from 0 to -0.7 p.u. at 1 s. This corresponds to a power of 420 MW from the eastern converter to the western converter. The reason for doing this is to compare the current controllers of the three different models. In Figure 4.13 the current in the d axis and the active power at the eastern converter is visualised and in Figure 4.14 the DC voltage and active power at the west converter is shown.

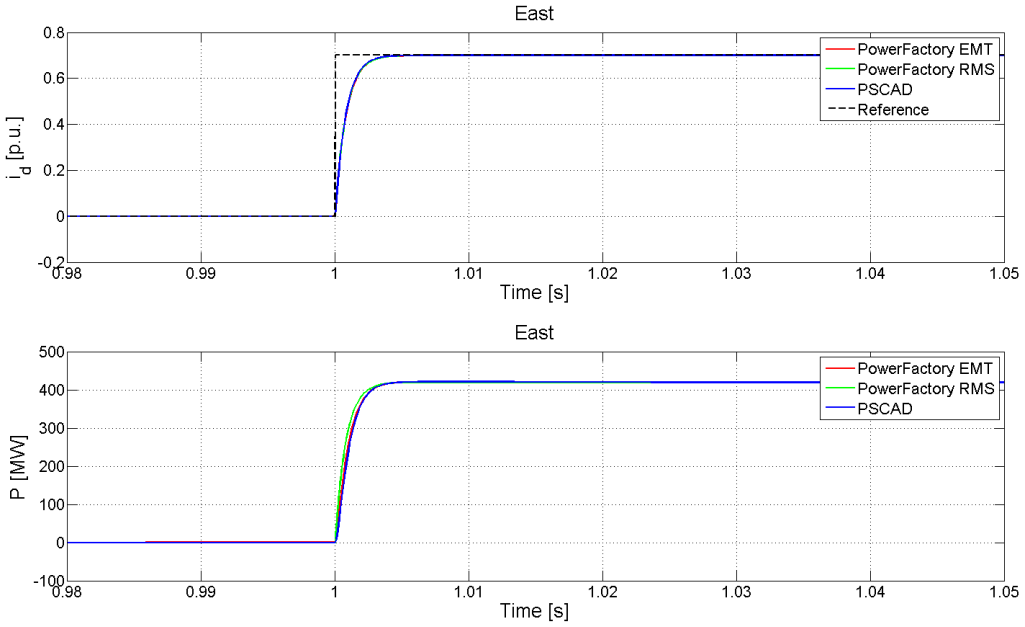

Figure 4.13: *d* axis current and active power following a negative setpoint change.

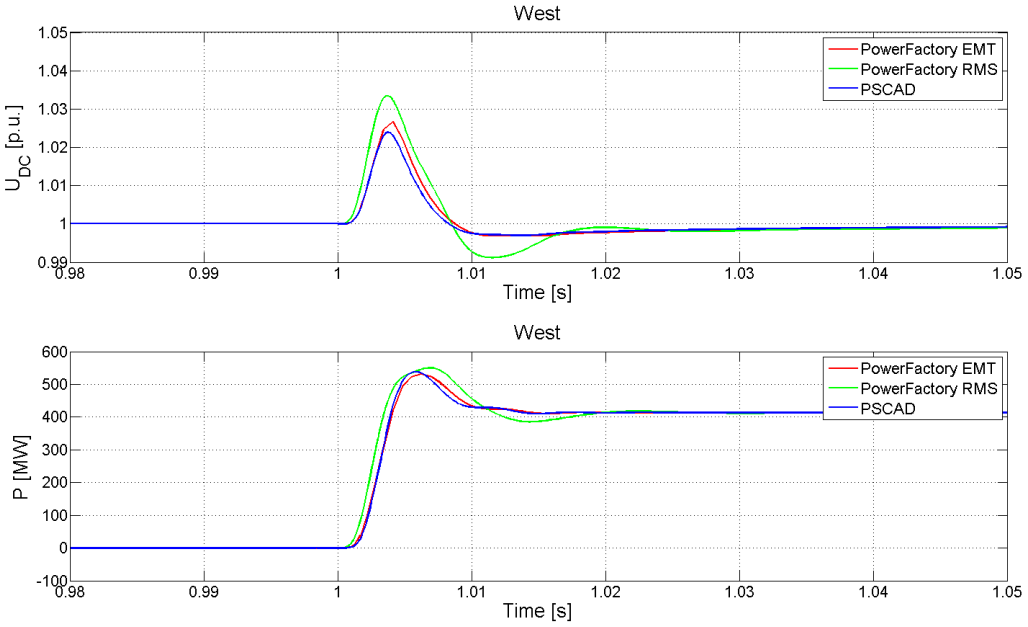

Figure 4.14: DC voltage and active power following a negative setpoint change.

As can be seen all models responds to the change equally following the current reference step. This indicates that the current controller implementation in the RMS model correspond well to the EMT models. The result also shows that, for the EMT models, the DC voltage and active power at the western converter are similar. However, the RMS model differ slightly from the EMT models during the transient.

Figure 4.15 shows the voltages in both the d and q axes for the western and the eastern converter.

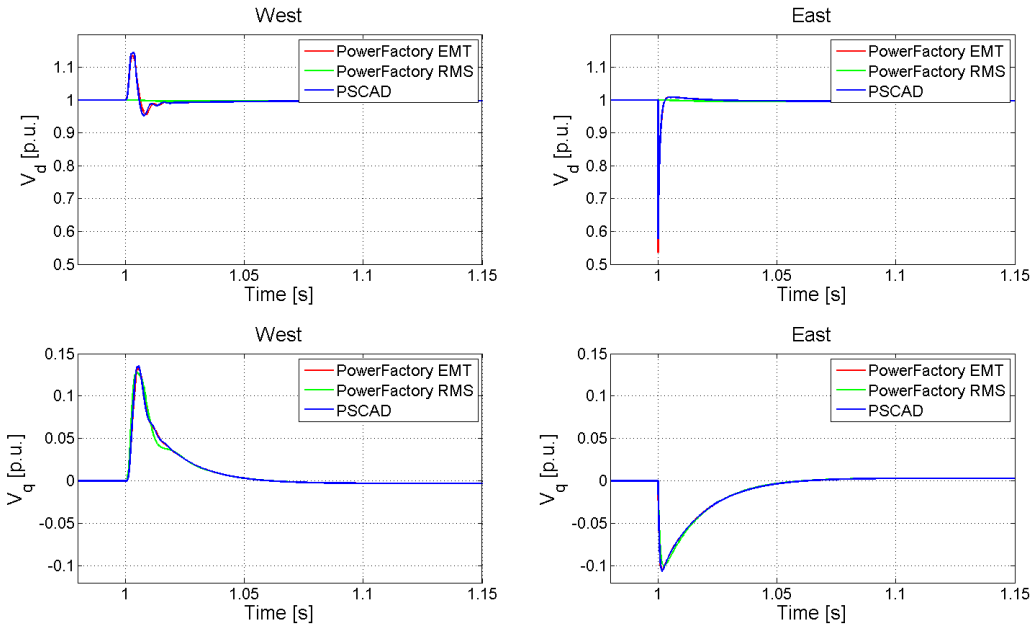

Figure 4.15: d and q axis voltages following a negative setpoint change.

For the voltages in the q axis, the RMS model perform well when compared to the EMT models, but the voltages in the d axis differ greatly during the transient. This is due to the fundamental difference in how AC grid elements are modelled in RMS simulations compared to EMT simulations, as discussed in Section 4.3, and it can be explained by looking at Eq. 3.7, 3.8, 4.11 and 4.12. The dominant term in the d axis voltage comes from the dynamics of the phase reactor, which is not present in the RMS model. In the q axis, however, the dominant term is the cross-coupling which is represented similarly in RMS and EMT simulations. Studying the d axis voltage over time, however, shows that the RMS model is a good indication of the steady state value.

Figure 4.16 shows the AC voltage magnitude and the reactive power at both converters.

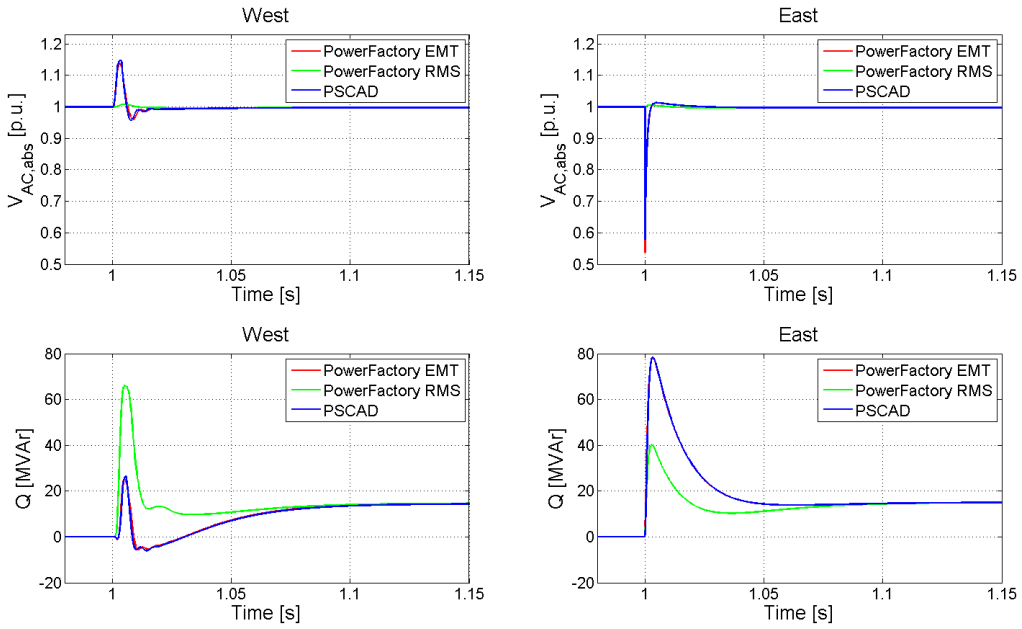

Figure 4.16: AC voltage magnitude and reactive power following a negative setpoint change.

The magnitude of the AC voltage will differ in the RMS model for the same reason as why the d axis voltage will differ during the transient. Studying the reactive power it can be seen that the RMS model differ from the EMT models during the transient, but it does not affect the steady state value after the transient. This is caused by the difference in the AC voltage magnitude which is used as the input for the AC voltage droop controller. Also, the reactive power of the western converter behave in a way that might seem counter-intuitive. When the voltage of the western converter goes up the reactive power increases as well, whereas the expected behaviour would be that it would decrease, in order to bring down the voltage. The reason for this is that the implemented AC voltage droop controller has a filter added to it which causes it to react slowly to changes. This means that even it the current controller follow the reference of the q axis current well, the reference itself will be slow. As the active and reactive powers consist of components from both the d and q axis voltages, as well as the fact that the q axis voltage will not be zero during the transient the reactive power will be influenced, causing this behaviour. However, in steady state it performs as expected.

4.6.2 Positive Setpoint change

In this simulation the power reference is changed from 0 to +0.7 p.u. at 1 s representing a power flow towards the eastern converter. Figure 4.17 visualize the current in the d axis for the eastern converter and the active power and Figure 4.18 show the DC voltage and active power of the western converter.

In this simulation the models follows the reference like they did in the previous case. However,

the difference between the RMS model and the EMT models is larger than in the simulation case with a negative setpoint change. Moreover, it can be seen that the response of the EMT models is more oscillatory compared to the negative setpoint change case, which is less apparent in the RMS model.

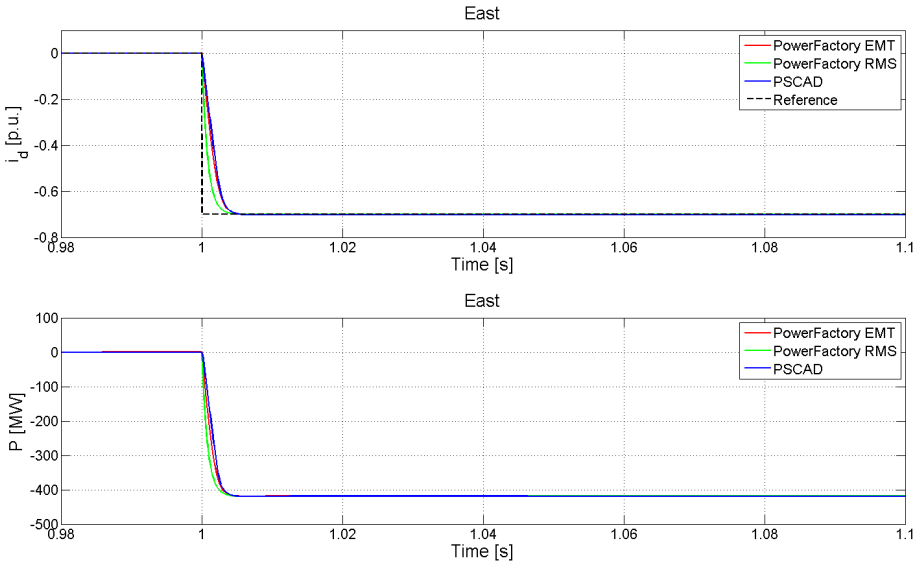

Figure 4.17: *d* axis current and active power following a positive setpoint change.

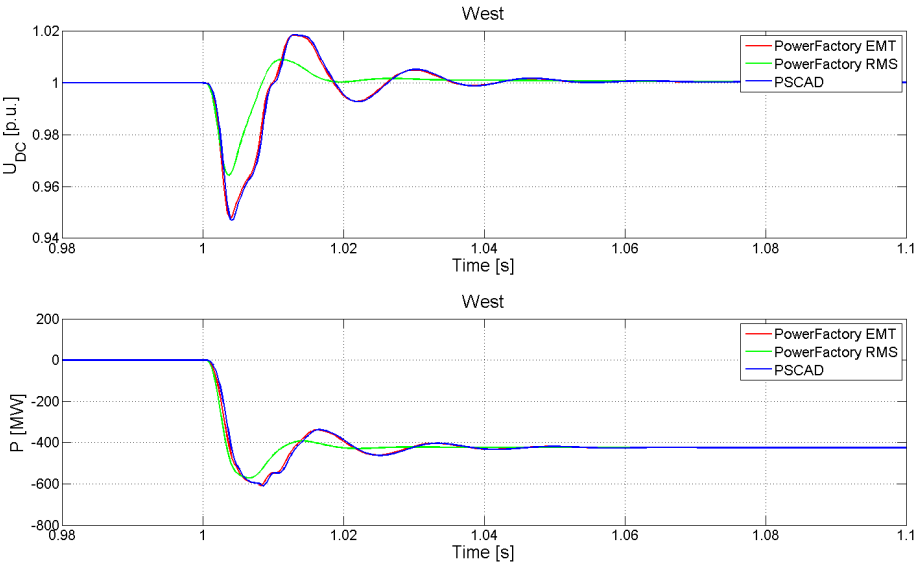

Figure 4.18: DC voltage and active power following a positive setpoint change.

Figure 4.19 and Figure 4.20 show the voltages in d and q axis, the voltage magnitude and the reactive power for the eastern and the western converter.

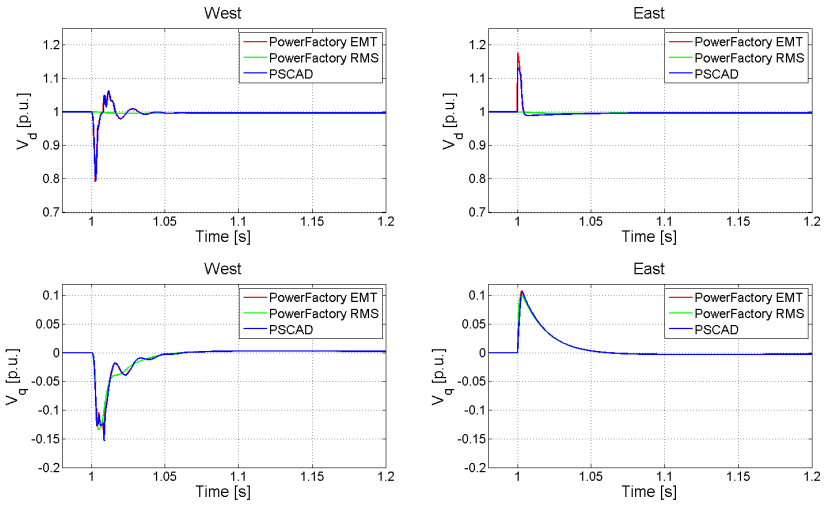

Figure 4.19: d and q axis voltages following a positive setpoint change.

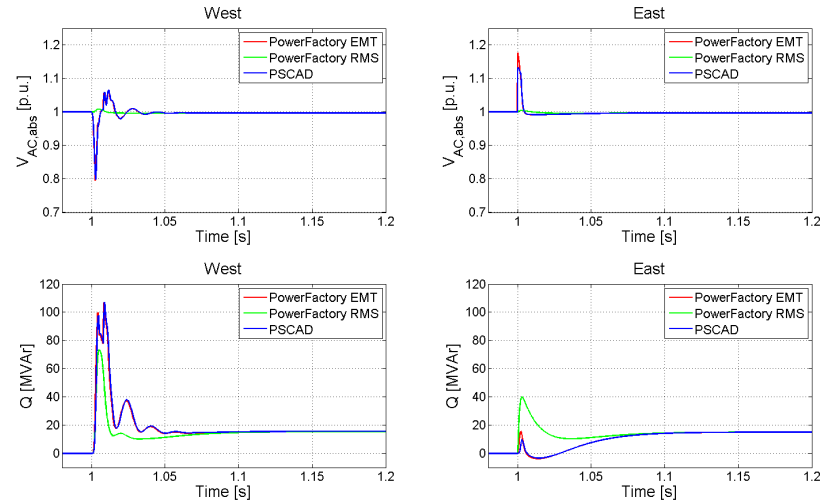

Figure 4.20: AC voltage magnitude and reactive power following a positive setpoint change.

Similarly to the previous case, the q axis voltage is represented well, and the d axis voltage and the AC voltage magnitude provide a good representation of the steady state values, even if they differ during the transient. As in the previous case, the reactive power during the transient behaves differently in the simplified model, but it does not affect the steady state value after the transient.

4.6.3 Single-Line to Ground fault east

In this simulation a Single-Line to Ground (SLG) fault at the eastern AC terminal is applied at 1 s with the active power transfer being -0.7 p.u. The fault is cleared after 0.1 s. Figure 4.21 show the active power and the current in the d axis for the eastern converter.

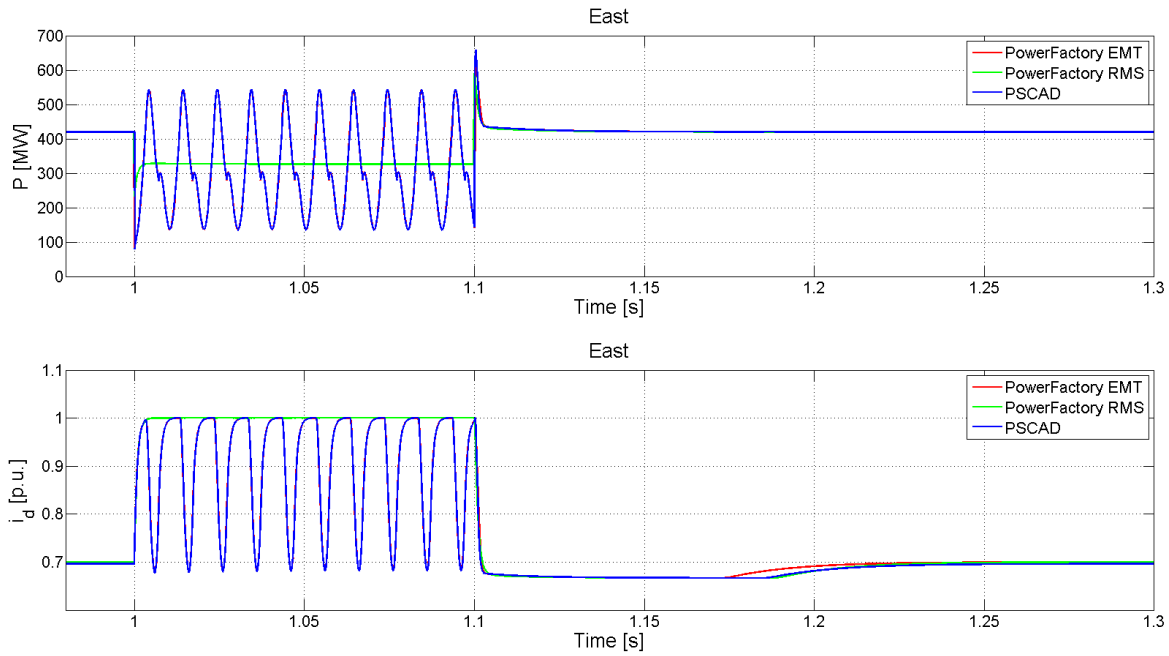

Figure 4.21: Active power and d axis current, following a SLG fault at the east converter

When the fault is applied, the power transferred over the HVDC link is reduced due to the voltage drop on the AC side of the converter. The d axis current is then increased by the power controller, eventually reaching its limit. During the fault both EMT models start to oscillate at twice the grid frequency, this is not represented by the RMS model. The absence of oscillations in the RMS model is due to the phasor representation. After the fault is cleared the RMS model coincide with the EMT models.

Figure 4.22 shows the DC voltage and active power for the western converter. As the DC voltage controller attempts to balance the power on the HVDC link, the oscillations in the active power of the eastern converter will spread to the western converter as well.

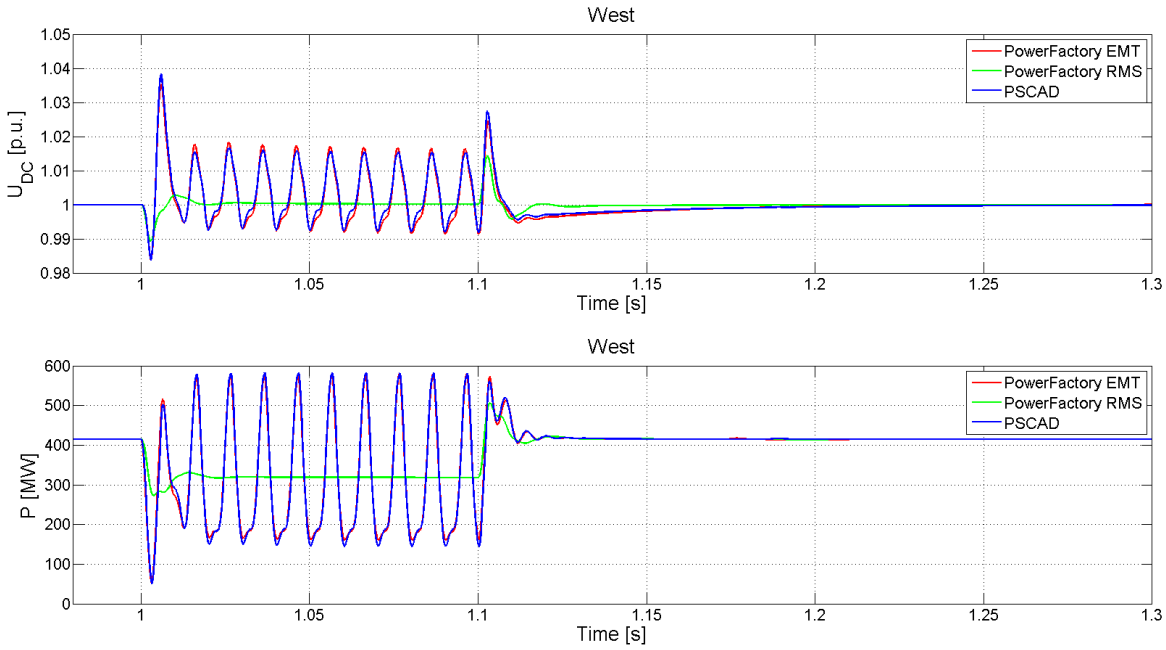

Figure 4.22: DC voltage and active power following a SLG fault at the eastern converter

Figure 4.23 show the voltages in d and q axis and Figure 4.24 show the voltage magnitude and the reactive power for the eastern and the western converter. The d and q axis voltages in both converters are not represented well by the RMS model during the fault, but when the fault is cleared the models coincide so the result can be considered acceptable. Again, the reactive power during the transient differs between the RMS and EMT models, but it has a small impact on the steady state result.

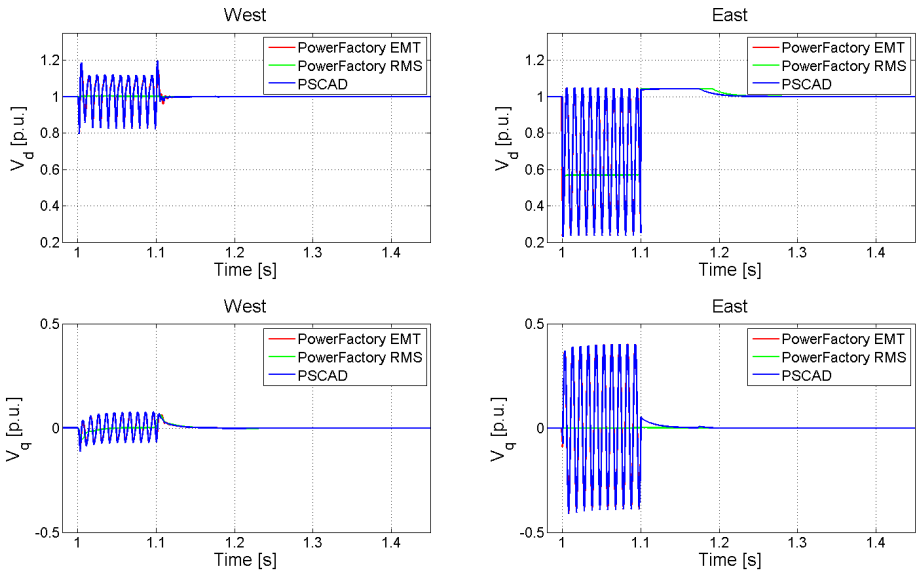

Figure 4.23: d and q axis voltages following a SLG fault at the eastern converter.

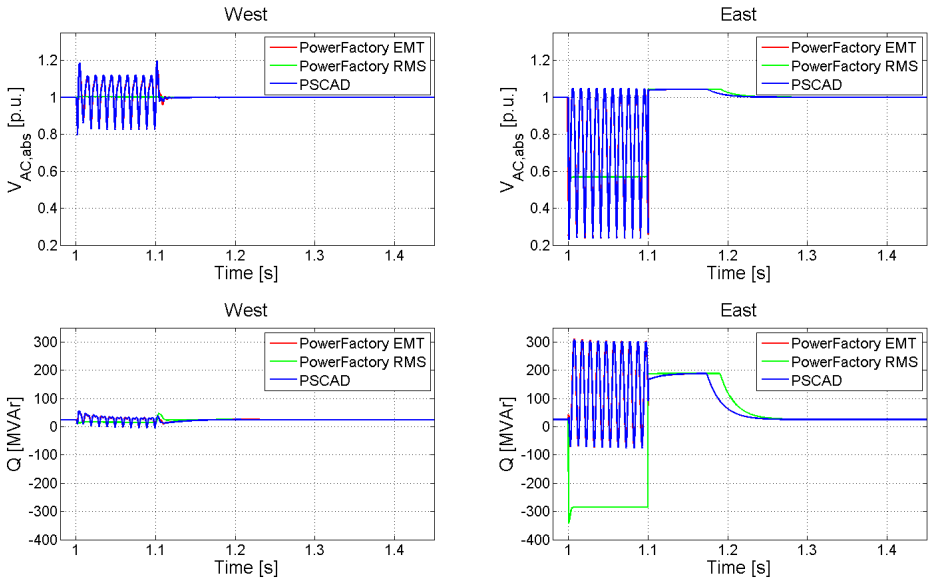

Figure 4.24: AC voltage magnitude and reactive power following a SLG fault at the eastern converter.

4.6.4 Single-Line to Ground fault west

In this case a SLG fault at the western AC terminal is applied at 1 s, with an active power flow of -0.7 p.u. The fault is cleared after 0.1 s. Figure 4.25 show the DC voltage, measured at the western converter, and the active power for both converters.

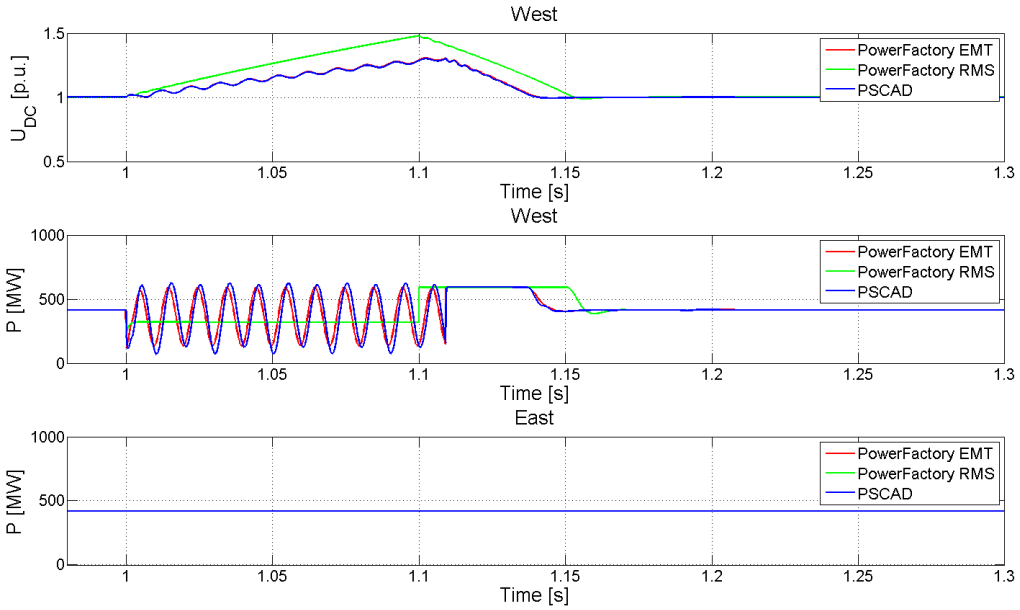

Figure 4.25: DC-link voltage and active powers following a SLG fault at the west converter

Due to the AC side fault, the power that the western converter can inject into the AC grid is reduced. In this case the loss of transmission capacity means that there will be an imbalance in power in the DC side. This will cause the DC side capacitors to be charged, and the DC voltage will rise. This behaviour is present for the EMT and RMS models, but during the fault the behaviour in the active power for the RMS model is different. Similarly to Section 4.6.3 oscillations are present in the EMT models but not in the RMS model. When the fault is cleared the capacitors will start to discharge bringing the system back to normal operation.

It is noticed that as the capacitors in the RMS model are charged faster than the EMT models, it will return to steady state slower. However, the impact on the transient stability is negligible as it would require a long time to reach a considerable difference between the DC voltages in the RMS and EMT models, but in reality the voltage increase will be prevented.

Figure 4.26 shows the voltages in the d and q axes for the west converter and Figure 4.27 shows the AC voltage magnitude and the reactive power for the western converter. Once again, the voltages in the d and q axis are different in the RMS model during the fault, but when the fault is cleared they return to the same value as the EMT models. The reactive power behaves similarly to the previous case, and the simplified model return to the same steady state value as the EMT models.

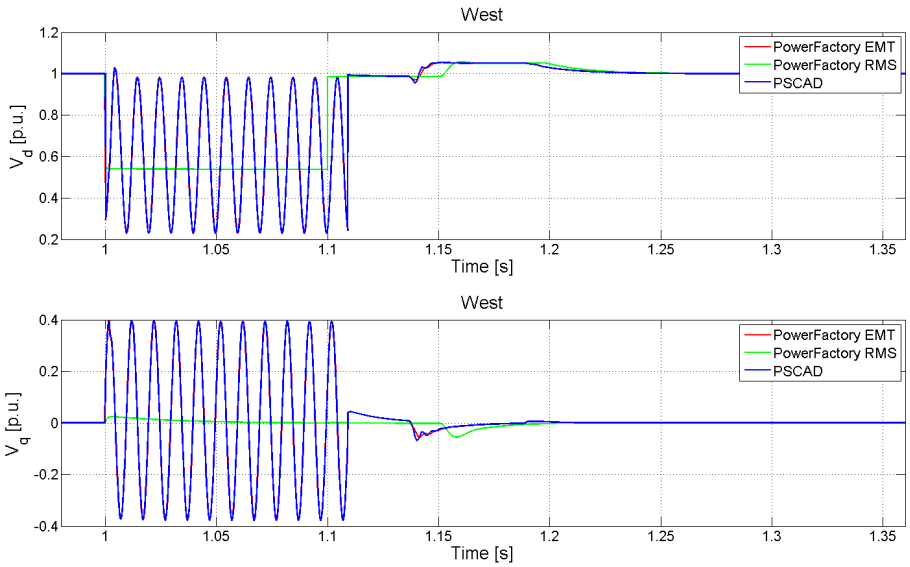

Figure 4.26: d and q axis voltages following a SLG fault at the western converter.

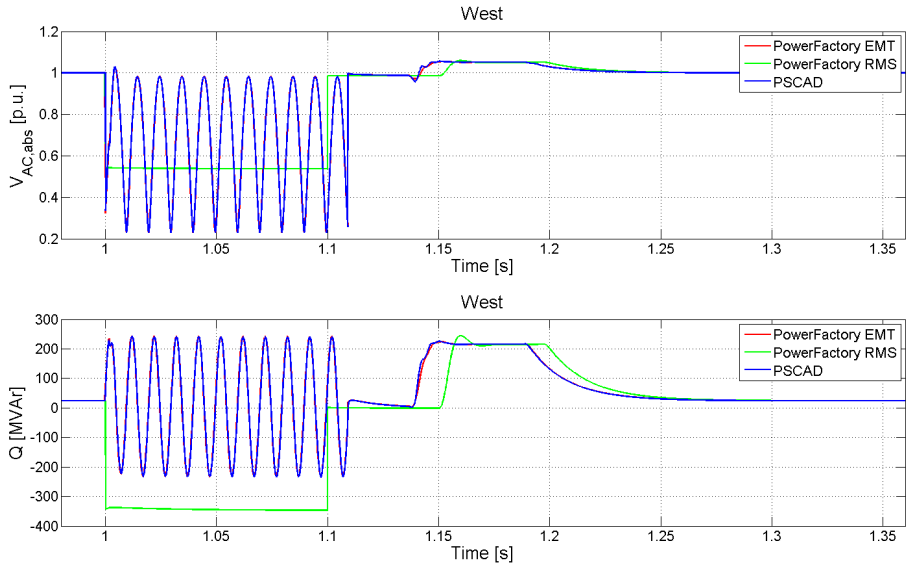

Figure 4.27: AC voltage magnitude and reactive power following a SLG fault at the western converter.

4.6.5 Three-Phase to Ground fault east

For this simulation a three-phase to ground fault is applied at the eastern AC terminal at 1 s with an active power flow of -0.7 p.u. The fault is cleared after 0.1 s. Figure 4.28 and Figure 4.29 show the DC voltage and active power at the western converter and the active power at the eastern converter.

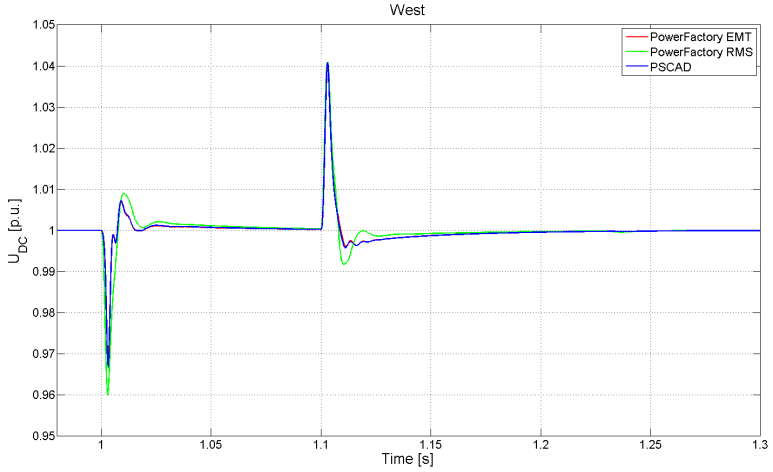

Figure 4.28: DC link voltage following a three-phase to ground fault at the eastern converter.

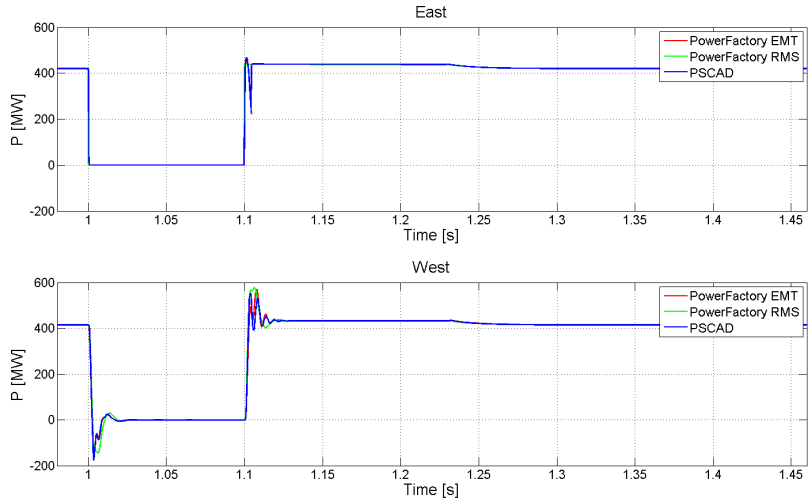

Figure 4.29: Active powers following a three-phase to ground fault at the eastern converter.

The results show that the RMS model is a good representation in this case. Figure 4.30 and Figure 4.31 show d and q axis voltages, AC voltage magnitude and the reactive power for both converters.

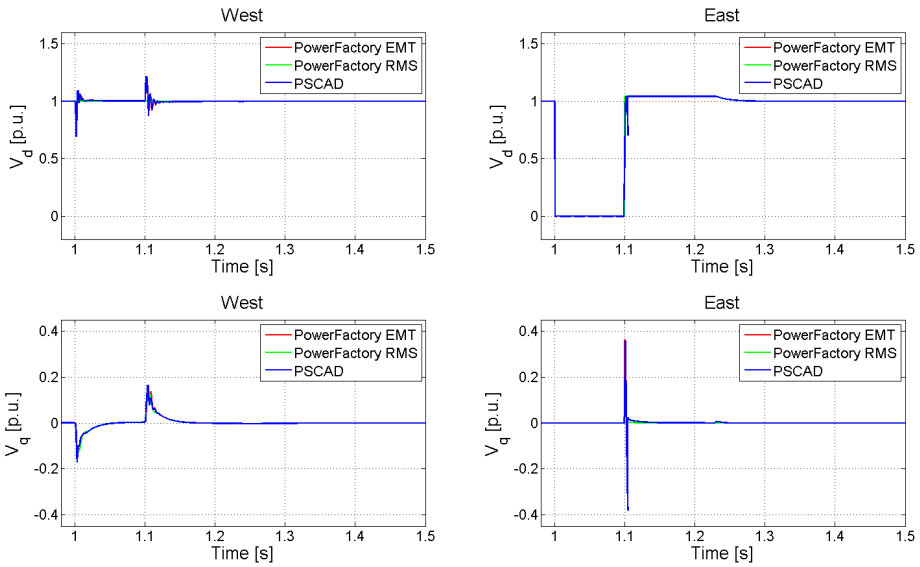

Figure 4.30: d and q axis voltages following a three-phase to ground fault at the eastern converter.

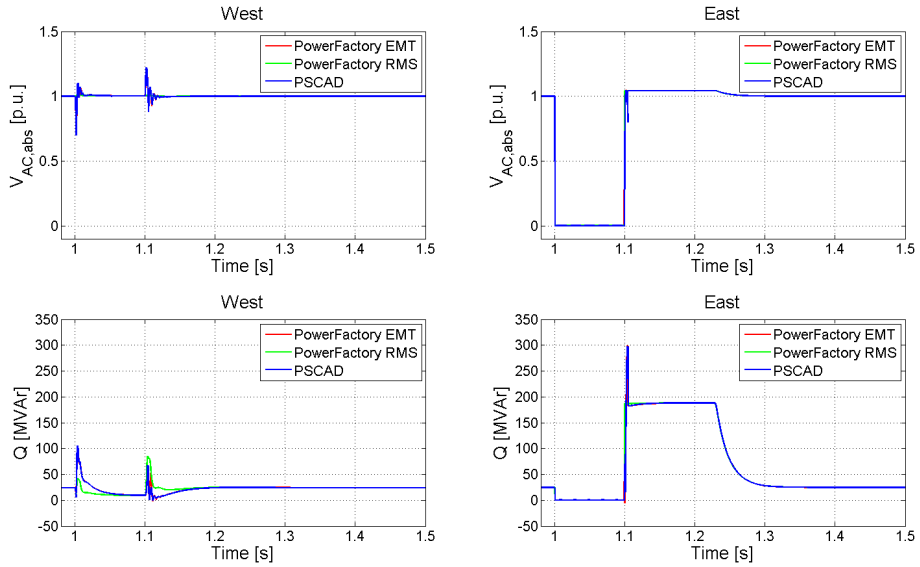

Figure 4.31: AC voltage magnitude and reactive powers following a three-phase to ground fault at the eastern converter.

Even though some deviations are noticed, the results from the RMS model are acceptable.

4.6.6 Three-Phase to Ground fault west

In this simulation a three-phase fault is applied to the western AC terminal at 1 s and cleared after 0.1 s. The active power flow is +0.7 p.u.

Figure 4.32, Figure 4.33 and Figure 4.34 visualize the DC voltage, active and reactive power, AC voltage magnitude and the voltages in d and q axis for the western converter.

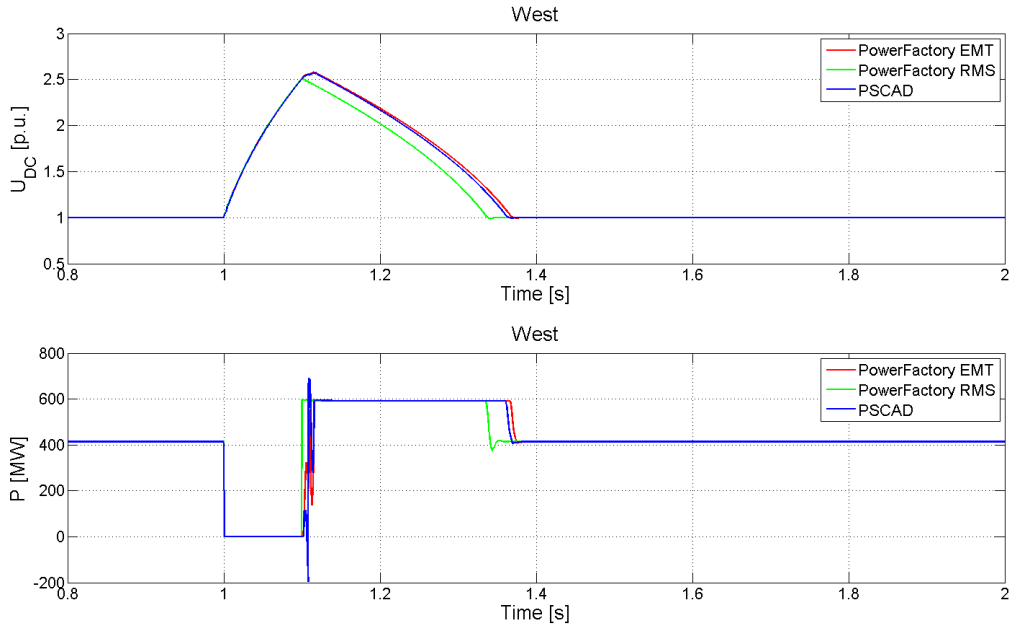

Figure 4.32: DC voltage and active power following a three-phase to ground fault at the western converter.

Similarly to case 4.6.4, the power that can be injected into the AC grid at the western converter will be reduced (in this case to zero). Thus, the voltage will increase as the capacitors are charged by the power flowing from the eastern converter. However, as the fault is symmetrical in this case, the charging will take place at the same rate for the RMS and EMT models but there is still a small difference in regards to how quickly the system returns to steady state following the fault clearing. In the EMT models each phase is cleared independently when the current crosses zero. In the RMS model, as it is not represented as a three-phase voltage, there will be no zero crossing and instead the fault is cleared instantaneously.

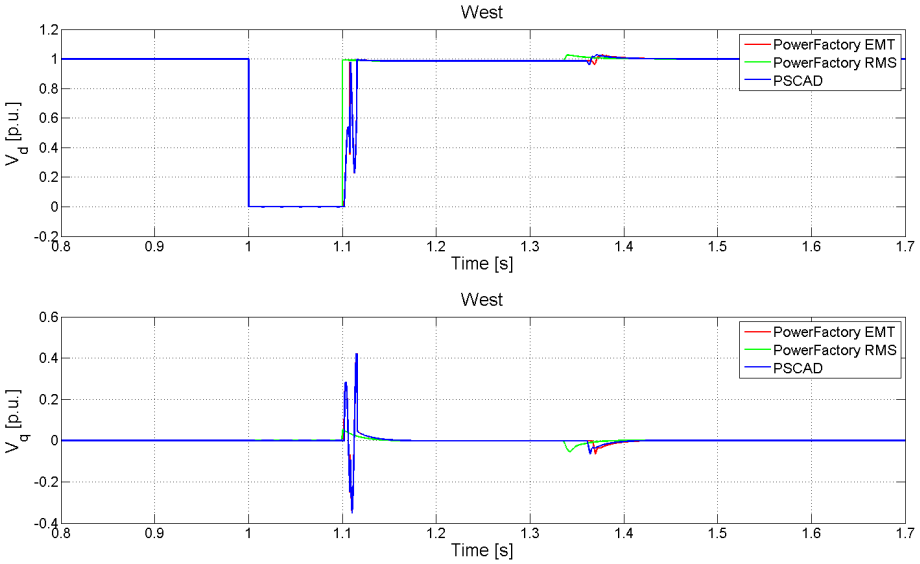

Figure 4.33: d and q axis voltages following a three-phase to ground fault at the western converter.

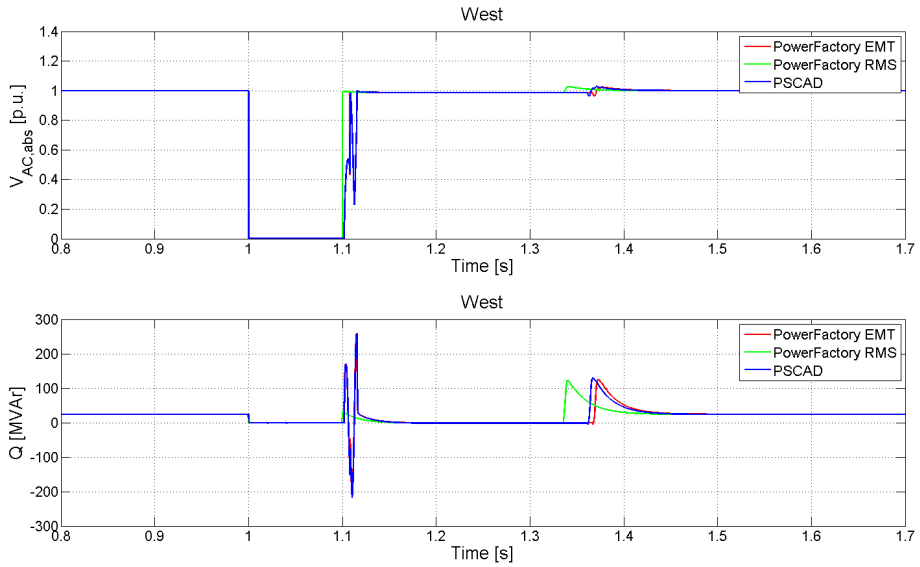

Figure 4.34: AC voltage magnitude and reactive power following a three-phase to ground fault at the western converter.

4.6.7 DC Line to Ground fault

In this simulation a DC line to ground fault was applied at the DC cable connecting the positive converter terminals at 1 s, and it was cleared after 0.1 s. The active power flow was -0.7 p.u. Figure 4.35 shows the pole voltages at the western converter.

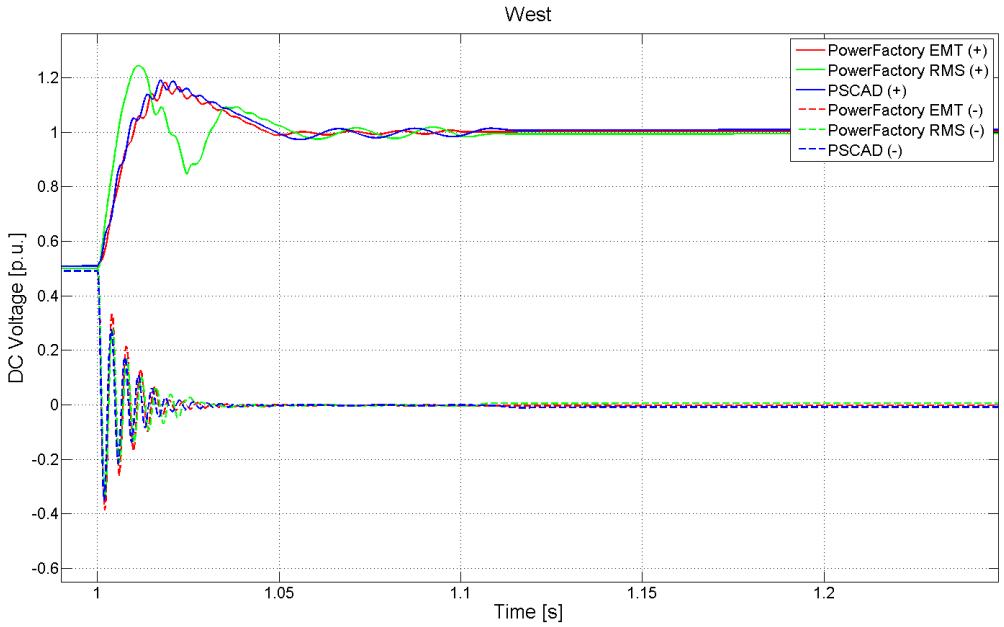

Figure 4.35: Pole voltages following a line to ground fault on the DC side.

When the fault occurs, the voltage of the faulted cable drop from 0.5 p.u. to zero. As the converter controls the voltage to 1 p.u. for the DC link, the voltage of the healthy cable will increase towards 1 p.u. When the fault is cleared the previously faulted cable will not return to 0.5 p.u. as the objective of the converter controlling the DC voltage is not to balance voltage in the DC cables. It should be noted that when the voltage drops initially in the DC link, the power flow at the western converter will be reversed in order to charge the capacitors, bringing the DC link voltage back to 1 p.u.

Figure 4.36 shows the DC voltage at the western converter. Figure 4.37 shows the active power at both converters.

In this case, the RMS model appears to be a bad representation of the behaviour of the EMT models during the fault. The active power behaves in a way that is difficult to explain, causing the DC voltage to differ from the EMT models. However, when the fault is cleared the RMS model returns to coincide with the EMT models. It should be noted that even if this difference in the active power between the RMS and EMT models could impact the transient stability of the connected AC grid.

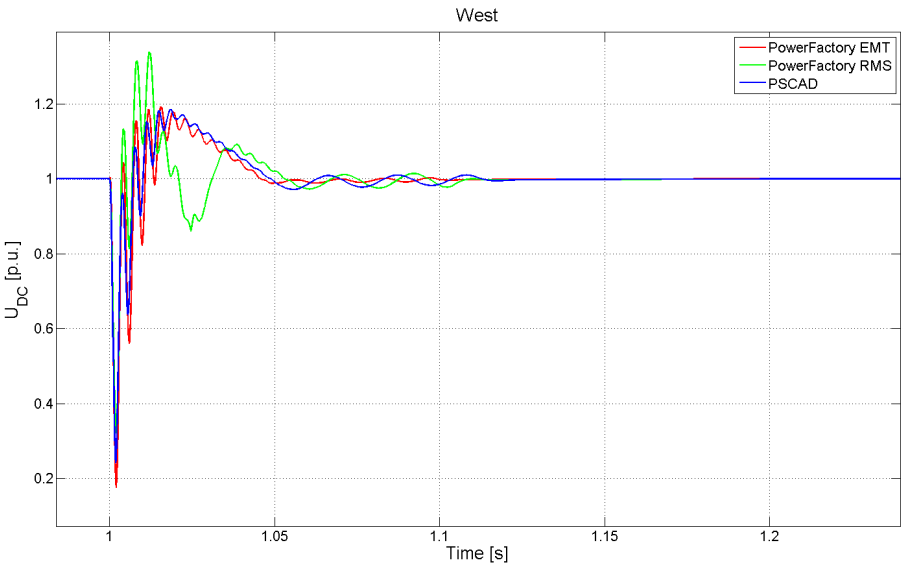

Figure 4.36: DC voltage following a line to ground fault on the DC side.

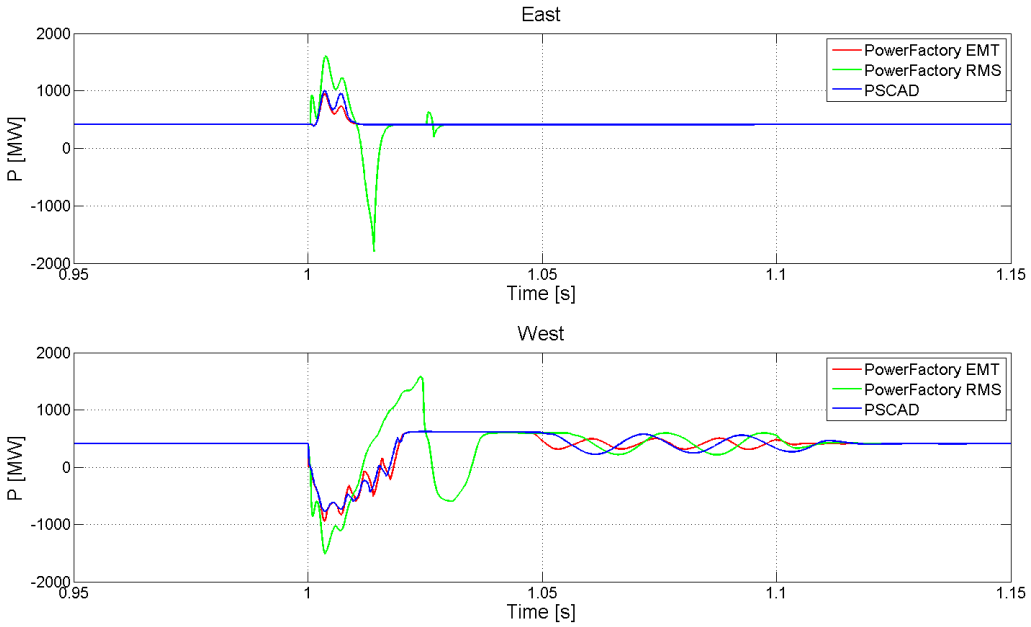

Figure 4.37: Active powers following a line to ground fault on the DC side.

4.6.8 Weak AC Setpoint change

In this case the strength of the western AC grid was lowered and a positive set point change occur at 1 s. Having a weaker AC grid will result in a bigger influence of the PLL on the system dynamics and if the AC grid is too weak, the control system should not be able to handle it in neither the RMS or EMT models. This is because the control system is based on vector current control, which is not suitable for control in converters connected to weak AC grids [23]. The simulation was performed in order to see if there is a point where the RMS model will fail to represent the EMT and PSCAD models.

With an SCR of 1.5, which is considered a very weak grid, the EMT models were found to be unstable and undamped oscillations were observed. In contrast to this, the RMS model manages to return to steady state following the setpoint change. Figure 4.38 show the DC voltage at the western converter.

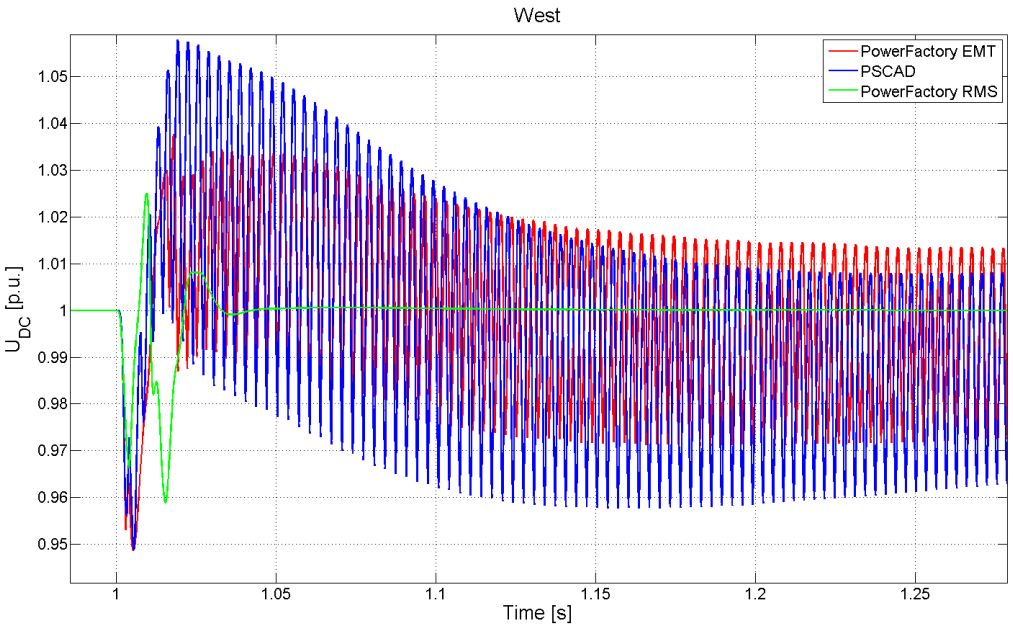

Figure 4.38: DC voltage following a positive setpoint change with weak AC

In this case the RMS model cannot represent the behaviour of the EMT models at all, and it can be concluded that for very weak AC grids, where the influence of the PLL will become more significant, the RMS model will be a bad choice.

4.7 Summary of Verification Results

A summary of the results from the verification is presented below.

- The changes in the current controller implementation resulted in almost no difference at all between the current in the RMS and EMT models following a reference step.
- As the dominant term in the d axis voltage is dependant on the dynamics of the phase reactor, it is not represented well by the RMS model during the transients. The q axis voltage, however, is represented well as the dominant term is then the cross-coupling, which is the same in both RMS and EMT simulations.
- For any event in which there will be an imbalance, such as an SLG fault, the RMS model cannot be considered good representation of the EMT models during the fault. After the fault, however, the RMS model will return to the same steady state value as the EMT models so for transient stability studies the RMS model can still be considered a good approximation of the EMT models.
- If an SLG fault occur at the converter controlling the DC voltage, the amount of power it can inject into the AC grid is reduced, which will lead to that the DC link capacitors are charged with an increase in the DC voltage as the consequence. In this case, the difference in behaviour of the different models during the fault will impact the rate at which the capacitors were charged. This means that when the fault is cleared, the DC voltage in the RMS model will be higher than in the EMT models so it will take a longer time for it to return to steady state. However, the voltage would have to rise to a high value in order for this difference to have any significant impact on the results, and in practice the active power controller should limit the power in case of an overvoltage on the DC link.
- In the case of a three-phase fault, the RMS model can be seen as a good representation of the EMT models up until the point when the fault is cleared. Then the RMS model will return to steady state faster than the EMT models. This is caused by the difference in modelling between RMS and EMT. When a three-phase fault is cleared each phase is cleared independently when there is a zero-crossing in the current. For the RMS model, however, the fault is cleared instantly causing a difference in settling time. This difference can be considered small, however, and as long as the clearing time is reasonably short the model should be a good enough approximation.
- In the case of a DC fault the RMS model does not coincide well with the other models during the fault, with a large difference in the active power. Depending on the strength of the system this might have an impact on the results.
- Caution should be exercised when using the RMS model under conditions involving weak AC grids, where the influence of the PLL on the performance of the controller will increase. It was found that when lowering the SCR of the AC system while under high loading conditions, the EMT models would become unstable earlier than the RMS model, which still appeared to be stable.

5

Results from Application Study

This chapter present results from simulations with VSC-HVDC in parallel with a multimachine AC system.

5.1 Introduction

With the model verified, it was included in a more complex system to be used for evaluation of the impact of VSC-HVDC on the transient stability when placed in parallel with an AC system. This was also an opportunity to see how the model performed in a more complex system and to investigate how the simulation times differed when using the RMS model. As the EMT models in PSCAD and PowerFactory performed similarly during the validation it was decided that the RMS model should only be compared to the PowerFactory EMT model for the simulations. The system used for the simulations is shown in Figure 5.1 and it is based on a two-area, four-machine system from [9], with a HVDC link added between buses 7 and 9. For each machine a speed governor, Power System Stabilizer (PSS) and Automatic Voltage Regulator (AVR) was implemented based on generic IEEE models as shown in [51, 52]. Parameters used for the system can be found in Appendix B.

The AC-system is split into two areas: area 1, to the left in the figure, and area 2 to the right. Machine 3, denoted $M3$ in the figure, is the slack machine and it is responsible for balancing the power in the AC system. In order to satisfy the loads, 400 MW is transmitted from area 1 to area 2. The converter in area 1 is set to control the active power in order to control the amount of power to be transmitted using the HVDC link, whereas the converter in area 2 is set to control the DC voltage.

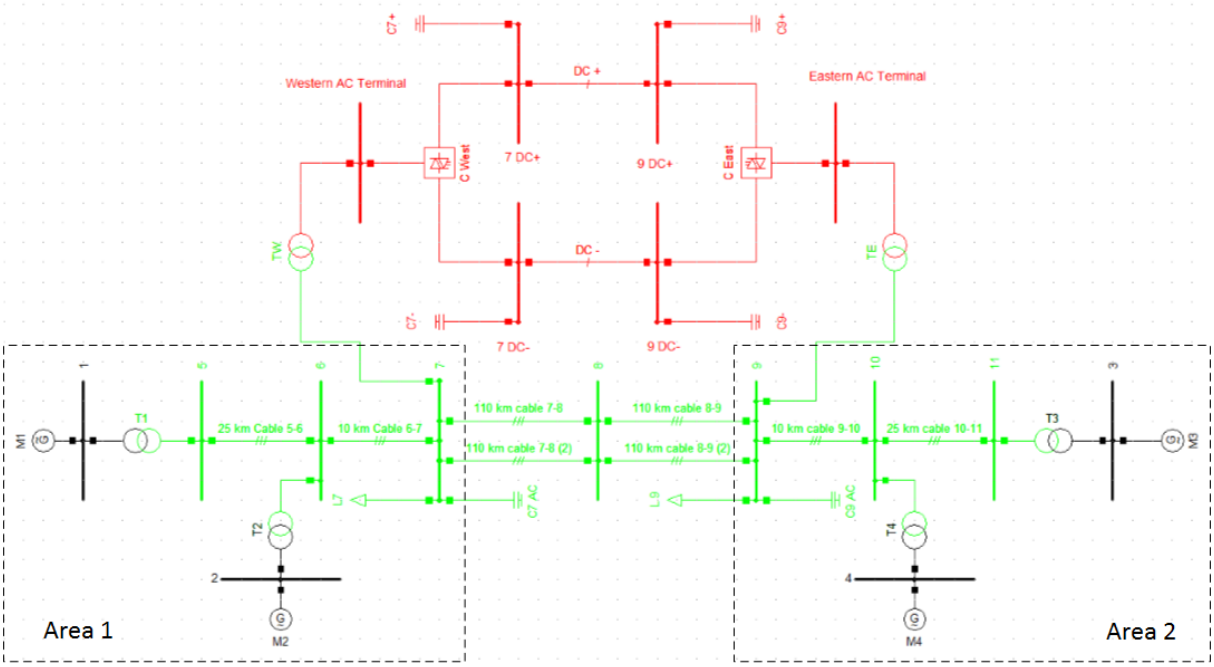

Figure 5.1: Overview of the multimachine system with a parallel HVDC link.

5.2 Simulations

All simulations were performed in both the RMS and EMT simulation modes in order to compare the computational speed and as an extra verification that the simplified model performs adequately. However, only results from the RMS simulations will be shown unless there is a discrepancy in the results.

5.2.1 Three-Phase to Ground Fault bus 8

The first case simulates a three phase AC fault close to bus 8. The fault is cleared by isolating the faulted line after 100 ms. The simulation is repeated for three different power loadings over the HVDC link:

1. Low loading - 0.1 p.u. (60 MW)
2. Medium loading - 0.35 p.u. (210 MW)
3. High loading - 0.65 p.u. (390 MW)

Where high loading correspond to almost all the power transmitted through the HVDC link. The results were compared to the case when there was no HVDC link at all. Figure 5.2 and Figure 5.3 show the machine speeds and mechanical power respectively.

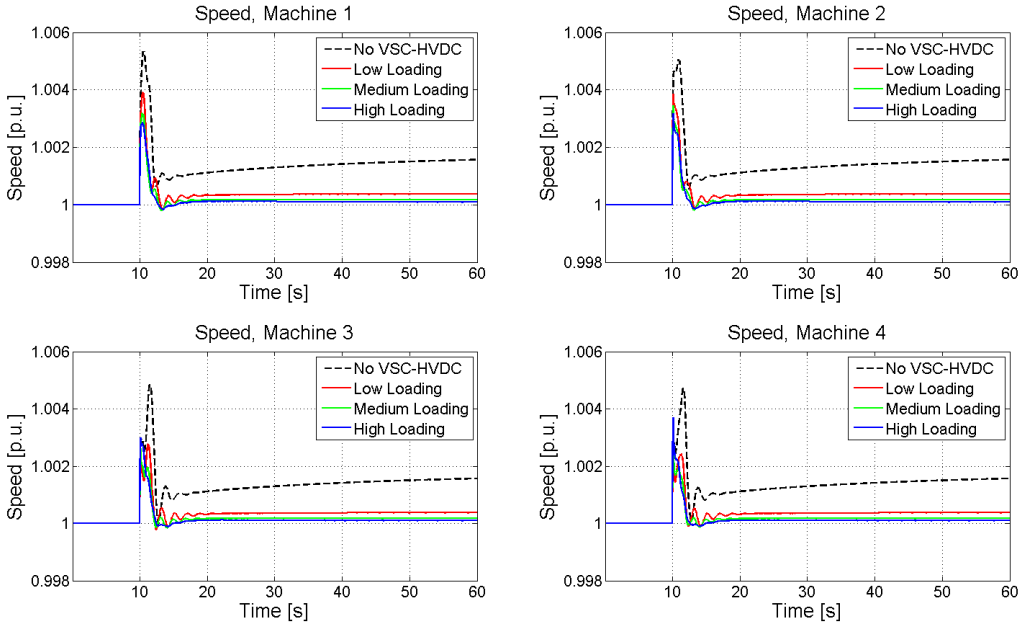

Figure 5.2: Machine speeds following the three-phase fault at bus 8.

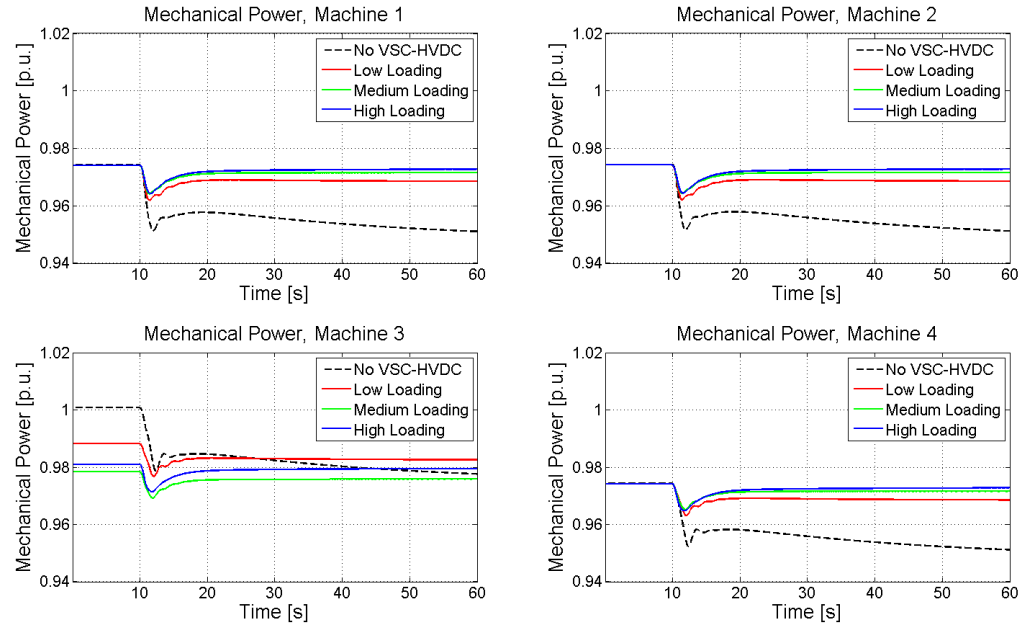

Figure 5.3: Mechanical powers following the three-phase fault at bus 8.

Studying the machine speeds following the fault it can be seen that with a parallel HVDC link, the speed will not deviate as much as the case when there is no HVDC link and it will return to steady state faster. When there is a parallel HVDC link, the deviation will be slightly different depending on the loading of the HVDC link. When the system return to steady state, the speeds will be different compared to before the fault. This is due to that the loss of a line will change the configuration of the system, with a following increase in losses as the power have to be transferred over only one line instead of two.

Comparing the case of low loading on the HVDC link with the other two cases (medium and high) it can be seen that the deviation is larger when the loading of the HVDC link is low. This is simply due to that if most of the power is transferred over the HVDC link the loss of a line will have a smaller impact.

It can also be seen that even if little power is transferred over it, the addition of a HVDC link will result in smaller deviations. One reason for this is that the HVDC link will provide reactive power support to the AC system, improving the voltage levels and reducing losses.

Also, the computational time and model accuracy is compared for the RMS and EMT models. This is illustrated in Figure 5.4 which show the machine speeds in both models following the fault. It is shown for the case when 0.35 p.u. of power is transmitted over the DC link.

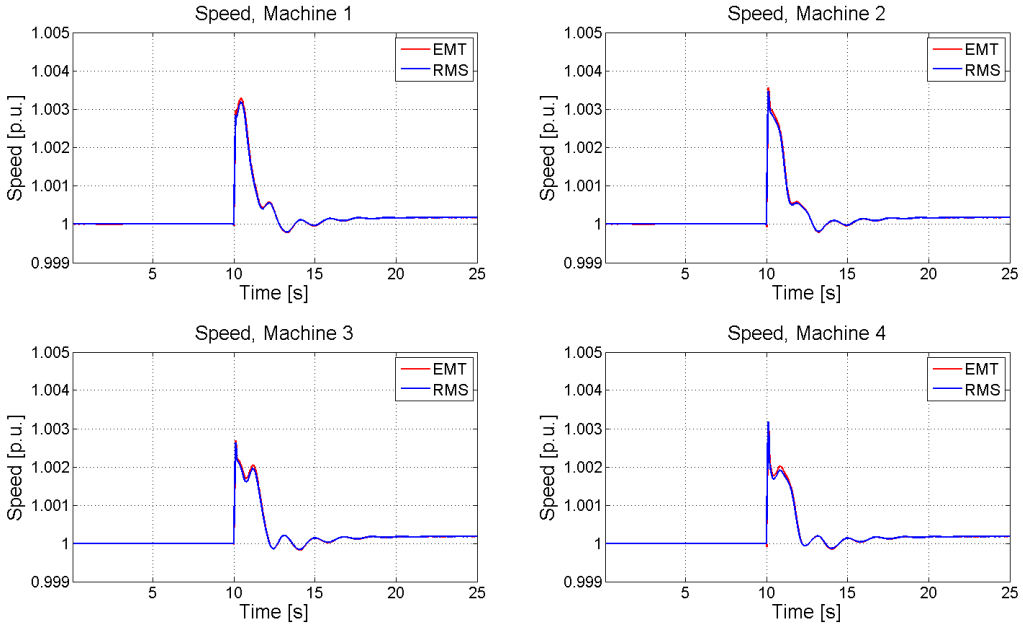

Figure 5.4: Machine speeds, comparison between RMS and EMT following the three-phase fault at bus 8.

The computational time for the RMS model was in this case 39 seconds, and for the EMT model it was 4 minutes and 28 seconds when using the same integration settings. These results show a great improvement in computational time with almost no difference in the results.

5.2.2 Converter Outage

The second case consist of a converter outage on the converter which is controlling the active power. This case was performed in order to observe how the system would respond when the power transfer suddenly had to shift from the HVDC link to the AC lines. The converter outage was simulated for two different loadings in the HVDC link, 0.35 and 0.65 p.u. Figures 5.5 and 5.6 show the machine speeds and mechanical power respectively.

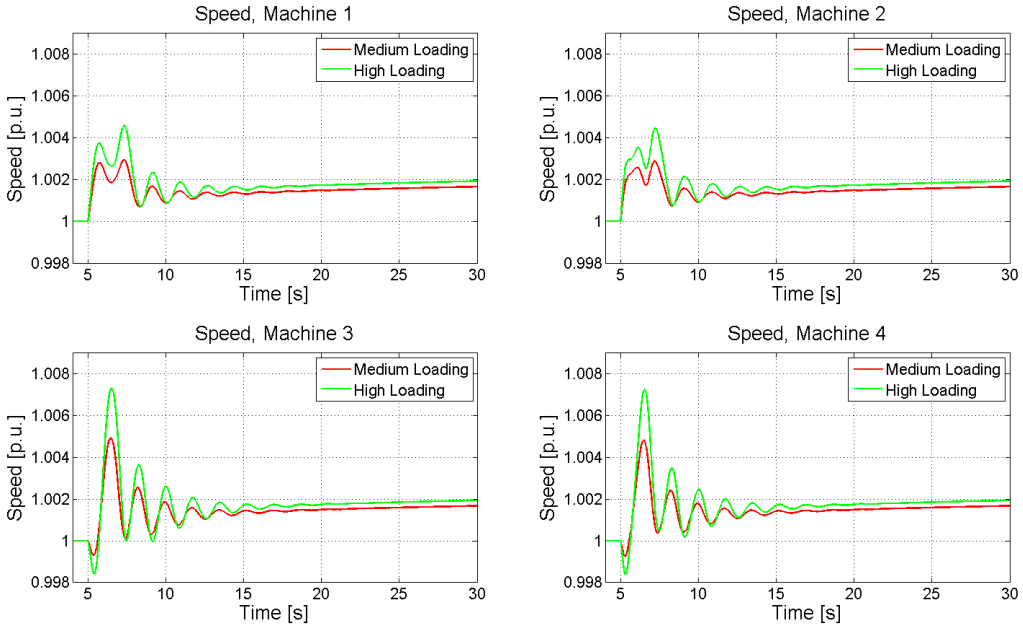

Figure 5.5: Machine speeds following the converter outage.

When the converter goes down the power transfer on the HVDC link goes down to zero and the reactive power support in area 2 is lost. For both loading scenarios, the system remained stable but if the loading of the HVDC link is higher the oscillations in the machine speeds will be larger.

From the mechanical power it can be seen that the mechanical power of all machines will differ compared to the initial value following the outage for the different loading scenarios.

Comparing the computational speed for this case, the RMS model completed the simulation in 1 minute and 46 seconds and the EMT model completed the simulation in 5 minutes and 22 seconds.

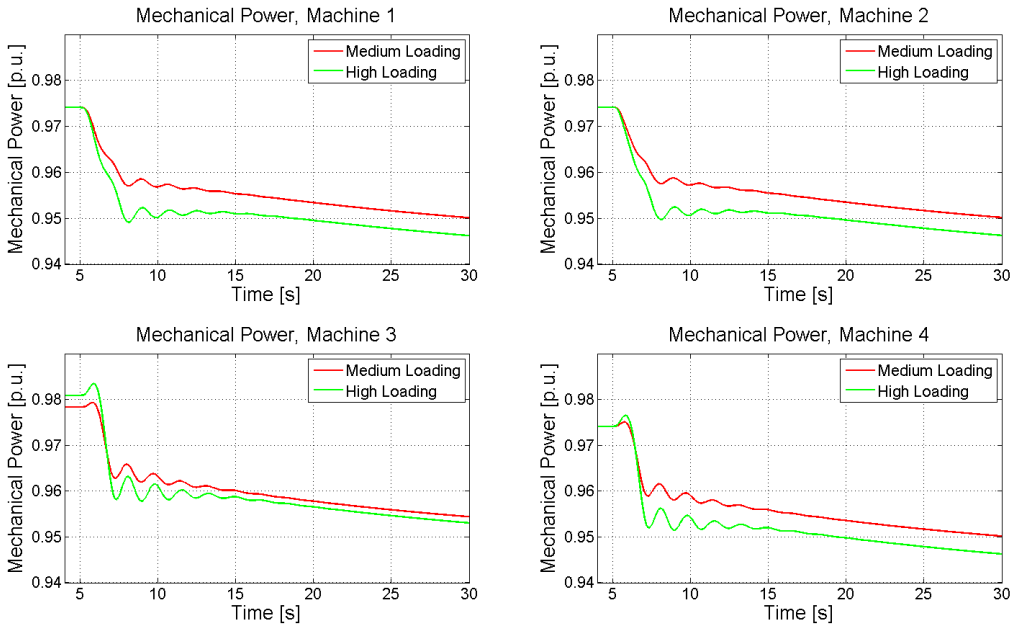

Figure 5.6: Mechanical powers following the converter outage.

5.2.3 DC Line to Ground Fault

In this case a DC side fault was simulated in order to study the impact on the AC system. Similarly to the converter outage, it was done for two different loadings, 0.35 and 0.65 p.u. The behaviour of the HVDC link was similar to what could be seen in Section 4.6.7. Following the fault, the voltage of the faulted pole went down causing the voltage of the HVDC link to drop significantly. This caused the converter controlling the DC voltage to reverse its power flow in order to bring back the HVDC link voltage to 1 p.u. Figures 5.7 and 5.8 show the machine speeds and mechanical power respectively.

Looking at the machine speeds, the loading of the HVDC link appear to have almost no impact on the results. Following the reversal in power flow at the converter controlling the DC voltage, the speed will go down for all machines as there will now be extra power flowing into the HVDC link in order to charge the capacitor as well as the power required by the loads.

This can also be seen from the mechanical powers of the machines, which will rise following the fault in order to compensate for the additional power needed in the system. As expected, machine 3 is the only one to be significantly affected by the loading of the HVDC-link as it is the slack.

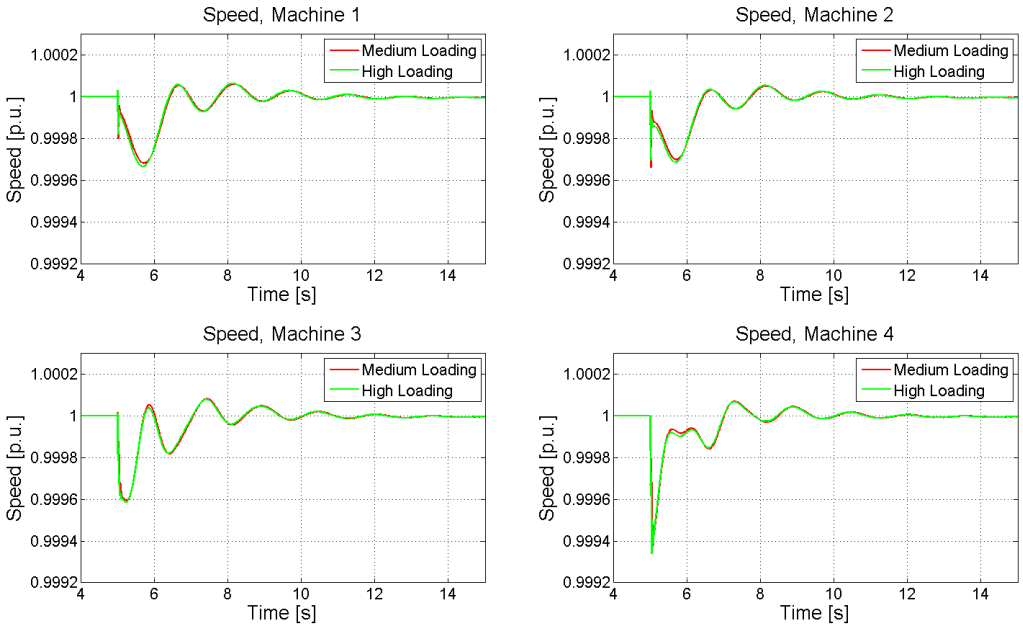

Figure 5.7: Machine speeds following the DC fault.

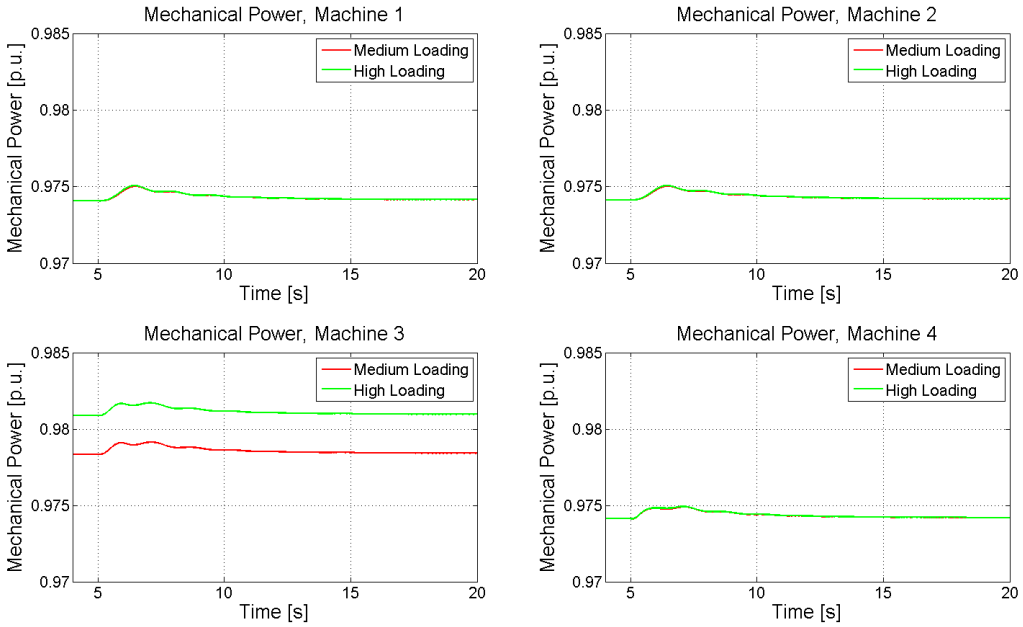

Figure 5.8: Mechanical power following the DC fault.

Considering the results from Section 4.6.7, there was some concern if the odd behaviour in the active power during the fault in the RMS model would have an impact on the results. In order to investigate this, the electrical power, mechanical power and speeds were compared for the RMS and EMT models. This is shown in Figures 5.9, 5.10 and 5.11.

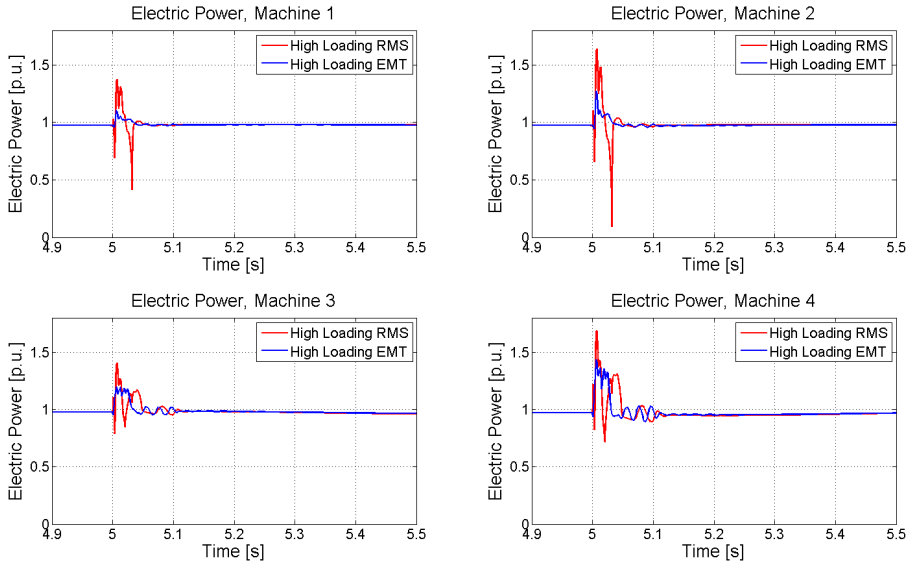

Figure 5.9: Electrical power for RMS and EMT following the DC fault.

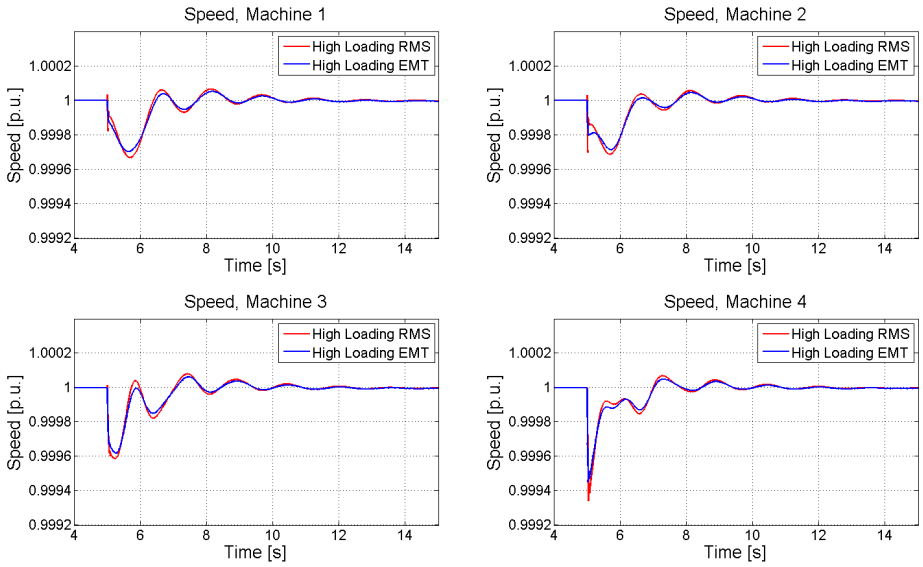

Figure 5.10: Machine speeds for RMS and EMT following the DC fault.

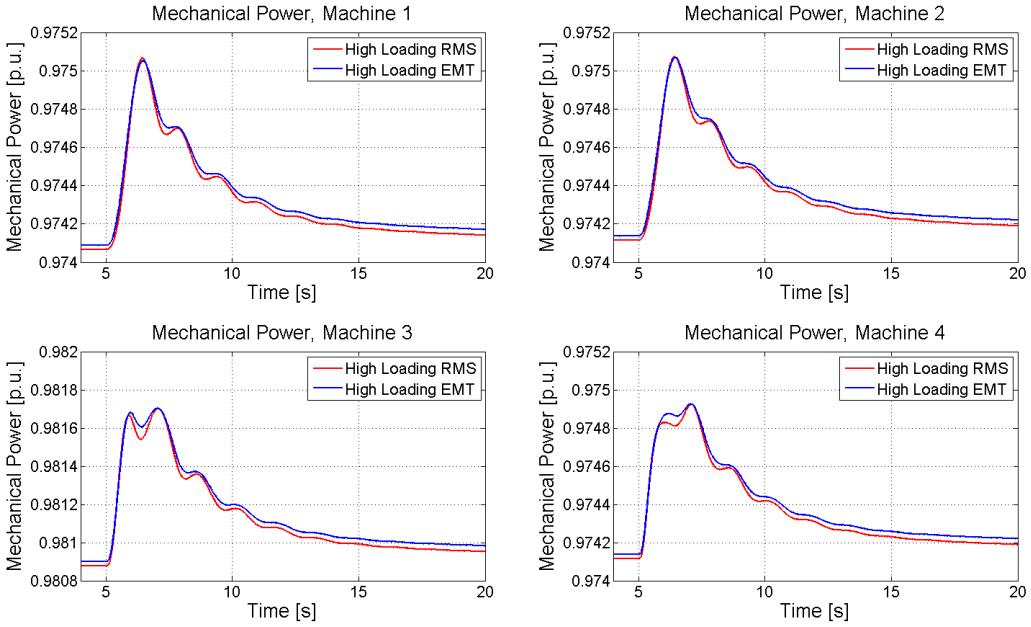

Figure 5.11: Mechanical power for RMS and EMT following the DC fault.

In this case, even though the electrical power differed greatly between the RMS and EMT models during the fault, the impact on the results can be considered negligible. This is in part due to the strength of the AC system used in the simulations.

Similarly to the previous two cases, the RMS model showed a significant reduction in computational time needed for the simulation. It completed the simulation in 20 seconds, whereas the EMT model needed 4 minutes.

5.3 Summary of Application Study

In the first case, the results have shown that the introduction of a parallel HVDC link decrease the deviations in machine speeds following the fault, even if little power is transmitted over it, thanks to the reactive power support it provides. The second case have investigated the consequences of a converter outage, when power is suddenly transferred back to the AC lines. It has been found that if the HVDC link is heavily loaded, the impact on the machine speeds is greater as more power has to be shifted from the HVDC link to the AC lines. For the third and final case there have been some concerns regarding the behaviour of the active power in the RMS model, and if it will have an impact on the results. Despite the difference in active power, in this case the impact on the machine speeds have been deemed negligible.

Table 5.1 shows the computational time of the different models for the simulation cases, and the maximum error in machine speeds for the RMS model when compared to the EMT model.

Table 5.1: Simulation Results

Simulation cases	**RMS Computational time**	**EMT Computational time**	**Maximum error [p.u.]**
Three-phase fault	39 s	4 min 28 s	2.0986e-4
Converter outage	1 min 46 s	5 min 22 s	5.209e-5
DC fault	20 s	4 min	5.610e-5

The results show that the RMS model give great gains in computational speed with almost no loss in accuracy.

6

Closure

This chapter present conclusions with some discussion as well as some suggestions for future work on this subject.

6.1 Conclusions

A detailed model of a VSC-HVDC was developed in PSCAD and PowerFactory for EMT simulations. This included developing and implementing a control system which was done based on vector current control. As the main goal of the thesis was to develop a model suitable for slow dynamic studies, it was investigated how the model would have to be adjusted for use in simplified RMS simulations. The RMS simulation mode of PowerFactory differs from the EMT simulation mode in several ways, and the control system had to be changed as follows.

- Due to the representation of AC dynamics in the RMS model, the current controller had to be adjusted in order to achieve the same response as the EMT models. It was concluded that in order to achieve this, the proportional part of the current controller should be put to zero, with the integrating part remaining the same.
- As the RMS model uses phasors instead of rotating quantities the PLL had to be adjusted accordingly. This meant removing the feed forward of the nominal frequency in the RMS implementation.

It was investigated to what extent the built-in models in PowerFactory could be used, rather than having to develop user-defined models. It was concluded that converters, cables, capacitors and phase reactors could be represented in a satisfactory way by the built-in models, whereas the current controller and PLL had to be implemented manually. The reasoning behind this was based on shortcomings in the implementation, as was the case for the current controller, and a lack of documentation corresponding to the model behaviour, which was the case for the PLL. As there were no built-in models for the outer controllers they had to be implemented manually.

A comprehensive validation has been performed in order to analyse the performance of the RMS model when compared to the more EMT models. This was done by simulating several different cases, including e.g. reference steps, single line to ground faults and DC side faults and comparing the results. It was concluded that the simplified RMS model performed very well in most cases, and that it could be considered an adequate representation of the EMT models considering transient stability studies. There are, however, some limitations in the model that should be considered.

With the model validated, it was then included in a larger four-machine system in order to compare the computational times between the RMS and EMT models, and to analyse the impact of VSC-HVDC on the AC grid.

- It could be seen that the RMS model produced similar results to the EMT models in all cases, with a major reduction in computational time.
- It was found that the introduction of VSC-HVDC into an AC system can help to improve the transient stability due to several reasons, including the ability to provide reactive power support to improve the voltage profile and its high controllability.
- It was found that the amount of loading of the HVDC link affected the machines following a fault. Considering the system as a whole it can be seen that consideration should be given as to how the VSC-HVDC should be operated in order to give the maximum improvement to the transient stability.

6.2 Future Work

In order to further evaluate the usefulness and performance of the simplified model, some possible areas of interest for future work are:

- Extending the system to an MTDC configuration. This will require changing the outer controllers but as one of the future uses of VSC-HVDC is expected to be in HVDC grids, further research should be done.
- It can be investigated if the model can be reduced further while still being accurate enough for transient stability studies. This can involve e.g. removing the π-model representation of the DC cables and replacing them with only a resistance, as mentioned in Chapter 2.
- As the system used in the simulations is strong, extended system studies can be performed using the RMS model in a weaker system.

References

[1] ABB (2013), "History of ABBs HVDC expertise." Available: http://www.abb.se/cawp/seitp202/7cfd9a3a7416a383c1256e8600406f4f.aspx.

[2] J. Pan, R. Nuqui, L. Tang, and P. Holmberg, "VSC-HVDC control and application in meshed ac networks," in *IEEE Power Engineering Society General Meeting*, pp. 20–24, Pittsburgh, Pennsylvania, 2008.

[3] ABB (2013), "HVDC projects by commisioning year." Available: http://www.abb.com/industries/ap/db0003db004333/2eaf1b10de87a2bec12574ea005127de.aspx.

[4] Svenska Kraftnät (2012), "The South West Link." Available: http://www.svk.se/Start/English/Projects/Project/The-South-West-Link/.

[5] G. Pinares, "Operation of HVDC grids in parallel with AC grids," Master's thesis, Chalmers University of Technology, Gothenburg, Sweden, 2010.

[6] P. Kundur, J. Paserba, V. Ajjarapu, G. Andersson, A. Bose, C. Canizares, N. Hatziargyriou, D. Hill, A. Stankovic, C. Taylor, *et al.*, "Definition and classification of power system stability IEEE/CIGRE joint task force on stability terms and definitions," *Power Systems, IEEE Transactions on*, vol. 19, no. 3, pp. 1387–1401, 2004.

[7] S. Cole, *Steady-state and Dynamic Modelling of VSC-HVDC Systems for Power System Simulation*. PhD thesis, Katholieke University Leuven, Leuven, Belgium, 2010.

[8] F. Gonzalez-Longatt, J. Roldan, and C. Charalambous, "Power flow solution on multi-terminal HVDC systems: Supergid case," in *International Conference on Renewable Energies and Power Quality (ICREPQ 12)*, Santiago de Compostela, Spain, 2012.

[9] P. Kundur, *Power system stability and control*. Tata McGraw-Hill Education, 1994.

[10] L. Tuan and J. Daalder, *Power System Analysis Compendium*. Department of Energy and Environment, Chalmers University of Technology, Gothenburg, Sweden, 2011.

[11] H. Latorre, *Modeling and Control of VSC-HVDC Transmissions*. PhD thesis, Royal School of Technology, Stockholm, Sweden, 2011.

[12] J. Paulinder, *Operation and control of HVDC links embedded in AC systems.* Licentiate thesis, Chalmers University of Technology, Gothenburg, Sweden, 2003.

[13] S. Cole, J. Beerten, and R. Belmans, "Generalized dynamic VSC-MTDC model for power system stability studies," *Power Systems, IEEE Transactions on*, vol. 25, no. 3, pp. 1655–1662, 2010.

[14] N. R. Chaudhuri, R. Majumder, B. Chaudhuri, and J. Pan, "Stability analysis of VSC-MTDC grids connected to multimachine AC systems," *Power Delivery, IEEE Transactions on*, vol. 26, no. 4, pp. 2774–2784, 2011.

[15] P. Rault, F. Colas, X. Guillaud, and S. Nguefeu, "Method for small signal stability analysis of VSC-MTDC grids," in *Power and Energy Society General Meeting, 2012 IEEE*, pp. 1–7, IEEE, 2012.

[16] M. P. Bahrman and B. K. Johnson, "The ABCs of HVDC transmission technologies," *Power and Energy Magazine, IEEE*, vol. 5, no. 2, pp. 32–44, 2007.

[17] T. M. Haileselassie, *Control of multi-terminal VSC-HVDC systems.* PhD thesis, Norwegian University of Science and Technology, Trondheim, Norway, 2008.

[18] C. Bajracharya, *Control of VSC-HVDC for wind power.* PhD thesis, Norwegian University of Science and Technology, Trondheim, Norway, 2008.

[19] C. Du, *VSC-HVDC for industrial power systems.* PhD thesis, Chalmers University of Technology, Gothenburg, Sweden, 2007.

[20] T. W. Shire, "VSC-HVDC based network reinforcement," Master's thesis, Delft University of Technology, Delft, Netherlands, 2009.

[21] L. Zhang, *Modeling and control of VSC-HVDC links connected to weak AC systems.* PhD thesis, Royal School of Technology, Stockholm, Sweden, 2010.

[22] L. Zhang, L. Harnefors, and H.-P. Nee, "Power-synchronization control of grid-connected voltage-source converters," *Power Systems, IEEE Transactions on*, vol. 25, no. 2, pp. 809–820, 2010.

[23] L. Zhang, L. Harnefors, and H.-P. Nee, "Interconnection of two very weak ac systems by VSC-HVDC links using power-synchronization control," *Power Systems, IEEE Transactions on*, vol. 26, no. 1, pp. 344–355, 2011.

[24] J. Beerten, D. Van Hertem, and R. Belmans, "VSC-MTDC systems with a distributed DC voltage control - a power flow approach," in *PowerTech, 2011 IEEE Trondheim*, pp. 1–6, IEEE, Trondheim, Norway, 2011.

[25] L. Tang and B.-T. Ooi, "Protection of VSC-multi-terminal HVDC against DC faults," in *Power Electronics Specialists Conference, 2002. pesc 02. 2002 IEEE 33rd Annual*, vol. 2, pp. 719–724, IEEE, Queensland, Australia, 2002.

[26] L. Tang and B.-T. Ooi, "Locating and isolating DC faults in multi-terminal DC systems," *Power Delivery, IEEE Transactions on*, vol. 22, no. 3, pp. 1877–1884, 2007.

[27] J. Candelaria and J.-D. Park, "VSC-HVDC system protection: A review of current methods," in *Power Systems Conference and Exposition (PSCE), 2011 IEEE/PES*, pp. 1–7, IEEE, Phoenix, Arizona, 2011.

[28] ABB (2013), "ABB solves 100-year-old electrical puzzle, new technology to enable future DC grid." Available: `http://www.abb.com/cawp/seitp202/65df338284e41b3dc1257aae0045b7de.aspx`.

[29] M. Callavik, A. Blomberg, J. Häfner, and B. Jacobson (2012), "The hybrid HVDC breaker." Available: `http://www05.abb.com/global/scot/scot221.nsf/veritydisplay/c9d5ba256e7e9671c1257ab6004b1feb/$file/hybrid-hvdc-breaker---an-innovation-breakthrough-for-reliable-hvdc-gridsnov2012.pdf`.

[30] J. Arrillaga, Y. H. Liu, and N. R. Watson, *Flexible power transmission: the HVDC options*. John Wiley & Sons, 2007.

[31] D. Gilles, "VSC-HVDC in meshed networks," Master's thesis, Katholieke Universiteit Leuven, Leuven, Belgium, 2008.

[32] B. Jacobson, B. Westman, and M. Bahrman (2012), "500 kV VSC transmission system for lines and cables." Available: `http://www05.abb.com/global/scot/scot221.nsf/veritydisplay/15adb38bd2044a5ec12579de002b08ad/$file/500%20kv%20vsc%20transmission%20system%20for%20lines%20and%20cables.pdf`.

[33] ABB (2013), "Jinping - sunan 7 200 MW UHVDC transmission." Available: `http://www.abb.com/industries/ap/db0003db004333/545527721af2bf14c12578690049fea4.aspx`.

[34] A. M. Alsseid, *Dynamics and control of high voltage DC grids*. PhD thesis, University of Aberdeen, Aberdeen, Great Britain, 2012.

[35] N. Mohan and T. M. Undeland, *Power electronics: converters, applications, and design*. John Wiley & Sons, 2007.

[36] C. C. Bonilla and S. M. Tigga, "Design and performance comparison of two-level and multilevel converters for HVDC applications," Master's thesis, Chalmers University of Technology, Gothenburg, Sweden, 2011.

[37] ENTSO-E (2011), "Offshore transmission technology." Available: `http://www.assoelettrica.it/wp-content/uploads/2013/01/Entso-E-Offshore-Transmission-Technology.pdf`.

[38] J. Yang, J. Zheng, G. Tang, and Z. He, "Characteristics and recovery performance of VSC-HVDC DC transmission line fault," in *Power and Energy Engineering Conference (APPEEC), 2010 Asia-Pacific*, pp. 1–4, IEEE, Chengdu, China, 2010.

[39] J. Arrillaga, Y. Liu, N. Watson, and N. Murray, *Self-Commutating Converters for High Power Applications*. John Wiley & Sons, 2010.

[40] C. Du, *The control of VSC-HVDC and its use for large industrial power systems*. Licentiate thesis, Chalmers University of Technology, Gothenburg, Sweden, 2003.

[41] C. Ismunandar, "Control of multi-terminal VSC-HVDC for offshore wind power integration," Master's thesis, Delft University of Technology, Delft, Netherlands, 2010.

[42] G. Pinares, L. A. Tuan, L. Bertling Tjernberg, C. Breitholtz, and E. Aty, "On the analysis of the DC dynamics of multi-terminal VSC-HVDC systems using small signal modeling," in *Power Tech Conference, Grenoble, France, 16-20 June*, IEEE, 2013.

[43] T. Midtsund, "Control of power electronic converters in distributed power generation systems," Master's thesis, Norwegian University of Science and Technology, Trondheim, Norway, 2010.

[44] R. Vilanova and O. Arrieta, "PID tuning for cascade control system design," in *Electrical and Computer Engineering, 2008. CCECE 2008. Canadian Conference*, pp. 001775–001778, IEEE, Niagara Falls, Canada, 2008.

[45] L. Harnefors and H.-P. Nee, "A general algorithm for speed and position estimation of AC motors," *Industrial Electronics, IEEE Transactions on*, vol. 47, no. 1, pp. 77–83, 2000.

[46] L. Angquist and M. Bongiorno, "Auto-normalizing phase-locked loop for grid-connected converters," in *Energy Conversion Congress and Exposition, 2009. ECCE 2009. IEEE*, pp. 2957–2964, IEEE, San Jose, California, 2009.

[47] DIgSILENT GmbH (2013), "Dynamic simulation with powerfactory." Available: `http://www.irena.org/DocumentDownloads/events/2013/March/Palau/04_StabilityHandling.pdf`.

[48] F. Gonzalez-Longatt, "Models for stability analysis." Available: `http://www.fglongatt.org/Tutorial_DigSilent_EN.html`, 2009.

[49] DIgSILENT GmbH, *Technical Reference - PWM Converter*. DIgSILENT GmbH, 2007.

[50] DIgSILENT GmbH, *Technical Reference - PLL*. DIgSILENT GmbH, 2005.

[51] X. Xu, R. Mathur, J. Jiang, G. Rogers, and P. Kundur, "Modeling of generators and their controls in power system simulations using singular perturbations," *Power Systems, IEEE Transactions on*, vol. 13, no. 1, pp. 109–114, 1998.

[52] C. Hamon, "Doubly-fed induction generator modeling and control in digsilent power factory," Master's thesis, Royal School of Technology, Stockholm, Sweden, 2010.

[53] X. Xu, R. Mathur, J. Jiang, G. Rogers, and P. Kundur, "Modeling of generators and their controls in power system simulations using singular perturbations," *Power Systems, IEEE Transactions on*, vol. 13, no. 1, pp. 109–114, 1998.

A

VSC-HVDC parameters

Converter Data

Ratings; $S = 600$ MVA, $V_{AC} = 300$ kV, $V_{DC} = 300$ kV, $f = 50$ Hz

$f_{sw} = 2$ kHz	$\tau_c = 0.005$ s	$\varepsilon = 3$
$L_{ph} = 0.25$ pu	$R_{ph} = 0.0025$ pu	$C_{DC} = 3.14159$ pu

DC Voltage Controller

K_P	4.61718
T_i	0.0206821
α	0.4 pu

Current Controller

	RMS	EMT
K_P	0	1
T_i	0.31831	0.31831
α	4 pu	4 pu

AC Voltage Controller	
R_{AC}	10
T_{AC}	0.05

B

Multimachine system parameters

Generator Data

Base; 900 MVA, 20 kV, 50 Hz

$X_d = 1.8$	$X'_d = 0.3$	$X''_d = 0.25$	$V_{sat} = 0.015$
$X_q = 1.7$	$X'_q = 0.55$	$X''_q = 0.25$	$B_{sat} = 9.6$
$X_l = 0.2$	$T'_{do} = 8.0$ s	$T''_{do} = 0.03$ s	$\psi_{T1} = 0.9$
$R_a = 0.0025$	$T'_{qo} = 0.4$ s	$T''_{qo} = 0.05$ s	$K_D = 0$
$S_{1,0} = 0.039$	$S_{1,2} = 0.223$		

$H = 6.5$ (For G1 and G2) $H = 6.175$ (For G3 and G4)

Transmission Lines

Base; 100 MVA, 230 kV

$r = 0.0001$ pu/km $x_l = 0.001$ pu/km $b_c = 0.00175$ pu/km

Transformers

Base; 900 MVA, 20/230 kV

$X = 0.15$ pu

Off-nominal ratio = 1.0

Operating Condition

$G1$	$P = 700$ MW	$Q = 185$ MVAr	$V_t = 1.03\angle 20.2°$
$G2$	$P = 700$ MW	$Q = 235$ MVAr	$V_t = 1.01\angle 10.5°$
$G3$	$P = 719$ MW	$Q = 176$ MVAr	$V_t = 1.03\angle -6.8°$
$G4$	$P = 700$ MW	$Q = 202$ MVAr	$V_t = 1.01\angle -17.0°$
$Bus\ 7$	$P_L = 967$ MW	$Q_L = 100$ MVAr	$Q_C = 200$ MVAr
$Bus\ 9$	$P_L = 1767$ MW	$Q_L = 100$ MVAr	$Q_C = 350$ MVAr

For the synchronous machines, a PSS, AVR and speed governor was implemented based on [53]. This is shown in Figure B.1 and Figure B.2.

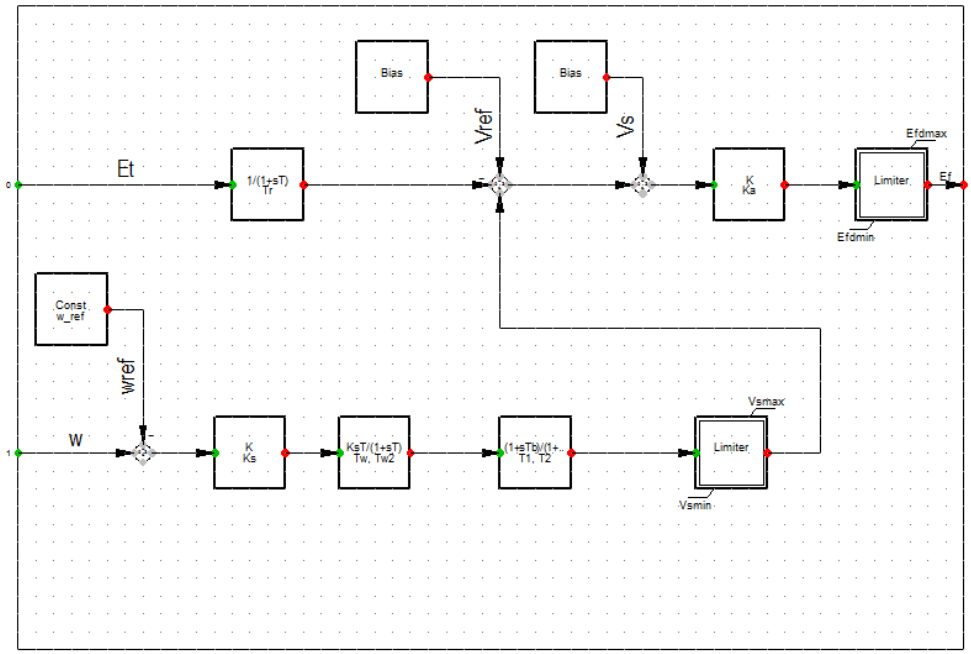

Figure B.1: PSS and AVR implementation.

PSSAVR parameters

$K_a = 200$	$T_r = 0.01$	$V_{s,max} = 0.2$
$K_s = 20$	$T_1 = 0.16$	$V_{s,min} = -0.2$
	$T_2 = 0.02$	$E_{fd,max} = 5$
	$T_\omega = 10$	$E_{fd,min} = -5$

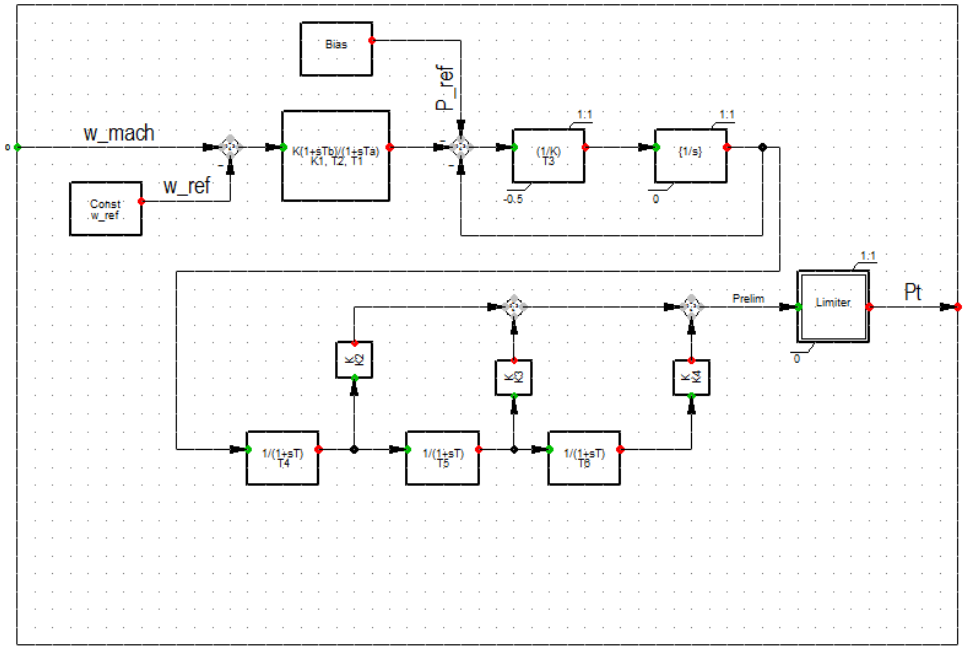

Figure B.2: Speed governor implementation.

Speed governor parameters

$K_1 = 15$	$T_1 = 0.1$	$T_5 = 4.25$	$R_{max} = 1.1$
$K_2 = 0.25$	$T_2 = 0$	$T_6 = 0.72$	$R_{min} = -0.5$
$K_3 = 0.25$	$T_3 = 0.25$	$P_{max} = 1.1$	
$K_4 = 0.5$	$T_4 = 0.42$	$P_{min} = 0$	